ESTIMATING THE ACOUSTIC ABSORPTION OF WOOD-INFUSED CONCRETES

Matthew Lorimer

A thesis submitted in partial fulfillment of the requirements for the

MASTER OF APPLIED SCIENCE IN MECHANICAL ENGINEERING

Department of Mechanical Engineering
Faculty of Engineering
University of Ottawa

Abstract

In architectural design, few materials compare to the degree of use of concrete. Due its high compressive strength and economic efficiency, concrete excels in architectural applications. While impressive, concrete has shortcomings in its acoustic absorption properties and ability to be used sustainably. To address both concerns, the proposed solution is to introduce waste wood fibers into concrete's composition. Due to wood's fibrous nature, acoustic absorption can be bolstered while improving sustainability by recycling waste wood products. While manufacturing wood infused concretes and measuring acoustic absorption is not difficult, it is time consuming and resource intensive. Therefore, a model to estimate acoustic absorption coefficients of fiber-infused concretes is developed to aid in bypassing the need for experimental trial-and-error. The model utilizes the Delany-Bazley (DBz) and Johnson-Champoux-Allard-Lafarge (JCAL) models to predict acoustic absorption coefficients of given fiber-infused concretes. The DBz model provides an estimate of the characteristic impedance and wave number of a sample based on a power-law relationship that considers sound medium and airflow resistivity. The DBz model estimates are then refined by the JCAL model using estimated viscous and thermal properties of the sample. Finally, using these refined acoustic property estimates, the acoustic absorption coefficients are estimated. Using varying wood-infused concrete samples, results are experimentally verified using an impedance tube and absorption coefficients are calculated using the transfer-function method. After comparing estimated and measured absorption values, the current model was found to have the potential of providing a relative comparison of acoustic performance between compositions. However, estimated values were not accurate, nor considered representative of samples. Further, multiple aspects of the model could be improved to better represent different concrete compositions in model estimations.

Acknowledgments

I would like to thank Ali Sheikh, Charly Kone, and Sebastian Ghinet at the National Research Council for kindly providing and assisting me with the impedance tube used in this study.

Table of Contents

List of Figures

List of Tables

Nomenclature

T: Air Temperature

P_0: Air Pressure

R: Universal Gas Constant of Air

ρ_0: Density of Air

c_0: Speed of Sound

K_a: Bulk Modulus of Air

μ: Viscosity of Air

C_p: Specific Heat at Constant Pressure of Air

C_V: Specific Heat at Constant Volume of Air

γ: Specific Heat Ratio

κ: Thermal Conductivity of Air

Pr: Prandtl Number

σ: Surface Airflow Resistivity

r: Radius of Fibers

d: Ratio of Fiber Densities

b: Average Square Root of Area per Fiber

ρ_{mat}: Density Sample

ρ_{fib}: Density Fibers

ϕ: Surface Porosity

V_{sol}: Dry Volume of Sample

V_T: Total Volume of Sample

V_{void}: Volume of Surface Voids of Sample

α_∞: High Frequency Limit of Tortuosity

ω: Angular Frequency

ρ: Dynamic Density

λ: Viscous Characteristic Length

k_0': Thermal Permeability

K_{dyn}: Dynamic Bulk Modulus

λ': Thermal Characteristic Length

Z_c: Characteristic Impedance

k: Wave Number

f: Frequency

$Z_{surface}$: Surface Impedance

α: Acoustic Absorption Coefficient

$\mathcal{R}$: Reflection Factor

$M1$: Microphone Position 1

$M1'$: Alternate Microphone Position 1

$M2$: Microphone Position 2

$X1$: Distance Between $M1$ and Speaker

$X1'$: Distance Between $M1'$ and Speaker

$X2$: Distance Between $M2$ and Speaker

$S0$: Distance Between Microphones

f_u: Upper Frequency Limit

D: Impedance Tube Diameter

λ_u: Upper Frequency Limit Wavelength

f_l: Lower Frequency Limit

λ_l: Lower Frequency Limit Wavelength

L: Total Length of Impedance Tube

x: Position in Impedance Tube

p: Acoustic Pressure

A: Incident Wave Soundwave Amplitude

B: Reflected Wave Soundwave Amplitude

S_{12}: Acoustic Cross-Spectrum

S_{11}: Acoustic Auto-Spectrum

H_{12}: Acoustic Transfer Function

Chapter 1

Introduction

In the construction industry, there is an increasing demand for sustainability, one aspect of which is human comfort [1]. A key factor in human comfort is acoustic health, which can be severely impacted by environments with poor acoustic design. Due to concrete's prevalence, the manipulation of concrete has the potential to have a large impact in creating more suitable acoustic environments within architectural spaces. In July of 2020 alone, over nine million tons of concrete were imported into the United States [2]. Being one of the most used construction materials, concrete (in the form of interior paneling, roadways, and highway barriers) presents a unique opportunity to foster acoustically controlled environments to absorb intrusive vehicle noise and inhibit excessive internal noise when combined with fibrous aggregates that enhance the porous nature of the concrete itself [3]. By improving the acoustic properties of concrete from the outset, both cheap and easily manufacturable sound absorbers could be integrated into structural designs and would avoid expensive retrofitting or intrusive alternatives later.

To understand how acoustics can impact architectural spaces, the modes in which sound travels between air and solid objects must be examined. Considering the situation in which a soundwave (a pressure wave propagating through a medium) collides with a barrier, there are three energy interaction modes that can be described. The kinetic energy of the

pressure wave can be transmitted through the barrier, can dissipate within the barrier, and can reflect off the surface of the barrier (Figure 1-1). Transmission is the phenomenon in which the pressure wave travels through the barrier and propagates out the other side. Absorption is the kinetic energy of the pressure wave that dissipates into heat while travelling within the barrier. Finally, the acoustic energy that does not enter the barrier and bounces off the surface to continue propagating in the initial medium is said to have reflected [4].

Levels of acoustic absorption vary as the soundwave frequency changes. This is because frequency represents the amount of soundwave repetitions over time. If wavelength is also considered, this means that wavelength must decrease as frequency increases. Therefore, if a high frequency wave is considered, more repetitions are required to travel the same distance as that of a lower frequency wave, requiring more energy to do so. For example, as a soundwave travels through a concrete sample, assuming wave amplitude is constant, higher frequency waves will be exposed to more viscous interactions, and therefore, will lose energy (be absorbed) more rapidly. This in turn reveals that lower frequency absorption should be considered more carefully due to the naturally higher transmissibility of low frequencies [5].

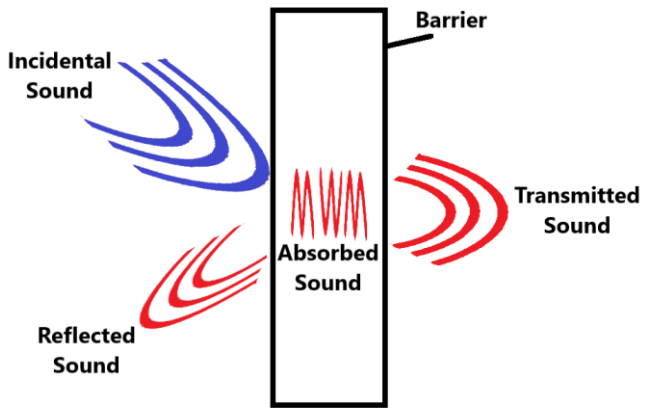

Figure 1-1: Interactions of Sound with Solid Objects

Concrete, by nature, is typically quite reflective of acoustic energy [6]. While beneficial in acoustic insulation, issues arise in indoor spaces when the desired result is acoustic absorption. One practice that has been proven to bolster acoustic absorption is increasing the porosity of concrete [7]. Porosity increases acoustic absorption as incident soundwaves become trapped within concrete pores and are then converted to thermal energy. The porosity of concrete is determined during the concrete curing process, in which hydration occurs and the concrete paste solidifies. Hydration is the chemical process in which water reacts with the concrete mix. If more water is used, more pores form [8]. Therefore, by tailoring the water content in the concrete mix with regards to porosity, acoustic absorption can be bolstered. Similarly, adding fibrous aggregates to concrete also acts to trap acoustic energy. Fibres convert acoustic energy to thermal energy as sound reflects between the fibres, and therefore, absorbs sound. The nuances of aggregate selection and quantity are complex, as a multitude of factors play a role in the overall energy absorbed [9]. These factors include specific density, porosity, aggregate size, aggregate quantity, aggregate material, water content, cement content, curing time, and frequency. Studies vary in which factors take priority with respect to influencing acoustic absorption. However, all of these factors play some role in the final absorption levels.

Acoustic absorption is a measure of how much acoustic energy is absorbed by a material once a sound wave has made contact with it. The remaining acoustic energy, that which has not been absorbed, will either be reflected from the material or transmitted through it. For example, if a material has an acoustic absorption coefficient of 1.00, all acoustic energy of the incidental wave has been absorbed by the material. It is worth noting that the acoustic absorption value typically varies based on the frequency of the wave. The acoustic absorption coefficient is directly related to the reflection factor (a similar property that denotes how much acoustic energy is reflected from a material when a sound wave makes

contact with it), as well as the acoustic impedance of the material. Acoustic impedance, as the name implies, is a quality that denotes the resistance of acoustic flow a system or medium applies (impedes) as sound travels through the system or medium [10]. For the purposes of this study, both the reflection factor and acoustic impedance will be found when solving for acoustic absorption.

When obtaining values of acoustic absorption from varying materials, the most common methodology is through experimentation using samples of the material and impedance tube testing. Impedance tube testing measures acoustic absorption with two microphones in a controlled environment. One microphone is used to measure the energy of an incidental sound wave and the second microphone is used to measure the amount of acoustic energy projected off the material once the incidental soundwave makes contact. This difference in energy provides an acoustic absorption value via a ratio of the acoustic energy picked up by each microphone. While this process for measuring acoustic absorption is fast and accurate, it can become a lengthy process when using concrete samples due to their slow curing times. Therefore, a need exists for being able to accurately model acoustic absorption of wood/concrete mixtures to circumvent the need to make experimental samples for each new material composition. These models use their own sets of specific parameters, both in terms of the sample itself and the medium in which the sound is travelling [11]–[13]. These models would greatly benefit the process of verifying the acoustic absorption of any given specific concrete composition, and thus, help improve the design and development of healthy acoustic architectural environments.

An analytical model combining the Delany-Bazley (DBz) model and Johnson-Champoux-Allard-Lafarge (JCAL) model will be used to solve acoustic absorption by estimating the acoustic impedance based on the thermal and viscous properties of the concrete [11]–[15]. These models are both used for the prediction of acoustic properties of fibrous, porous

materials such as concretes. The DBz model takes a much simpler approach (as was intended by its authors) in estimating the acoustic impedance of the material, only requiring the viscous property of static airflow resistivity in its calculations [15]. However, DBz estimations can be refined using the JCAL model by introducing a multitude of viscous properties (open porosity, the high frequency limit of tortuosity, and viscous characteristic length) and thermal properties (thermal characteristic length, and thermal permeability). The utilization of these models in tandem provides a much more refined and informed prediction of acoustic impedance that can be used to estimate the potential acoustic absorption of the desired concrete composition.

The purpose of this study is to verify the accuracy of acoustic absorption estimations made using the acoustic impedance values found by combining the DBz and JCAL models. To verify the accuracy of the acoustic absorption predictions using the models, acoustic absorption values of varying concrete samples will be experimentally observed using acoustic impedance tube testing. Impedance tube testing works by monitoring sound wave amplitudes before and after reflecting off the surface of the material being tested. Using the transfer function method, ASTM E1050-19, the amplitudes are used to solve for the acoustic reflection (which, just like acoustic absorption, varies based on the frequency of the wave) [16]. The reflection factor can be used to solve the acoustic absorption coefficient, allowing the verification of the analytical models by comparing the results with experimental data. Concrete samples will be manufactured, and densities and porosity values measured to ensure that the hybrid DBz – JCAL model can depict the concrete's acoustic properties as accurately as possible.

Chapter 2

Acoustic Properties of Wood-Infused Concretes

Like any solution to an issue, wood-infused concrete as an acoustic absorber has both advantageous and disadvantageous properties. Within this section, these advantages and disadvantages will be explored. Further, the research involving acoustic absorption related to wood-infused concrete, as well as other concretes and fibrous materials will be considered, along with some of their applications. This review of the current literature will provide an overview of the current state of this field. This information will also be key in developing a model for acoustic absorption of wood infused concrete in the following chapters.

2.1 Advantages of Wood-Infused Concretes

Sustainability is a term that can be understood in three ways, environmental conscientiousness, economic feasibility, and human desirability. The use of wood-infused concretes to improve the acoustic quality of a space has the potential to bolster all three of these areas. The first aspect of sustainability that will be considered, and most integral to this thesis, is human desirability in the form of the acoustic quality of architectural spaces.

Due to the porous nature of concretes and the fibrous contents of wood aggregates, wood-infused concretes have particularly useful qualities for bolstering acoustic absorption of a space [6], [17]. Regarding acoustic absorption's role in human comfort, sound control in architectural spaces is an increasingly significant factor in urban design [18]. In fact, all kinds of work environments, from offices to schools, are implementing more open designs to bolster human connections [19]. The sound quality in these spaces plays a large role in not only comfort, but in human productivity. A study by Kang et al. found that acoustic environment quality is the largest factor impacting productivity of those within university open-plan research office-spaces [19]. While open spaces generally work as intended and increase human communication, acoustic design becomes of great importance as unimpeded sound travel is found to be distracting. Haapakangas et al. found that in open workspaces, sound that can be heard from more than 8 meters away brought productivity down and reflected poor room acoustics [18].

Moreover, these concerns extend beyond places involving deskwork. Roadways produce large amounts of sound that can intrude on residential spaces or places of recreation. The importance of human comfort is well understood, as many urban centres now require transportation noise assessments before construction of housing [20]. A common solution to excessive road noise levels is the use of acoustic barriers. For example, highway barriers act as a wall to reduce the intensity of perceived sound that travels from traffic noise hotspots to surrounding areas. While multiple factors impact the effectiveness of an acoustic barrier, the acoustic absorption of the barrier plays a particularly important role [18]. A study by Peceño et al. investigated the impacts of course aggregate replacements in concrete acoustic-absorbing barriers with mollusk-shell waste [21]. They found the best acoustic absorption potential was provided when 80% of the concrete by weight was replaced by 2-to-7-millimeter scallop waste, providing greater acoustic absorption coefficients than concrete

alone, between the range of 0 and 3800 Hz, before plateauing [21]. While mollusk-shell waste and fibrous materials such as wood do not provide the same material properties, the acoustic potential found by using mollusk-shell waste shows the positive potential that aggregate replacement can have on highway barriers and other applications.

Another, more innovative, strategy in mitigating traffic noise is through the implementation of fibrous materials in the pavement of roadways themselves. While ceramic-like materials, such as concrete, have relatively low flexural strength, fibrous materials like wood have high flexural strength. When combining these two materials together via wood-infused concrete, the flexural strength of concrete can be bolstered. In these applications, the primary goal of the wood-infused pavement is to reduce road noise at the source, as the fibrous wood materials absorb sound and vibrations as the vehicles operate atop them. This idea translates to other non-structural loading applications as well [22].

The environmental sustainability of wood-infused concretes is also of utmost importance when discussing the benefits of wood-infused concrete sound absorbers. The environmental benefits stem from the use of wood as an aggregate. While wood-infused concrete can be manufactured using wood from a plethora of sources, sustainability can be bolstered with the use of waste wood products. A study by Aghimien et al. found that amongst 10 local sawmills in Kojola, Oyo, Nigeria, at most only 70-80% of each log being sawn was used for the final product [23]. While practices in the lumber industry may differ in different regions from those in Nigeria, this data provides insight on the amount of waste-wood product, of varying forms, available in sawmills. Furthermore, ash is another natural by-product of wood that is in great abundance and has been shown to be effective in acoustic absorptive concretes. As an example, “The North American pulp and paper industry generates more than one million tons of ash annually by burning wood in power boiler units for energy

production", revealing an untapped source of natural biomaterials for both the benefit of acoustic concrete, and environmental sustainability [24]. Using wood-waste products in acoustic concrete has great potential in decreasing the carbon footprint of both the concrete manufacturing process and those that produce waste-ash.

Finally, wood-infused concrete absorbers improve economic sustainability by being both cost effective, as well as being accessible and easy to manufacture. The acoustic properties, in combination with the simple manufacturing and relatively low cost of concrete, enables an easy implementation of acoustic damping barriers in sound sensitive spaces. The need for cheap sound control can be seen in the room acoustics of many open-style workspaces, where sound travels much easier due to the lack of divisions between spaces. Beyond affordability, the most significant benefit to utilizing concrete-based acoustic materials is the simplicity in which the properties of concrete can be altered. The potential to bolster the material properties of concrete with few alterations to the manufacturing process is highly beneficial. This allows the acoustic properties of sound absorbers to be adapted for different environments. This can be done by adjusting the composition of concrete itself [6].

Concrete's composition is made up of a number of elements, one of which is aggregates. Aggregates can be considered based on their size, material, and volumetric or mass-based fraction. Fediuk et al. compare numerous acoustic concrete compositions in terms of acoustic absorption and found that altering the fraction of aggregate by just 10% can greatly impact final values between samples made of the same materials [6]. For example, samples of a lightweight aggregate concrete that utilized crushed rubber as a fine aggregate replacement at 40% and 60% had a difference of acoustic absorption of 0.09 at 1000 Hz. A 9% change in acoustic absorption represents a significant difference in potential sound levels, depending on the environment [6]. Along with aggregates, another major factor affecting the final properties of concrete is the water content added during manufacturing,

as the porosity of a material has a significant impact on its acoustic absorption properties [9]. Water content in concrete plays perhaps the largest role in the overall porous nature of a concrete sample, both in terms of pore size and distribution [25]. Both changes in water-to-concrete ratio (W/C ratio) and the aggregates themselves impact the final density of a concrete sample. This is important because Fediuk et al. confirm that lower density samples tend to provide higher acoustic absorption values [6].

2.2 Disadvantages of Wood-Infused Concretes

While wood-infused concretes are considered beneficial in their overall impact on sustainability, they have complications that must be addressed. Particularly, these complications manifest in the form of a lower compressive strength, working around concrete's naturally reflective tendencies, and the inconsistent nature of concrete manufacturing and difficulties of wood-concrete bonding.

While concrete manufacturing is relatively simple and straightforward, there are some aspects that are more complicated than others. Specifically, when using larger aggregates, there is generally inconsistency in the material properties due to inhomogeneity of aggregate orientation. During the concrete mixing process, fibres orient themselves randomly, which in the case of coarse aggregates is very influential on the overall material properties. This random nature makes it difficult to define the acoustic properties of samples precisely, or obtain consistent acoustic absorption information. Moreover, this also makes it difficult to determine well understood properties, such as compressive strength, Young's modulus, or flexural stiffness. While material properties can be averaged to provide a general range of expected values, outliers that exceed or fall short of these ranges are expected, adding a risk factor to their potential application [26]. A possible solution to this is to create wood-infused concrete using methods like those used for traditional fibre

reinforced composite materials, by orienting wood fibres ahead of time and then adding liquid concrete as a matrix, controlling the resulting sample. However, it is worth noting that this is not a particularly practical solution, as orienting individual fibres on a large scale is a time-consuming process, especially when a major benefit of concrete is its ease of manufacturing.

Further, the compatibility of certain wood-cement compositions can be problematic in the structural integrity of the final product. The compatibility refers to how well cement sets after mixing with water and wood aggregates. This setting process is important, because if the cement and wood do not take to one another, the properties of the final concrete product can be detrimental to the usability of the sample. The compatibility of materials can be calculated using an inhibitory index that calculates the compatibility of materials based on the thermal properties of the composition during the mixing and setting processes. There are many potential factors that impact compatibility that go beyond the type of wood (aggregate size and geometry, composition percentages, additives, etc.). Therefore, making a prediction regarding compatibility can be very difficult. Furthermore, research looking at wood-infused concrete is commonly concerned with the structural stability of the final product, with little regard to incompatibilities as they relate to acoustic properties [27]. An issue that does arise when working with miscanthus fibres, which shares properties with wood, is that hydration can be interrupted due to the absorption of water by the fibres [7]. This can hinder the mixing process if not accounted for, extending the time required to form the concrete. Generally, conclusions state that by including biofibres, porosity and internal voids are increased, thus improving acoustic absorption [28].

While the intended application of infusing concrete with wood fibers in this study is to bolster acoustic absorption, a problem when using concretes of any kind is that it is

naturally acoustically reflective. An advantage when considering acoustic insulation, high reflection poses as an issue for absorption. While acoustic absorptive materials are also great at insulating rooms, this occurs through acoustic energy absorption, whereas concrete excels at reflecting acoustic energy. Highly reflective panelling will only amplify the effects of sound on dense roadways, in metropolitan spaces, and in enclosed work environments. In fact, since the acoustic absorption of most concretes is so low, the magnitude of the sound being reflected from the surface of the concrete is virtually the same as the incident wave. In smaller spaces, such as working areas or between buildings, this can create a reverberation effect, further increasing noise, as concrete can reflect up to 99% of the acoustic energy it is subjected to [6]. Specifically, "concrete is generally a preferred product to block noise transmitted … due to its excellent performance as [a] sound reflecting material ... However, it is extremely limited in terms of the sound absorbing capability" [28]. Concrete's excellent reflective properties pose a significant disadvantage to acoustic absorption since these are opposing properties. Therefore, significant interventions are required to boost absorption. The noise reduction coefficient (NRC) can be used to represent an average of acoustic absorption values over a frequency range. For example, values for lightweight aggregate concrete with lightweight cenospheres ranging from 20% to 60% volume and measuring between 10 and 300 micrometers boasts NRC values ranging between 0.11 and 0.15, which represents highly reflective values [28].

A point worth noting, beyond the acoustic applications of wood-infused concretes, is the impact of wood aggregates on the structural strength of concrete. Concrete, in general, is used in primarily structural applications and its great performance in this application has led to its industry standard in structural design. Unfortunately, using wood aggregates drastically decreases the compressive strength of concrete. When replacing aggregates with fibrous materials and increasing porosity and void spaces through increased water content,

density and compressive strength sharply decrease. For example, when examining concrete with fine aggregates (sand) replaced with olive wood waste, compressive strength quickly decreases as the wood content increases. Specifically, by replacing 25% of the sand by mass and utilizing curing accelerators and additives, a peak compressive strength of approximately 40 MPa can be achieved, representing a 10 MPa decrease when compared to Portland concrete. As replacement percentages increase, compressive strength is found to decrease sharply, with 50% sand replacement boasting a peak strength of approximately 36 MPa, and 100% replacement peaking at less than 2 MPa. Furthermore, strength of samples only increase as curing time is lengthened between samples [22]. This is a common theme found in concretes; as the volumetric void percentage increases with larger aggregates, the potential for the material to withstand large compressive loads decreases, as stresses are focused through smaller columns of concrete [26].

Despite this decrease in structural strength, within the same study examining olive wood waste concretes, an increase in flexural strength is observed. Antoun et al. examined the effects of replacing fine aggregates in concrete with olive wood waste for masonry applications and found that the flexural strength of the bricks increased substantially [22]. When fine aggregates (sand) were replaced with the olive wood waste, flexural strength was bolstered at replacement percentages up to 50% by volume. The greater the length of the curing process, the greater the flexural properties of the samples, with 25% replacement samples achieving comparable flexural strength to a reference Portland concrete. However, 100% aggregate replacement provided extremely low flexural strength potential, showing that wood aggregates cannot be used as a true aggregate replacement for strength purposes. It was hypothesized that these wood-infused samples would excel in road-noise control applications through their use as a roadway material. This is because of the improved flexural strength, as well as the acoustic absorption properties found with fibrous

materials [22]. Similarly, regarding flexural strength, a study by He et al. found that by utilizing waste timber formwork as a fibre aggregate in concrete, flexural strength could be increased [26]. Specifically, by breaking down the wood (Masson's pine) into 5 mm long fibres and adding it to a magnesium oxychloride concrete mix under varying proportions, flexural strength was found to reach a peak value of 22.5 MPa. This peak value was reached when utilizing a composition consisting of 30% incinerated sewage sludge ash (ISSA) by powder weight and 15% wood fibres by powder weight. Even without the use of concrete powder replacements, like ISSA, and only utilizing the wood fibres and magnesium oxychloride concrete mix, peak flexural strength was found to be 18.75 MPa when 25% of the powder weight was wood fibres. These values exceed typical industry standards for the flexural strength of concrete, revealing the potential of using wood fibres in concrete. It is worth noting that the other additives used in concrete also have great influence on the mechanical properties. For example, the use of magnesium oxychloride concrete was important in this study, as this admixture assisted in bonding the wood-fibres to the concrete during the hydration and curing processes [29].

Conflictingly, a study by Li et al. utilized wood aggregates that ultimately had a poor effect on the flexural strength [26]. Experiments found that the use of waste spruce tree shavings ranging in size from 0 to 10 mm in diameter in lightweight concrete provided flexural strength measurements at an average of 2.5 MPa [26]. These values are significantly lower than the values found in other studies when compared to other lightweight concrete flexural strength values [30]. It is worth noting that this concrete is categorized as lightweight concrete and differs in composition from those in the olive wood waste study [22]. However, this data still displays that simply adding wooding fibres to concrete will not on its own greatly improve flexural strength. A point worth considering is that this study was not looking to maximize wood-infused concrete's flexural properties, but

rather, was trying to develop a model that could predict structural properties. Samples of concrete using 0 to 10 mm wood shavings as coarse aggregate replacements at 43% specific mass had a flexural strength to compressive strength ratio of 47%. Values for compressive strength in this test were found to be about 5.3 MPa [26]. This is extremely low compared to Portland cement, which boasts compressive strengths between 20 and 40 MPa [31]. This demonstrates that wood infused concrete may be useful for flexural applications, but may not be viable for structural compressive loads.

2.3 Acoustic Properties of Wood

While the primary focus of this paper is on the acoustic performance of wood fibers in concretes, there are not a great number of resources that address this specific topic. Therefore, the acoustic properties of related wood-based materials will be examined to both improve the understanding of both concrete and wood in acoustic absorption and provide a basis of how other fiber-infused materials perform when absorbing sound. Nonetheless, how the varying properties of wood and the method in which they are oriented affect acoustic absorption are considered.

Many fibrous materials can be utilized to bolster the acoustic properties of varying spaces. The amount of energy absorbed by these materials is directly related to the size of the aggregate used to build the damper (amongst other factors). While numbers can vary, for the purposes of this section of the report, two aggregate classifications are defined: fine and coarse. Fine aggregates measure 9.5 mm thick or less and are used to make up the bulk of a concrete's composition and fill the void spaces of the final product. On the other hand, coarse aggregates measure between 9.5 mm and 38.1 mm [32]. These size ranges are based on the aggregate size sorting of the Portland Cement Association [32]. Used in acoustic absorption, both provide varying degrees of acoustic properties. Boubel et al. found that to

obtain the highest acoustic absorption coefficient possible using beechwood and redwood sawdust and chip aggregates (fine and coarse), 0.315 to 0.63 mm (PS2 – defined by the authors) and 1.25 to 2.5 mm (PS4 – defined by the authors) aggregate sizes should be used [17]. Fibres between 0.63 mm and 1.25 mm (PS3 – defined by the authors) had a higher peak acoustic absorption than PS2 but were lower for most frequencies. Specifically, PS3 aggregates boasted a peak acoustic absorption value of 1.0 at 700 Hz. Tested between 0 and 1000 Hz, the acoustic absorption of PS2 remained higher than all other aggregate sizes throughout the entire frequency range, except for PS3 and PS4 peaks. While PS4 boasted the second highest peak acoustic absorption value of 0.95 at 700 Hz, it did not maintain this high acoustic absorption across all frequency bands, like PS2. Furthermore, it was found that the larger the aggregate size, the worse the acoustic absorption properties of the sample became due to drastic increase in large voids and pores in the material. When below the aggregate range of 0.315 to 0.63 mm, it was found that acoustic absorption decreased due to low surface porosity and few internal voids. This in turn caused the material to reflect high amounts of acoustic energy and revealed that there is an aggregate size in which peak acoustic absorption values can be obtained [17]. While the specific values for this peak acoustic absorption in relation to aggregate size is different for different fibre types, this phenomenon is seen in other materials as well, including in concretes that use non-biofibres. Unfortunately, few papers delve into large ranges of aggregates sizes to provide complete confirmation of this.

Beyond just the fibers themselves, the method in which they are oriented will impact sound absorption as well. When assembling aggregates to form an acoustic absorber, the orientation of fibres impacts the acoustic absorption potential of a sample. However, fibre orientation can only be considered for coarse aggregates, because fine aggregates are typically too small to orient in any practical specific direction (e.g. sawdust sized fibres).

Tudor et al. studied the impact of fibre orientation and size using larch wood bark as an absorber [33]. The smallest fibre length examined was 4 mm and the largest length was 30 mm in samples measuring 30 mm and 100 mm in diameter, and 30 mm and 60 mm in thickness. 100 mm diameter samples were used in low frequency NRC measurements (20 to 1600 Hz) and 30 mm diameter samples were used in high frequency NRC measurements (1600 to 6400 Hz). The two orientations considered when examining aggregate orientation were parallel and perpendicular. In this case, parallel refers to aggregates that are perpendicular to the trajectory direction of the incident sound wave, whereas perpendicular refers to the case where fibres are parallel to the incident soundwave's trajectory direction. Considering frequency values between 0 and 6050 Hz, acoustic absorption values were found to vary. Acoustic absorption coefficients for 30 mm-thick samples containing fibres 4 to 11 mm long and of similar densities were found to have similar acoustic absorption coefficient peaks between parallel and perpendicular fibres. In this case, however, the peak absorption for perpendicular fibres is found to be 0.85 at 4700 Hz and for parallel fibres is found to be 0.92 at 2150 Hz. Longer fibres, 10 to 30 mm in 30 mm-thick samples had higher acoustic absorption peaks (up to almost 1.0) that were maintained over a smaller frequency range. Finally, when samples using these fibre lengths had their thicknesses extended to 60 mm, acoustic absorption trends altered again. When increasing thickness, the peak acoustic absorption of samples with larger aggregates decreased. However, acoustic absorption across the overall frequency range increased. Acoustic absorption values became more consistent, and fell within a smaller range, as opposed to one large peak. Increasing the thickness of the fine aggregate samples also created more consistent acoustic absorption values. However, the denser samples steeply dropped in acoustic absorption, while less dense samples increased in acoustic absorption. In 60 mm samples, the density was found to have a significantly larger effect on acoustic absorption than any other factor. Parallel

fibres measuring between 4 and 11 mm and having a density of 688 kg/m^3 had an average acoustic absorption level of 0.35, whereas a density of 362 kg/m^3 had an average acoustic absorption of 0.70. A similar, but less significant difference can be found amongst 60 mm-thick samples with fibres in the range of 10 to 30 mm. While some conclusions can be drawn from the results of these samples, fibre orientation did not appear to be a driving factor in the effectiveness of acoustic absorption. These results showed that absorption values vary widely based on the thickness of the aggregate and the density of the sample (how much aggregate is used). Other factors, such as percent resin used, and frequency band being examined also played a role in determining the effectiveness of the acoustic absorber [33]. It is worth noting that while fibres can be oriented for good reason, the most common orientation used in practice (due to simplicity of the manufacturing process), when considering fibre-infused concretes, is random.

Finally, the amount of potential acoustic energy absorbed by a sample of fibrous material is related to the density of the sample. Since aggregate size is directly related to the porosity and void content of the final product, a sample of higher density than another of equal volume will have a lower void content and porosity. This, in turn, increases the reflective properties of the sample. The same logic can be used when looking at low density samples, in which the void spaces are too large, facilitating the transmission of sound through the sample. Investigations regarding the acoustic absorption of spruce and larch trees by Tudor et al. found that spruce composite panels with densities of less than 500 kg/m^3 were able to attenuate up to 60% more sound when compared to densified larch boards of 700 kg/m^3 [34]. Specifically, fine and coarse spruce, being less dense than larch woods, had peak absorption coefficients of 0.55 and 0.60, respectively, whereas coarse larch peaked at approximately 0.35 in the frequency range of 500 to 4000 Hz. This was found to be due to the observed low-density particleboard (pine) having higher porosity than that of

the comparable medium-density particleboard (larch). When increasing the thickness of the higher density larch board, an increase of 0.05 in acoustic absorption was recorded, pushing the peak value to 0.40 [34]. This increase in acoustic absorption can be attributed to the 'law of mass' [35].

2.4 Acoustic Properties of Concrete

Next, the acoustic absorption of concrete and other granular, aggregate based materials (asphalt, cement, etc.) are examined. The material properties of concrete are significantly different than those of wood and other biomaterials, but many of the properties that relate to the acoustic absorption potential of concrete are the same. Particularly important properties include aggregate sizes within the concrete, the porosity of the material, and the density. These properties stem directly from the mixing composition, the main determinate in the final product's properties. This considers the water content, fine and large aggregate content, and concrete and plasticizer content. Beyond these more general material properties, acoustic absorption is also directly related to several specific material properties that are used directly to find the numerical estimate for acoustic absorption. These include surface airflow resistivity, open porosity (porosity at the surface), tortuosity, and standard deviation of pore size, however these will be examined more in depth later in this report.

Concretes, by nature, have extremely high reflection coefficients that work against absorption. Values for acoustic absorption tend to trend around 0.02, or in other words, reflect 98% of acoustic energy. However, the reflective nature of concrete does trend downward as specific density and mass are increased. This trend has less to do with the material itself and more to do with the fact that acoustic transmission loss increases as there is more material to pass through. This idea is described in the "law of mass" that states that by increasing the mass of a sample, the acoustic transmission loss will increase,

as does the absorption (marginally), as there is more opportunity for absorption as the sound travels through the material [35]. Due to the relation between acoustic absorption, open porosity, and total porosity, potential methods for improving the acoustic absorption of basic concrete (no specialized aggregate substitute) include using foaming agents or water content to obtain increased void ratios. Foaming agents and calculated void ratios were found to increase acoustic absorption significantly at low frequency bands, up to 0.9. Unfortunately, at higher frequency bands, the impact on acoustic absorption is low, only raising absorption by about 0.1 to 0.3 [6].

Beyond concrete density, aggregates are an integral aspect of the composition. Fine and coarse aggregates can be detrimental to the structural integrity of concrete samples. Aggregates also play an important role in the acoustic viability of concretes. Labeled as "porous concrete", fine aggregates are reduced or removed to increase void spaces within the sample, as there is less fine material to fill in these gaps. An increase in void space, or pores, traps acoustic energy and converts it to heat, reducing sound levels as the energy dissipates. A study by Kim and Lee used aggregates, crushed gravel, measuring 8 to 13 mm and 13 to 19 mm at varying paste/aggregate ratios and air entrainment (AE) admixtures/cement ratios in concrete samples to achieve varying cement paste flow rates [3]. Interestingly, smaller coarse aggregates boasted better acoustic absorption properties than larger aggregates, demonstrating that while coarse aggregates may bolster porosity, the acoustic absorption relationship is not so simple. 8 to 13 mm aggregate samples without AE admixtures boasted acoustic absorption rates up to 1.0 at 900 Hz, while 13 to 19 mm aggregate samples peaked at 0.92 at 1100 Hz. Similarly, lightweight aggregates of expanded shale measuring between 4 and 8 mm (the smallest aggregate size of this kind) peaked at 1.0 at 1000 Hz, while peak values decreased as aggregates got larger. The largest lightweight aggregate size used was 12 to 19 mm, which reached a maximum peak acoustic

absorption of 0.82 at 850 Hz. It is also worth noting that the well known relationship between sample thickness and acoustic absorption was also observed (i.e. samples measuring 100 mm in thickness were found to be more absorptive over a larger frequency range than samples of the same composition measuring 70 or 50 mm) [3].

Similar results were found by Pereira et al. using lightweight aggregates, expanded clay, in samples of porous concrete [36]. In this case, varying material properties were examined as they relate to acoustic properties. Specifically, grain size, thickness, and water/aggregate/cement ratios were examined. The aggregate grain sizes examined ranged from 0 to 2, 2 to 4, and 3 to 8 mm (all of which are considered fine). After running impedance tube experiments on their samples, it was found that samples using finer aggregate sizes, regardless of thickness, outperformed their larger aggregate counterparts in acoustic absorption. All samples that used aggregates measuring between 0 and 2 mm were found to have acoustic absorption values greater than 0.95, while samples using aggregates measuring between 2 and 4 mm brought down acoustic absorption values by at least 0.05. This is noteworthy, as this shows that despite coarse aggregates being effective in increasing porosity of the concrete sample, fine aggregates can still be used exclusively to bolster acoustic absorption to great effect. Thicker samples were found to have the greatest acoustic absorption values (close to 1.0), with peaks occurring at lower frequency ranges (550 to 700 Hz) than thinner samples (up to 1500 Hz at 40 mm thick). Furthermore, it was found that by increasing the amount of cement content within a composition of concrete, acoustic absorption values were found to be lower than those of the same aggregate size and thickness. Samples with more concrete in their composition also boasted higher densities, which in turn reduced void content and lowered acoustic absorption properties [36].

Aggregates are not the only significant factor influencing concrete porosity, the amount of water in a concrete's composition impacts the number of pores and void spaces. The

water content is quantified by its water-to-cement (w/c) ratio, a ratio comparing the amount of water by weight to the amount of cement by weight. Typically, the more water that is added during the concrete mixing process, the more it results in a more porous sample, as pore structure is determined during hydration. Hydration is the phenomenon during the concrete curing process in which the cement and water chemically react with one another. This relationship has been shown by Kim et al in their study regarding the w/c ratio on porosity [25]. It was found that when keeping concrete and sand quantities constant and increasing the w/c ratio from 0.45 to 0.6, porosity increased by 150% after 91 days of curing. If increasing the water content by merely 33% can impact porosity so drastically, the acoustic properties with respect to porosity will also naturally be affected. This provides an easy way to increase the acoustic absorption potential with little input (simply adding more water). However, it should be noted that while porosity was increased by 150%, compressive strength was also reduced by 24.4% [25]. While porosity is beneficial in sound absorption, excessive pores and void spaces is detrimental to compressive strength. This is observed through Abram's Law, a general mathematical relation used in predicting concrete's compressive strength via the w/c ratio. Having a higher w/c ratio results in a lower compressive strength, as more void spaces result in less cross-sectional area, and therefore, higher stress concentrations. Due to fewer structural applications of sound absorbers, this decrease in strength may not be particularly detrimental to most acoustic applications.

2.5 Acoustic Properties of Fiber-Infused Concretes

The final group of materials worth acknowledging are those of other fibrous concretes. Even more informative than general fibrous concretes are those using bio-fibers. These concrete compositions may have similar properties and can be used to provide a more rounded understanding of the wood-infused concretes developed in section 4.1. There are also few studies specifically related to the acoustic performance of wood-infused concretes. Unfortunately, due to the complexities of the properties of concrete, any change in the composition between studies causes the properties of the final product to be completely different. While there is some data on how wood-infused concretes perform acoustically, there are a multitude of materials that can be used to enhance acoustic absorption and they can all provide insight on how potential wood-concrete compositions can perform due to their similar aggregate sizes and fibrous natures. Of the studies examined, acoustic absorption values were primarily found using impedance tube testing before being compiled and compared.

In an innovative concrete review paper, Fediuk et al. compiled the acoustic absorptive and insulative properties of a wide variety of hybrid concretes [6]. While wood-infused concretes were not covered, the study did reveal the effects of fibrous aggregates in concretes amidst other aggregate types. NRC values of aggregate concretes were compared to basic building materials (not implemented into concrete), and it was found that fibrous materials have significantly higher NRC values than those that are non-fibrous. Heavy textiles (carpets), cork, fibreglass, and sprayed cellulose fibres boast NRC values ranging between 0.55 and 0.75, whereas base concretes measure 0.2 or below (except for smooth

unpainted concrete that peaks at ~0.3). It is worth noting that different types of wood (hardwood, softwood), in the form of planks, were included and do not have particularly high NRC values (less than 0.3). Furthermore, it was found, based on data compiled for varying concrete-aggregate compositions, that many biomaterials boast comparatively high acoustic absorption values. Particularly, coconut fibre concretes had peak acoustic absorption values between of 0.42 and 0.8 in the range of 1250 and 3200 Hz. Other materials that were found to have great absorption values were oyster shell waste, peaking between 0.43 and 0.53 at 1000 to 1800 Hz, crumb rubber concretes, peaking between 0.30 and 0.70 at 400 to 2500 Hz, polymer concretes, peaking between 0.9 and 1.0 at 64 to 1600 Hz, and some forms of recycled concrete aggregates, peaking between 0.01 and 1.0 at 1500 to 2000 Hz. A more in-depth summary of specific concrete mixes was also compiled, comparing NRC values, density, and acoustic absorption at 250, 500, 1000, and 2000 Hz. Materials found to boast the highest NRC values include varying forms of hemp concrete ranging between 0.40 and 0.59, foam glass concrete with NRC values of 0.56 (however non-foam glass concrete had a peak acoustic absorption value of 0.37), and lightweight aggregate mortar with 80% bottom ash powder had an NRC value of 0.61. While not particularly consistent, concrete with lower densities were generally found to boast greater NRC values. Despite this trend, lightweight aggregate mortar with 80% bottom ash powder had the highest NRC value, while also having a density of 1470 kg/m^3, relatively high compared to the other materials. Finally, comparing the acoustic absorption at previously stated frequencies, many materials that used coarser aggregates had less homogenous values across frequencies. For example, comparing hemp concrete using 30% ground granulated blast furnace slag and hemp concrete using hemp shiv at a 1:2 ratio, values of acoustic absorption were found to be 0.49 and 0.31 at 500 Hz, 0.42 and 0.81 at 1000 Hz, and 0.44 and 0.48 at 2000 Hz, respectively. Of interest is that light weight aggregate concrete

with expanded shale and using a 1% air entraining agent was found to have acoustic absorption of 1.0 at 1000 Hz. While this value is very good, the acoustic absorption is found to be poor at 250 and 500 Hz, with values of 0.08 and 0.24, respectively, and a moderate NRC value of 0.44 [6].

An introspective comparison on the impact of wood fibres on the acoustic properties of concrete was performed by Hussein et al., in which they compared waste-wood concrete (specifically sawdust) with concretes infused with other waste aggregate products (glass and plastic) [37]. Using lightweight mortars, fine aggregates (sand) were replaced at varying weight percentages (20%, 40%, and 60%). The amount of cement mix and water remained constant. Unfortunately, the species of tree used in the study is not disclosed in the report itself. This report examined the acoustic insulation of the samples as opposed to the acoustic absorption values. Through testing, it was found that sawdust infused concrete provided the greatest acoustic insulation at all replacement percentiles, and that the acoustic absorption was directly related to the quantity of sawdust added. The peak insulation levels were found to be 99% for concretes with fine aggregates replaced with 60% sawdust by weight. This reveals that wood-fibres in the form of sawdust infused concrete bolsters the insulation of concrete substantially. It is worth noting that sawdust was also found to have very low thermal conductivity, which continued to lower as more aggregate replacement was introduced [37].

Like wood aggregates, miscanthus, a type of grass, can be used to bolster the acoustic properties of concrete. Chen et al. performed an in-depth study on the mechanical properties of bio-based lightweight concretes containing miscanthus fibres [7]. Miscanthus, a fibrous plant similar to hemp or straw, is a widely available biomaterial that has the potential to offer acoustic damping properties. Within the study, miscanthus fibres measuring 2 to 4 mm wide and 2 to 20 mm long were used in amounts of 10%, 20%, and

30% replacement by volume of the concrete binder. In this concrete study, rather than replacing fine aggregates with biomaterials, the actual bonding agent was replaced. In this range, miscanthus fibres have very porous internal structures that are beneficial to absorption of acoustic energy, whereas smaller fibres were found to have closed pores. Samples made from the fibres measured 40 mm in diameter and were tested in an impedance tube. By introducing the porous fibres, the cement's porosity increased, while its density decreased, both of which bolster acoustic absorption. Acoustic absorption was measured in the frequency range of 200 to 2500 Hz, where miscanthus fibres were found to bolster values in all binder replacement percentages (10%, 20%, and 30%). The reference Portland cement had a peak acoustic absorption value at 750 Hz, with an acoustic absorption value of 0.27. As finer fibres were added, the peak acoustic absorption was pushed to higher frequencies. With 10% binder replacement by volume, acoustic absorption was raised to 0.5 at 715 Hz. At 20%, the peak was 0.65 at 1100 Hz, and at 30%, the peak was 0.55 at 1300 Hz. Values dropped back down quickly once reaching their peak. With the exception of 20% replacement, all acoustic absorption values plateaued at a range greater than that of the reference plateau [7].

Another form of biofibers is that of palm kernel shells. Khankhaje et al. utilized biomaterials native to Malaysia, including oil palm kernel shells (plant material) and cockleshells (mollusk shells) in porous concrete [9]. Due to its limited structural integrity, this form of concrete was restricted to low traffic roadways, where it was found to be useful in its ability to reduce traffic noise. Portland cement with coarse limestone aggregates measuring 6.3 mm was used as a control sample when comparing samples containing cockleshells (CS) and kernel shells (KS) as replacement to the limestone aggregates. Varying amounts of aggregate replacements were used in sizes ranging between 4.75 mm and 6.30 mm. CS was shown to have a crystalline microstructure, whereas KS was made of

porous fibres, each having significantly different acoustic absorption properties. Up to frequencies of approximately 1000 Hz, acoustic absorption was found to be virtually the same for each. Beyond this, however, 25% aggregate replacement by weight of 6.30 mm KS (KPC1 – defined by the authors) and 50% aggregate replacement by weight of 4.75 mm (KPC2 – defined by the authors) drastically increased acoustic absorption values, reaching peaks between 0.8 and 0.9 in the frequency range of 1500 to 2000 Hz. CS gradually increased in acoustic absorption until approximately 2000 Hz, where it peaked at an acoustic absorption value of 0.5. The reference concrete followed a similar trend, peaking around 2700 Hz at an acoustic absorption value of 0.45. All samples had acoustic absorption trend downwards after peaking until plateauing at approximately 4000 Hz, where the acoustic absorption of KS is found to be 0.17, 0.2 for CS, and 0.22 for the reference concrete. Data past 4500 Hz was not provided. Finally, it was suggested that by replacing the finer aggregates of concrete with KS or CS, the concrete would have the flexural strength to support light volume traffic [9].

2.6 Acoustic Modelling

The primary goal of this report is to develop a model that can estimate the acoustic absorption of wood-infused concrete, an analytical model that does not require experimental data. The information covered thus far has all been provided through experimentation and documentation of varying material compositions providing insight on the potential for bolstering the acoustic properties of concrete, and ultimately, be used as an absorber. Unfortunately, due to the complex nature of concrete and variance of material properties based on composition, not only is it very difficult to model the acoustic properties of concrete, but there is limited information on how to do so. The most explored models for estimating acoustic properties will be explored in this section, with the exception of the

Johnson-Champoux-Allard-Lafarge (JCAL) model. The JCAL model is an analytical model that utilizes the complex viscous and thermal properties of a porous material to predict acoustic absorption. However, as a core element of the hybrid model developed in this report, it will be covered on its own in Chapter 3. The models mentioned in this section will be briefly compared to provide a basis for understanding the limited state of the current literature in this field.

Pereira et al. investigate the Horoshenkov and Swift model, which calculates the acoustic absorption of a material by solving the dynamic density and the bulk modulus (compressibility) using material properties, air-flow resistivity, open porosity, tortuosity, and the standard deviation of pore size [36]. These attributes, used in tandem with the properties of air (sound travel medium), and the sound wave, can be used to estimate the acoustic absorption of the material. The study found that this model, when used to approximate the acoustic absorption of concretes, was accurate at frequency ranges above 400 Hz (values recorded up to 1600 Hz) [36]. This model is similar to the Johnson-Champoux-Allard-Lafarge (JCAL) model in that it uses the same parameters to estimate acoustic absorption [13].

Another model that is particularly useful in representing acoustic absorption when studying granular materials is the Johnson-Zwikker-Kosten (JZK) model. This model is a hybrid of the Johnson model, a precursor to the JCAL model, and the Zwikker-Kosten (ZK) model. The ZK model is an early representation of fluids in a porous material and is mathematically similar to the JCAL model. The ZK model is different from the JCAL model in that it defines density as rigid rather than dynamic and viscous properties are defined using the Womersly number. Conversely, the JCAL model utilizes the characteristic pore lengths (thermal and visco-inertial) when defining the viscous (and thermal properties). The Womersly number relates pore geometry to the viscous penetration depth, a measure

that provides an understanding of the viscous boundary layer thickness [38], [39]. The Johnson model, developed by Johnson et al., is a model developed to derive analytical properties of a porous isotropic medium [11]. This model is the basis for the JCAL and Johnson-Champoux-Allard (JCA) models and is used to solve for the complex viscous properties, which in turn can be used to define the dynamic density by using the viscous characteristics of the material [11]. The JZK model referenced above utilizes the viscous properties to define granular material. However, it ignores the thermal aspects of the material. Further, details on the relations used to derive this method were not provided [38].

The creation of an analytical model that can be used to predict acoustic absorption of wood-infused concretes is beneficial to the development of sustainably sourced concrete acoustic absorbers. While creating samples of wood-infused concrete and measuring the acoustic absorption of the samples is not difficult, the process to do so is time consuming and requires access to a number of resources. Furthermore, should a desired composition not be as acoustically absorptive as expected, the fabrication and testing time is wasted. By developing a model to estimate the acoustic absorption coefficient of fiber-infused concrete compositions via material properties, the experimental trial-and-error process could be bypassed, greatly improving the efficiency of the entire process, and providing a simplified design process by which ideal concrete compositions can be determined. This application is what the model developed in this thesis hopes to achieve.

As seen in this chapter, there is a great deal of research that can be applied to bolstering the acoustic properties of concrete through the introduction of wood aggregates. Regarding the use of concrete, porosity plays a key part in increasing the absorption coefficient. Through the use of concrete foaming additives to bolster porosity in concrete samples, Fediuk et al. found that when compared to basic concrete, acoustic absorption

increased by up to 0.9 at low frequency bands and 0.2 at higher frequency bands [6]. Further, concrete absorption is impacted through aggregate selection and water-to-concrete volumetric ratios in the concrete composition. Research by Kim and Lee indicated that as aggregate size decreased, absorption generally increased where the largest aggregates tested, 12 to 19 mm, boasted an absorption of 0.82 while the smallest aggregates, 4 to 8 mm, boasted an absorption of 1 [3]. Through the understanding that porosity impacts absorption, research revealing that w/c ratio impacts porosity therefore reveals w/c ratio control in concrete manufacturing can be utilized to bolster acoustic absorption as well. Kim et al. found that by simply increasing the w/c ratio by 15% increased porosity by up to 150% [25]. Of course this is also based on the concrete composition, but the w/c ratio impact shows great potential in bolstering acoustic absorption [25]. Similar to concrete, research regarding the absorption of varying woods has been found to be related to fiber size. Research indicates that when selecting fiber size however, there is an ideal size to maximize absorption as found by Boubel [17]. When comparing samples of varying beechwood and redwood samples, it was found that fibers from 0.315 to 0.63 mm and 1.25 to 2.5 mm boasted the max absorption while other sizes smaller and larger decreased acoustic performance [17]. While understanding how these materials interact to predict acoustic absorption, there is research both examining actual wood-infused and other fiber-infused concretes. For example, Fediuk et al. found that the NRC value of hemp concretes can boast absorption values up to 0.59 and other non-bio fibers like foam glass up to 0.61 [6]. The amount of absorption is also related to sample density as seen through comparing hemp concrete using 30% ground granulated blast furnace slag and hemp concrete using hemp shiv at a 1:2 ratio where absorption reached 0.42 and 0.89 at 1000 Hz respectively [6]. While absorption values are higher in fibrous concretes, an issue arises in that concrete is naturally reflective of soundwaves reflecting up to 99% of acoustic energy [6]. Further,

beyond acoustic properties, wood-fiber infusion has been found to drastically decrease compressive strength to 5.3 MPa from typical concrete compressive strengths of 20 to 40 MPa [26], [31]. However, wood-fibers have also been found to bolster flexural strength [22]. This research that has been done investigating the acoustic and material properties of wood-infused concretes is significant in the development of acoustic absorption models. The model of particular interest in this paper that this information will be put towards is a hybrid of the Johnson-Champeux-Allard-Lafarge model and Delany-Bazley model [13], [15].

Chapter 3

Acoustic Absorption Model

3.1 JCAL-DBz Model Description

While some models have been shown to provide some potential in estimating the acoustic properties of concretes, there is limited information on the topic. One model that has been used for predicting the acoustic absorption of fibrous and porous materials is the Johnson-Champoux-Allard-Lafarge (JCAL) model [11]–[14]. The Delany-Bazley (DBz) model has also been used in predicting the complex acoustic properties of fibrous materials [15]. Wood-infused concretes can be considered both fibrous, due to the nature of wood fibers, and porous, due to the void spaces created during the concrete's hydration process. Fibrous and porous materials excel at absorbing sound, as sound waves, when interacting with fibers and/or pores, become trapped and dissipate into thermal energy [8], [9]. Therefore, by utilizing the DBz and JCAL models in tandem, the acoustic absorption values of wood-infused concretes can be estimated.

Both the DBz and JCAL models have been used previously to estimate the acoustic properties of more traditional porous, fibrous materials (textiles and wools for example) [13], [15], [40]. Acoustic properties are estimated by calculating varying complex thermal and viscous properties of the material. While concrete is not a traditional porous or fibrous material, studies have shown that there is potential for these models to be utilized in

estimating the complex properties of denser, more reflective composites, such as concretes and asphalts. In the literature examined, the JCAL model has been used to predict the sound absorption of asphalt, as well as to predict the complex viscous properties of some hemp concretes. On the other hand, the DBz model has been used to predict the airflow resistivity of concrete-like porous, dense materials [40]–[42]. Further, the tandem use of the DBz and JCAL models have been shown to provide successful estimates of the acoustic absorption of complex textiles, providing a basis for the model's accuracy [43]. Under the pretext that these models, when utilized together, can provide accurate estimates of the complex thermal and viscous properties of a fibrous, porous concrete, a model can be developed for wood-infused concretes. The details of how acoustic absorption is predicted by the hybrid model will be covered in this chapter. MATLab code for the model is provided in Appendix A.

3.2 Model Parameters

The hybrid DBz and JCAL model utilized in this study is used to estimate the acoustic properties of wood-infused concrete compositions. However, to do so, a multitude of non-acoustic properties related to the material and the medium in which the sound will be travelling must be defined. Once defined, these variables can be used to estimate acoustic absorption. The air properties, viscous material properties, and thermal material properties must all be considered.

3.2.1 Air Properties

The JCAL and DBz models both consider the properties of the medium in which the sound is travelling, in this case air. These properties are non-acoustic in nature, as they are independent of the material. Important properties of air are provided in Table 3-1.

The air properties that are required include the air temperature (T) [K], air pressure (P_0) [Pa], the universal gas constant for air (R) [J/kgK], and the density of air (ρ_0) [kg/m^3], which is calculated using the other properties. These properties are all assumed to be constant for the environment in which the testing process is being performed. The universal gas constant is assumed to be ideal, while pressure and temperature values are equal to those measured during impedance tube testing. Using the calculated gas constant relationship, the air density can be solved using the gas constant equation:

$$\rho_0 = \frac{P_0 T}{R} \tag{1}$$

The next two values that must be considered are the speed of sound in air (c_0) [m/s], and the bulk modulus of air (K_a) [Pa]. The equation utilized for calculating the speed of sound in air is provided by ASTM E1050-19, the ASTM standard for acoustic absorption used for impedance tube testing, and scales with temperature [16]. The bulk modulus for fluids is calculated using the simple Netwon-Laplace relation between the bulk modulus, density, and the speed of sound [44].

$$c_0 = 20.047\sqrt{T} \tag{2}$$

$$K_a = {c_0}^2 \rho_0 \tag{3}$$

The final properties of air are more elaborate in their relation to temperature. The viscosity of air (μ) [Ns/m^2] can be calculated using equation (4), and is valid in the range of 100K – 600K for both ideal and non-ideal gas scenarios. This is because air is treated as both ideal and non-ideal increases in viscosity monotonically as temperature increases [45].

$$\mu = 7.72488 \cdot 10^{-8} T - 5.95238 \cdot 10^{-11} T^2 + 2.71368 \cdot 10^{-14} T^3 \tag{4}$$

Like viscosity, the specific heat at constant pressure (C_p) [J/kgK] is temperature dependent. Once calculated, the simple relation between the ideal gas constant and specific

heat at constant pressure can be used to solve for the specific heat at constant volume (C_V) [J/kgK]. The equation for C_P is specific to air and is accurate for the temperature range of 260K – 610K with slight alterations required if exceeding this range. An error of 0.2% was found between theoretical and empirical values showing this equation is accurate for both ideal and real representations of air [46]. The specific heat ratio (γ) of air is also required for defining the properties of air and can be easily calculated once C_p and C_V are known.

$$C_P = 4168.8(0.249679 - 7.55179 \cdot 10^{-5}T + 1.69194 \cdot 10^{-7}T^2 - 6.46128 \cdot 10^{-11}T^3) \quad \textbf{(5)}$$

$$C_V = C_P - R \quad \textbf{(6)}$$

$$\gamma = {}^{C_P}/_{C_V} \quad \textbf{(7)}$$

The final property of air that will be defined through temperature dependence is the thermal conductivity of air (κ) [W/mK]. Thermal conductivity is a measure of how well a medium can conduct heat or permit heat transfer. The formula used for the thermal conductivity of air has been proven to be accurate through semi-empirical data based on the molecular makeup of air and kinetic theory. Thermal conductivity is defined in equation (8) [47].

$$\kappa = 2.624e^{-2}\left(\frac{\left(\frac{T}{300}\right)^{\frac{3}{2}}\left(300 + 245.4e^{-\frac{27.6}{30}}\right)}{T + 245.4e^{-\frac{27.6}{T}}}\right) \quad \textbf{(8)}$$

The properties of thermal conductivity, viscosity, and specific heat at constant pressure of air can then be related to one another using the dimensionless Prandtl number (Pr). The Prandtl number will be needed in solving the thermal characteristic length.

$$Pr = \frac{\mu C_P}{\kappa} \quad \textbf{(9)}$$

Table 3-1: Properties of Air and Their Values Used in this Study

Air Property	Value
Temperature (K)	295.96
Pressure (Pa)	101650
Density (kg/m^3)	1.20
Universal Gas Constant (J/kgK)	287.03
Speed of Sound (m/s)	344.88
Isentropic Bulk Modulus (Pa)	$1.4232 \cdot 10^5$
Viscosity (Ns/m^2)	$1.8352 \cdot 10^{-5}$
Thermal Conductivity (W/mK)	0.026
Specific Heat at Constant Pressure (J/kgK)	$1.0025 \cdot 10^3$
Specific Heat at Constant Volume (J/kgK)	715.46
Specific Heat Ratio	1.40
Prandtl Number	0.71

3.2.2 Viscous Properties

The properties of air must be used in tandem with the material properties to calculate the acoustic properties of the material being analyzed. These material properties, for the DBz and JCAL models, can be divided into the viscous and thermal properties of the concrete. The viscous properties include the airflow resistivity, tortuosity, and viscous characteristic length.

Airflow resistivity (σ) [Ns/m^4] is a parameter that describes the potential for airflow over a material. Tarnow describes airflow resistivity over fibers via equation (10) [48]. In calculating the airflow resistivity over fibers, the fiber orientation, fiber scattering, material

density, and air viscosity must all be considered. Airflow resistivity is calculated under the assumption that airflow is constant and that fibers are represented as parallel, cylindrical, and of equal diameter. Further, that fibers are randomly spaced from one another (without intersecting) and that airflow is perpendicular to the fibers [48]. Variations on these stipulations are also provided by Tarnow. However, the stipulations adequately represent the fiber infused concrete compositions used [48].

$$\sigma = \frac{4\pi\mu}{b^2\left(0.64\ln\left(\frac{1}{d}\right) - 0.737 + d\right)} \quad \textbf{(10)}$$

$$b = r\sqrt{\pi\rho_{fib}/\rho_{mat}} \quad \textbf{(11)}$$

$$d = \rho_{mat}/\rho_{fib} \quad \textbf{(12)}$$

where variable d is a ratio of the material to fiber densities, r is the fiber radius [m], and b [m] is defined to be an average of what is the square root of the area per fiber. To be more specific, b is an average area of the Voronoi cells that the material is subdivided into based on fiber placement to describe the flux across the material. However, this equation has been simplified to be scalar. This simplified version of the b variable is used to describe the homogeneity of the material surface. It is worth noting that the general application of the resistivity equations are for foams and more traditional fibrous materials (wools and textiles) [48].

Surface porosity (ϕ) is a property used to define the amount of void space along the surface of a material represented as a ratio between the volume of surface pore void space to the total volume of the piece. While not a viscous property, porosity is required in calculating the complex viscous and thermal properties used in estimating absorption. Specifically, as acoustic waves contact the surface of the material, the pores of the concrete trap acoustic energy causing it to dissipate, quantified as absorption. Therefore, being able

to quantify porosity is important. Unfortunately, porosity is an extremely difficult property to estimate due to the complexity of the chemical interactions of the concrete curing process. Therefore, for the purposes of this report, porosity of each composition will be measured directly to ensure more accurate model values. Below is the method for calculating porosity by measuring the sample surface void volume in relation to the material volume [49].

$$\phi = \left[1 - \frac{V_{sol}}{V_T}\right] \tag{13}$$

$$V_{sol} = V_T - V_{void} \tag{14}$$

In this case, V_{sol} represents the dry volume of the piece [m^3], or the volume of the solid material (including internal pores), V_{void} represents the volume of the surface voids [m^3], and V_T represents the total volume of the sample [m^3]. The experimental method for observing the volume of the void space is found through water saturation of the sample, based on the methods provided in ASTM C642-21 [50]. The specifics of the water saturation process performed are covered in detail in section 4.1. V_T is assumed to be equal to the dimensions of the concrete mold. After baking the sample, the dry mass V_{sol} can be weighed, then the sample is submerged in water. Once the water saturates the pores of the sample, the sample is weighed again and the difference between the dry weight is calculated to solve the amount of water trapped in the pores. Knowing the density of water, 997 kg/m^3, the volume of water can be calculated and is assumed to be equal to V_{void} [51]. Porosity can then be calculated. It is worth noting that during development of the DBz-JCAL hybrid model, to verify model accuracy, porosity values were input based on results of other concrete compositions by Glé et al. [40]. Values of porosity for the concrete samples can be found in Table 4-1.

The higher frequency limit of tortuosity and the viscous characteristic length requires solving for the dynamic density and dynamic bulk modulus. The dynamic bulk modulus and dynamic density are calculated using the DBz model and JCAL model, and therefore, will be discussed in further detail in the analytical calculations of acoustic absorption in section 3.3.

The higher frequency limit of tortuosity (referred to herein as simply tortuosity or α_∞) is a dimensionless parameter used to describe the complexity of the pore shape, or the ease in which fluid can flow through the pores. As the value of tortuosity increases beyond 1, pore shape complexity and difficulty for fluid flow increase. To describe tortuosity, both viscous properties of the material and air properties must be considered [52].

$$\alpha_\infty = \frac{1}{\rho_0}\left[\mathrm{Re}(\rho) - \sqrt{\mathrm{Im}(\rho)^2 - \left(\frac{\sigma\phi}{\omega}\right)^2}\right] \quad \textbf{(15)}$$

where ω represents the angular frequency and ρ represents the dynamic density of the material [kg/m^3]. The terms $\mathrm{Im}(\rho)$ and $\mathrm{Re}(\rho)$ refer to the imaginary and real aspects of the dynamic density, respectively [53]. Once the tortuosity value has been calculated, the viscous characteristic length can be calculated. Similarly, the viscous characteristic length (λ) [m] takes into consideration the viscous properties of the material, as well as the air properties [52].

$$\lambda = \alpha_\infty \sqrt{\frac{2\rho_0\mu}{\omega * \mathrm{Im}(\rho)\left(\rho_0\alpha_\infty - \mathrm{Re}(\rho)\right)}} \quad \textbf{(16)}$$

The viscous characteristic length is a measure of length that describes the average radius of the interconnections between pores, or in other words, the smallest radius of the pores [11]. It is worth noting that despite calculations for the complex properties of tortuosity and viscous characteristic length being frequency dependent, in reality they are

not and only the values found as frequency approaches infinity can be used as intrinsic material properties [53].

3.2.3 Thermal Properties

There are two thermal properties that must be considered when modelling acoustic absorption using the JCAL model: thermal permeability and thermal characteristic length.

Static thermal permeability (referred to as thermal permeability) (k_0') [m^2], is a term that relates the properties of air to both the thermal properties and porosity of the material. By doing so, the thermal energy exchanges that occurs between the material and the air as sound travels within the pores can be defined. Specifically, it is used within the JCAL model to describe thermal interactions occurring at lower frequencies [54].

$$k_0' = \phi \frac{\delta_t^2}{2} \left\{ -\mathrm{Re}\left[\left(\frac{1 - \frac{K_{dyn}}{K_a}}{1 - \gamma \frac{K_{dyn}}{K_a}} \right)^2 \right] \right\}^{-\frac{1}{2}} \tag{17}$$

$$\delta_t = \sqrt{\frac{2\mu}{\rho_0 \omega \mathrm{Pr}}} \tag{18}$$

where K_{dyn} is the dynamic bulk modulus [Pa] of the material, which like the dynamic density, is calculated using the JCAL and DBz models, and therefore, will be examined in depth by looking at the models themselves. δ_t is a variable that is used to simplify the lengthy nature of the thermal permeability formula.

The other thermal property required is the thermal characteristic length (λ') [m]. The thermal characteristic length, like the viscous characteristic length, is a measure of the average radius of the pores. The difference between the two is that, while the viscous characteristic length defines the interconnections between pores, the thermal characteristic length defines the radius of the pore at the widest point. In other words, it is the maximum radius of the pore [52].

$$\lambda' = \delta_t\sqrt{2}\left\{-\mathrm{Im}\left[\left(\frac{\phi - \frac{K_{dyn}}{K_a}}{\phi - \gamma\frac{K_{dyn}}{K_a}}\right)^2\right]\right\}^{-\frac{1}{2}} \quad \textbf{(19)}$$

3.3 Acoustic Absorption Calculation

Utilizing the properties of air and viscous and thermal properties, acoustic absorption can be estimated. The modelling process can be split into four stages, the first of which is to estimate the acoustic properties of the material being modelled utilizing the DBz model. These properties are characteristic acoustic impedance (Z_c) [Pa-s/m] and wave number (k, also referred to as propagation coefficient) [m^{-1}] [15]. The DBz model is useful as it was developed with the intent of simplifying the process of obtaining Z_c and k by only requiring σ and the properties of air (speed of sound and density). The DBz model is a power-law relation that is based on empirical data by Delany and Bazley [15]. The model used in this paper is a variation developed by Allard et al. that puts emphasis on the density of air [14]. It considers the material being modelled as homogenous in its fiber makeup, such that wave propagation is through plane-wave propagation in a single direction. The original model developed by Delany and Bazley to solve for Z_c and k takes in the same parameters. However, exponentials and coefficients vary [14], [15]. Despite the differences between the forms, when comparing equations during the development of the model used in this thesis, difference between the values observed were less than half of a percent. The Allard model is as follows, where f is the frequency [Hz] [14]:

$$Z_c(\omega) = \rho_0 c_0\left[1 + 0.0571\left(\frac{\rho_0 f}{\sigma}\right)^{-0.754} - j0.0870\left(\frac{\rho_0 f}{\sigma}\right)^{-0.732}\right] \quad \textbf{(20)}$$

$$k(\omega) = \frac{\omega}{c_0}\left[1 + 0.0978\left(\frac{\rho_0 f}{\sigma}\right)^{-0.700} - j0.1890\left(\frac{\rho_0 f}{\sigma}\right)^{-0.595}\right] \quad \textbf{(21)}$$

$$\omega = 2\pi f \tag{22}$$

Due to the nature of the power-law, the DBz model has a limited range in which the impedance and wave number values examined reflect the empirical data utilized by Delaney and Bazley [15]. The limit proposed is one based on the relation between frequency and airflow resistivity [15].

$$0.01 < \frac{f}{\sigma} < 1.00 \tag{23}$$

It is worth noting that this method was based on glass-fiber and rockwool porosity values that were close to unity. Further, at lower frequency values, it was noticed that materials show structural non-rigidity, rendering the simple normalization of the values impossible. Finally, this relation is said to work most accurately when

$$0.04 < \frac{f}{\sigma} < 1.00, \tag{24}$$

and fibers used are larger than $1.5 \cdot 10^{-6} m$ in diameter [15]. This frequency range limit is important to ensure estimates of the acoustic properties are accurate.

The second step in estimating the acoustic absorption is using a simple relation to predict the dynamic density and dynamic bulk modulus of the material. The dynamic density (ρ) [kg/m^3] is a semi-phenomenal property that describes the density of an acoustic porous material. The dynamic bulk modulus (K_{dyn}) [Pa] is a property that describes the compressibility of an acoustic porous material. The dynamic properties assume that the porous medium is motionless – that vibrations of the medium caused by the acoustic waves are negligeable, and therefore, can be treated as an equivalent fluid [53]. Both properties are frequency dependent, and therefore, a relation can be used to relate the dynamic density, dynamic bulk modulus, characteristic impedance, and wave number [55].

$$Z_c(\omega) = \sqrt{\rho(\omega) K_{dyn}(\omega)} \tag{25}$$

$$k(\omega) = \omega\sqrt{\frac{\rho(\omega)}{K_{dyn}(\omega)}} \tag{26}$$

Then, using simple substitution, the dynamic properties can be solved:

$$\rho(\omega) = \frac{k(\omega)Z_c(\omega)}{\omega} \tag{27}$$

$$K_{dyn}(\omega) = \frac{\omega Z_c(\omega)}{k(\omega)} \tag{28}$$

The third stage in estimating the acoustic absorption of a fibrous concrete is to utilize the JCAL model to refine the estimations of the dynamic density and dynamic bulk modulus made with the DBz model. The JCAL model uses both the viscous and thermal characteristics of the material to predict the dynamic properties [11], [13], [14]. The viscous properties used are airflow resistivity, tortuosity, and viscous characteristic length, and the thermal properties used are thermal characteristic length and thermal permeability. While the airflow resistivity value has already been solved, the remaining viscous and thermal values must be calculated using the dynamic property values found with the DBz model, as seen in equations (15), (16), (17), and (19). The JCAL equations for the dynamic properties are shown below [11], [13], [14].

$$\rho(\omega) = \frac{\alpha_\infty \rho_0}{\phi}\left[1 + \frac{\sigma\phi}{j\omega\rho_0\alpha_\infty}\sqrt{1 + j\frac{4\alpha_\infty^2\mu\rho_0\omega}{\sigma^2\lambda^2\phi^2}}\right] \tag{29}$$

$$K_{dyn}(\omega) = \frac{\gamma P_0/\phi}{\gamma - (\gamma-1)\left[1 - j\frac{\phi\kappa}{k_0' C_P\rho_0\omega}\sqrt{1 + j\frac{4k_0'^2 C_P\rho_0\omega}{\kappa\lambda'^2\phi^2}}\right]^{-1}} \tag{30}$$

The dynamic density is defined using the complex viscous properties, and the dynamic bulk modulus is defined using the complex thermal properties. Like the DBz model, the JCAL model is less accurate at lower frequencies, approaching 0 Hz, than at a higher frequency range, especially for the dynamic density. This is because the dynamic bulk

modulus utilizes the thermal permeability to specifically address the complex interactions between pores and air during low frequency thermal exchanges. The viscous properties do not have such a variable in this model. Further, despite the equations for the complex properties being frequency dependent, material properties are independent of frequency. When the viscous and thermal property values are calculated over frequency, they can only be assumed to be intrinsic material properties once having reached a state of relative stasis. This occurs as the frequency approaches infinity, where the model is exact. Therefore, the values of the complex thermal and viscous properties used in calculating the dynamic density and bulk modulus are those found as the frequency approaches infinity [13], [53], [54].

Once more accurate estimates of the dynamic properties have been made using the JCAL method, they are used to recalculate the characteristic impedance and wave number. This is done using the relationships between the acoustic and dynamic properties of equations (25) and (26).

The final step is to utilize the acoustic properties to estimate the acoustic absorption (α). The characteristic impedance and wave number are used to estimate the impedance on the surface of the material ($Z_{surface}$) [kg/m^{2}s], where h [m] represents the thickness of the sample [55].

$$Z_{surface} = -j\frac{Z_c}{\tan(kh)} \tag{31}$$

By defining the acoustic interaction between soundwaves and the surface of the sample, $Z_{surface}$, acoustic absorption can be solved. Specifically, the surface impedance is used to calculate the reflection factor ($\mathcal{R}$) of the sample, a dimensionless measure that expresses how acoustically reflective the surface of the material is. This is done using the difference between the sample surface impedance and impedance of air, the two media in which a

soundwave will interact when reflecting. The model assumes that the sample is rigidly backed, meaning no sound will be transmitted through the material, and therefore, all energy that is not reflected is absorbed [10], [52].

$$\alpha = 1 - \left|\frac{Z_{surface} - \rho_0 c_0}{Z_{surface} + \rho_0 c_0}\right|^2 \quad \textbf{(32)}$$

$$\alpha = 1 - |\mathcal{R}|^2 \quad \textbf{(33)}$$

While the mathematics involved are significantly different, the impedance tube testing method uses this same logic to calculate the acoustic absorption of the material. Results found using the DBz and JCAL models are examined in Chapter 5.

3.4 Model Limitations

While the models and methods used in the estimation of the acoustic absorption of the porous concrete are based on empirical and semi-empirical data from their respective sources, there are still sources of estimation inaccuracy. General errors stem from the varying methods in which the properties of the material (viscous, thermal, dynamic, and acoustic) are estimated, as well as the conditions assumed of the air. Therefore, the inaccuracy of each of these properties will be examined individually in the same order as they appeared in previous sections.

The properties of the air are relatively straight forward and are accepted as accurate due to the extensive work done in examining the properties of air. Conditions for air are, however, assumed to be ideal, which do not accurately reflect the properties of air under all conditions. This error is not expected to be substantial. For example, in the calculations of specific heat at constant pressure for air, a maximum error of 0.2% was seen by a number of authors when compared to measured values while utilizing the temperature dependent

equation (5). This error is deemed acceptable, and while negligible, is worth noting [45]–[47].

Most of the material properties estimated are found through manipulation of the JCAL equations. However, two viscous properties are found separately: surface air resistivity and porosity. The method used to estimate the surface airflow resistivity of the material was developed by Tarnow to estimate the airflow resistivity of fibrous materials [48]. While the concrete being utilized contains fibers in its composition, the wood-infused concrete is not as accurately depicted by Tarnow's model as other more traditional fibrous textiles and wools [48]. First, while Tarnow's model has the potential to account for randomly distributed fibers (relative to one another), the estimation used assumes that fibers are all equal in size, parallel to one another, and that air flow over the fibers is perpendicular to the fiber orientation [48]. Due to both the random nature of fiber orientation in the concrete during the manufacturing process and the inconsistent nature of woodchip, wood-shaving, and sawdust generation (size and shape), this assumption is not the most accurate depiction of the fibers in the concrete. Further, Tarnow's model does not utilize much information on the material between the fibers, it simply estimates the airflow resistivity of the fibers themselves in relation to one another (as would be expected in textiles and wools where air can penetrate freely between fibers), only using the overall material density as a reference to the concrete [48]. In other words, the airflow resistivity estimate does not consider how the concrete matrix between the fibers will impact airflow resistivity. How these estimations will impact the model values is not fully understood. However, values projected during analytical estimations provided somewhat accurate resistivity values when compared to other bio-fibrous concretes [40].

Porosity is an extremely complex material property that is particularly difficult to estimate easily or accurately. Porosity is dependent on both the contents of the material

(water/cement ratio, cement type, aggregates, additives) and the complexities of the curing process (how the hydration process proceeds) which will differ between samples [8]. Therefore, for the purposes of this study, porosity values will simply be measured using the water saturation method. The method used for measuring porosity is similar to the method proposed by ASTM C642-21. However, due to a lack of resources, a simplified methodology was used [50]. Nonetheless, calculating the water saturated void space to total volume ratio is a widely used method for measuring porosity [3], [49]. There should be minimal error in the model when utilizing the porosity values measured through dry and water saturated mass comparisons.

Errors are introduced via the simplifications used in the Delany-Bazley model [15]. While the power-law relation that the DBz model uses is based on empirical data taken from acoustic data of varying glass-fiber and mineral wools, the relation is simply a line of best fit. In other words, the model does not take into account the complexities of the specific material used herein [15]. Further, the material being used in this study, wood-infused concrete, is not similar in structure to the varying wools used in the initial development of the DBz model, as Delany and Bazley assumed that the materials were comprised of homogenous, equally distributed fibrous layers (of which the wood-infused concrete is not) in which material porosity was near unity (1.00) [15]. The concrete utilized does not suit this material description, and porosity values peaked at 0.174. Finally, the DBz model is based upon a limited permissible frequency range of accuracy (equation (23)), in which the frequency range is dictated by the airflow resistivity value. To fit the limits imposed by Delany and Bazley, resistivity values become less practical as the examined frequency range decreases [15]. Concretes tend to have higher resistivity values, and therefore, will likely struggle to provide accurate estimations of acoustic properties at lower frequencies. For reference, Delany and Bazley examined a frequency band of 250-4000Hz for materials

with resistivities ranging from 2000-8000 kg/s-m^3 [15]. Looking at concrete resistivity values for varying concretes, typical resistivity values are in excess of 5000 kg/s-m^3 [40], [56], [57]. For example, Lemeurs et al. found that resistivity values ranged from 5000 to 50000 Ns/m^4 (it is worth noting that kg/s-m^3 and Ns/m^4 are equivalent units) [57]. As such, the limits on the Tarnow model must be addressed before the Delaney-Bazley model can be used [15], [48]. Utilizing the varying fiber sizes, estimated average resistivity values of each sample and frequency range using the Tarnow model are shown in Table 3-2 with the corresponding acceptable DBz frequency range.

Table 3-2: Airflow Resistivity Based Frequency Limits

Composition Number	**Average Estimated Air Flow Resistivity [Ns/m^4]**	**DBz Low Freq Average [Hz]**	**DBz High Freq Average [Hz]**
3	17184.7	171.8	17184.7
4	294.5	2.9	294.5
5	289.1	2.9	289.1
6	97.0	1.0	97.0
6.3	94.2	0.9	94.2
7	93.3	0.9	93.3
8	13.7	0.1	13.7
9	14.0	0.1	14.0
10	17598.7	176.0	17598.7

As can be seen in Table 3-2, the estimations for airflow resistivity found using the Tarnow model, with the exceptions of compositions 3 and 10, are significantly lower than those found by Lemeur er al.'s measurements, but the acceptable DBz frequency range is

extremely limited [57]. To ensure estimations made are within a useful frequency range and depict relatively accurate resistivity values of the concrete, the value of resistivity found utilizing composition 10, 17598.7 Ns/m^4, will be the estimated resistivity value used across all trials. This is due to the value being the highest of Tarnow's estimations, and thus, most accurately reflects the observed range of values for fibrous concretes. Interestingly, this great discrepancy in Tarnow's resistivity values found between samples of varying fiber sizes displays the dependency that Tarnow's model has on fiber size [48]. Unfortunately, verification through direct measurement of resistivity of the samples was not possible during this study, and therefore, the accuracy of the resistivity value is strictly based on results found in the literature [40], [56], [57].

The remaining viscous and thermal properties, tortuosity, viscous and thermal characteristic lengths, and thermal permeability are all solved for with the JCAL model, and therefore, their accuracy is limited by the limits of the JCAL model. Regarding the viscous properties estimated using the JCAL model, the dynamic density is bound by four limits on the real and imaginary values of the higher and lower frequencies. These limits are exact, except for the limit imposed on the real, low frequency limit [53]. This, however, only impacts frequencies approaching 0 Hz, a range that falls below what will be examined with the impedance tube, and therefore, will not be of great impact on the frequencies considered.

Finally, the last source of potential error comes from the final calculation of acoustic absorption. The calculation of acoustic absorption stems from the calculation of acoustic reflection that is based upon the surface impedance of the material. This calculation is under the assumption that the rigid backing of the material causes zero acoustic energy transmission. This assumption is obviously not accurate in reality as there will always be some lost energy even when surfaces are optimized for minimal acoustic transmission.

Chapter 4

Materials and Experimental Methodology

While the goal of the hybrid JCAL-DBz model developed in this paper is to reduce the need to develop concrete samples when trying to understand the acoustic absorption of a fibrous concrete composition, the model must first be verified. Therefore, to verify the accuracy of the model, multiple concrete samples were developed and tested to compare predictions made by the model. The concrete fabrication process and acoustic absorption process are both explained in this chapter.

4.1 Concrete Composition

Multiple sample concrete compositions were used in both the analytical and experimental measurements of the acoustic absorption coefficient. In this section, the process for manufacturing the concrete is illustrated.

The manufacturing of concrete is not particularly difficult in practice. Concrete consists of few ingredients: cement mix (which contains adhesives, sand, and potentially, aggregates), water, aggregates, and any number of special additives. The concrete used in this study consists of aggregate-less cement, water, varying wood fibers based on composition, and an air entraining admixture (AE).

Samples of concrete were molded to the dimensions of the impedance tube in which they were to be tested on. Therefore, samples were molded to be cylinders having a diameter of 44.5 mm and a length of 47 mm (73098.4 mm^3). For every sample composition, three samples were made (with three exceptions) providing a total of 31 samples of 11 compositions. Compositions varied based on wood-fiber contents, use of AE admixture, and water/cement (W/C) ratios. Four sizes of spruce fibers were used in the concrete compositions: fine sawdust (FSD), sawdust (SD), 2 mm wide fibers (2F), and 5 mm wide fibers (5F). Samples with no fibers were also made as a control group for the concrete. The specific cement mix used to create the concrete was *Rapid Set Cement All* multi-purpose cement, an aggregate-less cement. For the samples utilizing the AE additive, the specific additive used was *MasterAir AE 200*. AE additives are a form of chemical that when added to concrete, perform a chemical reaction during the curing process increasing the porosity of the final concrete composition. This is beneficial, as porosity and acoustic absorption are directly related. It is important to note that using AE additives cause the structural strength of concrete to decrease due to an increase in void space [3]. However, the structural tolerances of the concrete compositions utilized in this thesis are beyond the scope of this study.

The molds were made using both *Nerpa Polymers* casting epoxy to mold the inner surface of the impedance tube (the shape of the samples), and *SmoothOn* silicone to provide the female mold. The silicone mold was then used to mold appropriately sized concrete samples. The stages of concrete sample manufacturing are shown in Figure 4-1.

From Left to Right: Sifted 5mm Fibers, Concrete Paste, Molding of Samples, and Complete Sample in Impedance Tube

Figure 4-1: Concrete Sample Manufacturing Process

A variety of composition trials were performed until ideal fiber/cement (F/C) and W/C volumetric ratios were found that bolstered porosity while retaining structural rigidity. Specific sample W/C and F/C values for each composition can be found in Table 4-1. Prior to sample manufacturing, fibers were first sifted and then baked. FSD, SD, and 2F were sifted through a mesh with holes 2 mm in diameter to remove any contaminants or larger fibers. Naturally, the same was done for 5F using a mesh with holes of 5 mm in diameter. Once sifted, all fibers were baked in an oven for two hours at 95ºC to remove as much water from the fibers as possible. The creation of the concrete samples was then started. Each sample was made in the same manner, fibers and cement were mixed at the desired F/C ratios. Once thoroughly mixed, the appropriate amount of water was added incrementally while the concrete was mixed by hand. The amount of water was specific to each sample as W/C ratios varied between compositions. For samples that required AE, it was added to the mix using a baster after the water was added at the desired volumetric ratio. Samples were mixed for approximately ten minutes until components had been evenly mixed and water had saturated, forming a smooth paste. Samples were then set to cure in the molds for three hours to ensure an adequate hardness had been reached.

Sample compositions were made based on volumetric ratios of water, wood fiber, cement, and for those that used them, AE additive. Originally, composition ratios were based on the work of Istoan et al. to bolster acoustic absorption [58]. However, alterations to each composition were required, as it was found that the 2/1 F/C ratio suggested did not provide the desired structural rigidity. The discrepancies with respect to Istoan et al samples were likely due to the use of differing aggregate material and form in the concrete, providing different results than the initial study [58]. Compositions 1.1 to 2.3 do not utilize fibers and are control samples. Images of single samples of each composition are found in Figure 4-2.

Top Row, Left to Right: Samples 1.1, 2.1, 3.1, 4.1, 5.1, 6.1, Bottom Row, Left to Right: Samples 6.3, 7.1, 8.1, 9.1, 10.1

Figure 4-2: Concrete Samples of Each Composition

Table 4-1: Concrete Compositions and their Physical Properties

Sample #	Fibre Type	F/C Volume Ratio	W/C Volume Ratio	AE/C Volume Ratio	Measured Porosity (%)	Measured Dry Density (kg/m³)
1.1	-	-	5/22	-	1.65	2175.2
1.2	-	-	5/22	-	1.10	2220.3
1.3	-	-	5/22	-	0.96	2236.7
2.1	-	-	5/22	1/22	2.20	2094.4
2.2	-	-	5/22	1/22	3.70	1963.1
2.3	-	-	5/22	1/22	3.16	2011.0
3.1	FSD	10/14	10/14	-	14.00	1362.5
3.2	FSD	10/14	10/14	-	14.82	1380.3
3.3	FSD	10/14	10/14	-	13.86	1400.9
4.1	SD	10/14	10/14	-	16.74	1119.0
4.2	SD	10/14	10/14	-	15.23	1177.9
4.3	SD	10/14	10/14	-	17.84	1132.7
5.1	SD	10/14	10/14	1/14	13.45	1316.0
5.2	SD	10/14	10/14	1/14	12.07	1191.5
5.3	SD	10/14	10/14	1/14	13.04	1160.1
6.1	2F	10/14	10/14	-	11.39	1253.1
6.2	2F	10/14	10/14	-	9.19	1320.1
6.3	2F	2/3	1/2	-	10.02	1473.4
7.1	2F	2/3	1/2	1/30	7.82	1543.1
7.2	2F	2/3	1/2	1/30	6.45	1506.2
7.3	2F	2/3	1/2	1/30	7.14	1606.1
8.1	5F	10/14	4/14	-	6.04	1918.0
8.2	5F	10/14	4/14	-	6.59	1878.3
8.3	5F	10/14	4/14	-	6.72	1841.4
9.1	5F	10/14	4/14	1/14	6.17	1600.6
9.2	5F	10/14	4/14	1/14	4.80	1619.7
9.3	5F	10/14	4/14	1/14	6.59	1682.7
10.1	FSD	10/14	10/14	1/28	11.53	1231.2
10.2	FSD	10/14	10/14	1/28	14.00	1249.0
10.3	FSD	10/14	10/14	1/28	10.70	1261.3
10.4	FSD	10/14	10/14	1/28	12.90	1242.2

F = fibre, C = cement, W = water, AE = Air Entrainment Additive, FSD = fine saw dust, SD = saw dust, WF = wood fiber, WS = wood shavings

An F/C ratio of 10/14 was found to provide an ideal balance between structurally sound compositions, yet still porous and fibrous in nature. When testing fiber ratios, it was found that too large an F/C ratio inhibited the concrete's ability to form, causing samples to be extremely fragile. Further, it was found that too much water, when mixed with concrete, lowered the surface porosity, based on visual examination. Water content in each composition changed based on fiber type as differing fiber sizes absorbed differing amounts

of water. If more water is absorbed by the fibers, more water is required to bond with the cement mix, altering the required W/C ratio. Regarding the amount of AE additive used in each composition, volumetric ratios varied to monitor the impact of the AE agent on acoustic absorption. To examine the impact of AE, each fiber type had a composition with and without AE that utilized the same F/C and W/C ratios. The amount of AE used was always 10 mL for each AE composition. It is worth noting that the recommended amount of AE for structural concrete is 0.8 to 4 fl oz AE / 100 lbs. concrete (23.7 to 119.3 ml AE / 45.4 kg concrete). This is to ensure that the structural integrity of the concrete is not put into check for high compressive loads. However, due to the nature of the concrete in this study being non-structural, and because an increased porosity was desired, this recommended volumetric ratio was exceeded to bolster potential acoustic properties.

All compositions had three samples, with the exception of compositions 6, 6.3, and 10. First, composition 10 (samples 10.1, 10.2, 10.3, 10.4) had four samples instead of three, as excess materials permitted another sample be made. Composition 6 is split into two different compositions containing 2F. 6.1 and 6.2 shared the same F/C ratios as the previous compositions, but 6.3 was altered. This was done to examine the effects of changing the volumetric ratios of a composition. The W/C ratio and F/C ratio were both lowered in 6.3 when compared to 6.1 and 6.2, increasing the concentration of concrete within sample 6.3. As a result, an increase in density was observed. Therefore, composition 6 had two samples, and 6.3 is a stand-alone composition. Composition 7 (7.1, 7.2, and 7.3) were used to examine the 6.3 composition in combination with the AE agent.

Once concrete samples were constructed, porosity and density were measured for use in model estimations. It is worth noting that porosity measurements were performed after impedance tube testing was completed to ensure concrete absorption measurements were uninhibited by the potential effects of drying and soaking the concrete. To measure density,

each concrete sample was baked for 2 hours at 110ºC to evaporate any water contained within the pores. Once baked, samples were weighed to obtain the dry mass (Figure 4-3). Density was then calculated by simply dividing the dry mass by the volume of the mold. Once the dry masses were recorded, samples were submerged in water for 144 hours to allow water to saturate within the pores of the concrete. Once saturated, samples were then weighed once again to obtain a wet mass (Figure 4-3). The wet mass and dry mass were then used in tandem with equations (13) and (14) to solve for porosity. The methodology for drying the samples and measuring porosity were based upon those of ASTM C642-21 and Lie et al. [49], [50]. These material properties are required in the calculation of all complex thermal and viscous variables utilized in the JCAL model [53], [54]. Once these measurements were completed, the acoustic analysis of the samples could be performed.

Left: Dry Mass of Sample 1.1, Right: Wet Mass of Sample 1.1

Figure 4-3: Comparison of Sample 1.1 Dry Mass and Wet Mass

4.2 Impedance Tube Method

To measure the acoustic absorption of the fibrous concrete samples, an impedance tube was used. In this section, the methodology and mathematics used for impedance tube

testing will be explained. The impedance tube setup is based on the specific impedance tube used to collect the acoustic absorption data. This impedance tube was originally developed by Champoux, and used to develop the JCAL model [59].

An impedance tube is a device that uses projected soundwaves to calculate the acoustic absorption of a material sample. The device consists of a closed cylinder with a speaker at one end and the material sample placed at the other. The sample is mounted such that the surface facing the speaker is normal to the axis of the tube. Two microphones are mounted along the tube at the end closest to the sample, in this case, two ICP *Bruel & Kjær* 4135 condenser microphones. The testing process starts once the speaker, an *Altec Lansing* ID60C8 University 60w Horn Driver, emits a plane wave of a desired frequency toward the material sample. The frequency of the wave is controlled using a *Bruel & Kjær* Power Amplifier in tandem with a supervisory control and data acquisition system (SCADAS). Specifically, an *LMS Instruments* SCADAS and *SIEMENS Simcenter Testlab Sound Absorption Testing with Impedance Tube* software. The SCADAS and software allow for simple data collection over a large range of frequencies. This incident wave has its amplitude measured by the microphone nearest the speaker (M1) as it passes by. The incident wave is then reflected off the material sample, and as the reflected wave passes by the microphone closest to the sample (M2), the amplitude is measured again. The microphones record the soundwave amplitudes, which are then processed by the SCADAS and software. Acoustic absorption is calculated using a two-way transfer function. A diagram and the specific dimensions of the impedance tube are noted in Figure 4-4.

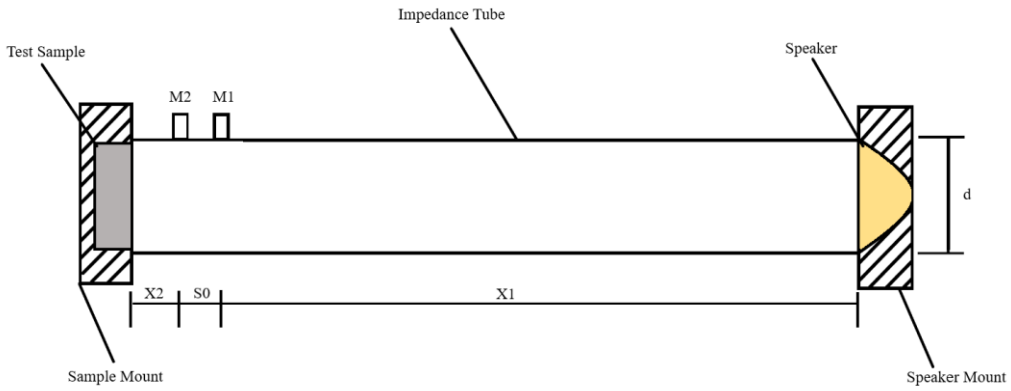

Figure 4-4: Impedance Tube Diagram

Values for each impedance tube dimension are provided in Figure 4-4. The acceptable frequency range in which acoustic absorption values can be measured is dependent on the distance between the microphones, $S0$ [m]. Therefore, each concrete sample was measured twice, once with microphones at distances $X1$ [m] and $X2$ [m], and again moving $X1$ to $X1'$ [m]. Note, $X1'$ is labeled $X1$ in Table 4-2 under the M1'-M2 microphone arrangement. When using the M1-M2 microphone setup, absorption measurements are accurate within the range of 137.2 Hz to 4516.8 Hz. The M1'-M2 setup increases $S0$, lowering the frequency range to between 58.1 Hz and 2922.7 Hz. The calculations for these frequency ranges are covered later in this section, while the microphone setup on the impedance tube is shown in Figure 4-5.

Table 4-2: Impedance Tube Dimensions

Microphone Arrangement	**M1-M2**	**M1'-M2**
***D* (m)**	0.0445	0.0445
***S0* (m)**	0.025	0.059
***X1* (m)**	0.931	0.897
***X2* (m)**	0.044	0.044
Upper Frequency Limit (Hz)	4466.0	2922.7
Lower Frequency Limit (Hz)	137.2	57.2

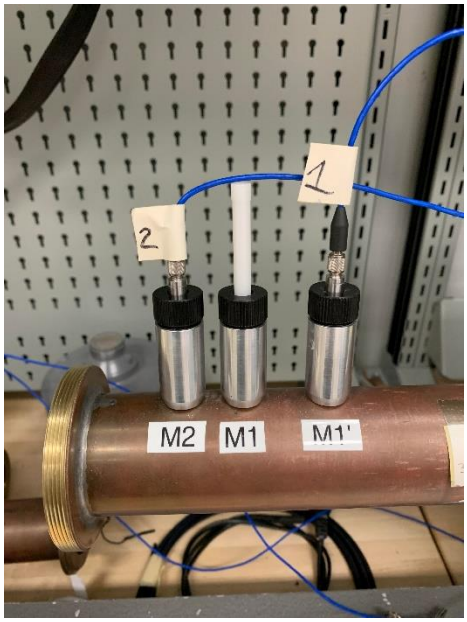

Figure 4-5: Microphone Positions on the Impedance Tube

Prior to the measurement of acoustic absorption for all samples, calibration of the microphones and system was performed. Microphones were first calibrated to ensure accurate measurement of sound. This was done by exposing them to a soundwave of 113.95 dB at 250 Hz generated by a *GRAS* 42AA Pistonphone. It is worth noting that in perfect air conditions, 114 dB would be generated. However, due to microphone sensitivity being impacted by air pressure, a correction of -0.05 dB was applied. This in turn ensures accurate microphone sensitivity in mV/Pa. Readings were within the required accuracy range for both microphones. A phase calibration was then performed to ensure microphones were accurately recording the transfer function between the microphones. This was done by performing two tests of an anechoic simulation in which M1 and M2 were placed in alternating positions ($X1$ and $X2$) and measurements of coherence and frequency response functions are compared, respectively, to calculate the correct microphone calibration factor [16]. Finally, once the phase calibration was completed, two final tests were done to ensure readings were accurate: a rigidly backed test (a brass, flat surface at the sample end) and

an anechoic test (a foam-filled tube at the sample end). The rigidly backed test was required to provide an absorption reading below 5% (near complete reflection), the anechoic test provided 100% absorption (complete absorption). Once calibrations and test trials were completed, the concrete samples were then tested. Once all acoustic absorption measurements were made in positions M1 and M2, the phase calibration and rigid and anechoic trials were repeated for the second round of testing where M1 was moved to $X1'$.

The mathematics used to develop the impedance tube setup follow ASTM E1050-08, a standard for building impedance tubes and calculating acoustic absorption [60]. It is worth noting that this standard has been updated since the construction of the tube used in this study, the latest standard is ASTM E1050-19 [16].

The physical dimensions of the tube dictate the frequency range in which accurate measurements of acoustic absorption can be obtained. The limitation on the upper limit of the frequency range is based on the diameter of the tube and distance between the microphones, while the lower limit is based only on the distance between the microphones. Firstly, the maximum upper frequency limit (f_u) [Hz] can be determined based on the inner diameter of the tube (D) [m] [16].

$$D < 0.586\lambda_u \quad \textbf{(34)}$$

$$f_u = c/\lambda_u \quad \textbf{(35)}$$

As shown, the inner diameter of the impedance tube must be less than 58.6% of the upper frequency wavelength (λ_u) [m]. This in turn can be used to solve for the diameter-based maximum upper frequency limit, which is 4466 Hz.

The lower frequency limit (f_l) [Hz] is constrained by the distance between the two microphones ($S0$) within the impedance tube and the lower frequency limit wavelength (λ_l) [m]. For the impedance tube used, three microphones are used to allow for varying frequency limits. By having two positions for the microphone closest to the speaker (M1 and

M1'), different values for $S0$ will allow for different lower frequency limits [16]. As seen in equation (36), the lower frequency wavelength must be less than ten times $S0$.

$$S0 > 0.01\lambda_l \tag{36}$$

Like the lower limit, the upper limit is also bound by $S0$. The relation relates the upper frequency to $S0$, as well as the speed of sound within the tube, c.

$$f_u S0 < 0.5c$$

$$f_u < \frac{0.5c}{S0} \tag{37}$$

This in turn means that there are two limits imposed on the upper frequency, the lower of which is the true limit [16]. In the instance of the M1-M2 microphone setup, the tube diameter constraint provides a high frequency limit of 4466 Hz while the $S0$ constraint provides a constraint of 6897.6 Hz. Therefore, the upper frequency limit is 4466 Hz.

Beyond the limits imposed on frequency, the following limits on the length of the impedance tube must be met to avoid measurement interference. Firstly, the length between the speaker and M1 ($X1$) must be greater than at least triple the diameter. This is because a combination of both plane and non-plane waves are generated by the speaker. However, non-plane waves, if picked up by the microphones, will interfere with measurements. Making $X1$ at least three times the diameter of the tube ensures that non-plane waves subside before reaching the microphones, providing clear measurements. Second, the length between the material sample and M2 ($X2$) has varying constraints based on the sample's surface. The concrete samples used have a flat, symmetrical surface, and therefore, the following constraint on $X2$ is recommended, as per ASTM E1050-08 [16], [60]. The $X1$ constraint and total length (L) [m] of the tube are also provided.

$$X1 > 3D \tag{38}$$

$$0.5D \leq X2 \tag{39}$$

$$L = S0 + X1 + X2$$

The impedance tube used has an $X2$ value greater than $0.5D$ which is suggested for materials with flat surfaces [16], [60]. Absorption measurements can then be performed, as all imposed limits are satisfied.

Once testing is completed, the soundwave amplitude measurements [Pa] recorded must be processed to solve for acoustic absorption. This is done using a transfer function (H_{12}). The amplitudes of the waves are denoted as A and B [Pa], A being the amplitude of the incidental wave and B being the amplitude of the reflected wave. Amplitudes are used to calculate the complex acoustic pressure [Pa] of the wave ($p(x)$) at each position of the microphones ($X1$ and $X2$). The equation is as follows [61]:

$$p(x) = Ae^{-ikx} + Be^{ikx} \quad \textbf{(40)}$$

$$p(X2) = p_2 \, , p(X1) = p_1 \quad \textbf{(41)}$$

Using the acoustic pressure equations, the cross-spectrum (S_{12}) equation can be solved using the complex conjugate of the complex pressure. Similarly, the auto-spectrum (S_{11}) can be found by relating the position to itself [62].

$$S_{12} = p_2 p_1^* \quad \textbf{(42)}$$

$$S_{11} = p_1 p_1^* \quad \textbf{(43)}$$

where, p_1^* refers to the complex conjugate of p_1. Finally, the transfer function can be solved using the cross and auto-spectra to find the reflection factor, $\mathcal{R}$, and therefore, the acoustic absorption coefficient [16].

$$H_{12} = \frac{S_{12}}{S_{11}} \quad \textbf{(44)}$$

$$R = R(\omega) = \frac{H_{12} - e^{-jks_0}}{e^{jks_0} - H_{12}} e^{2jk(s_0 + x_2)} \quad \textbf{(45)}$$

$$\alpha = \alpha(\omega) = 1 - |\mathcal{R}|^2 \quad \textbf{(46)}$$

where $\mathcal{R}$ represents the interaction between the air and the sample surface, as seen in the DBz-JCAL model, despite being solved using a different method. $\mathcal{R}$ is directly related to the acoustic absorption coefficient, as seen in equation (46), and is dependent on the frequency via the wave number (k).

4.3 Sources of Error

The experimental process for measuring acoustic absorption with an impedance tube is an accepted and accurate method for observing the acoustic properties of materials [16]. While true, there are still causes for experimental error.

Although the microphone calibration accuracy fell within the recommended range of accuracy, readings were not perfect. The microphones were subject to 113.95 dB at 250 Hz via a pistonphone for calibration. Calibrations, if perfect, should provide a sensitivity reading of 45 mV/Pa. However, both microphones fell short of this value. Measurements were done over two groups of tests, and therefore, two sensitivity readings were found for both M1 and M2, as shown in Table 4-3***: Microphone Sensitivity***.

Table 4-3: Microphone Sensitivity

Test Group	M1 Sensitivity (mV/Pa)	M2 Sensitivity (mV/Pa)
1	44.15	38.28
2	43.58	37.83

M1 was found to be more accurate in its sensitivity reading than M2. Further, while both microphones do not display significant error, M2 displays potential sensitivity error up to 15.93%, and M1 up to 3.17%. The sensitivity of the microphones can be impacted by the air pressure of the testing chamber, and therefore, a correction factor of -0.05 dB was applied to the microphone calibration using the pistonphone. -0.05 dB was used as recommended, to scale with larger air pressure discrepancies. A correction of only -0.05 dB shows that the pressure was close to ideal. This correction mitigates some of the potential

error found in calibrating the microphones. The other calibration required was a phase calibration of the system in which there were no noticeable sources of error identified.

Two types of experimental error can be identified related to the geometry of the samples. Firstly, the diameter of the samples should be as close to the inner diameter of the impedance tube as possible. Otherwise, potential interference caused by resonant waves generated between the walls of the tube and the sample's surface is possible. These resonant waves at the wall can propagate and interfere with the acoustic measurements made by the microphones. A larger gap between the sample wall and the inner surface of the tube results in larger interference. The inner diameter of the impedance tube is 44.5 mm, and all samples were molded based on this dimension. While the diameter of the samples were approximately 44.5 mm, minor variations were observed. Gaps between the samples and the impedance tube remained below 1 mm. However, even the smallest gaps can lead to potential resonant waves. A likely cause for this variation in sample diameter is due to concrete contraction during the hydration process of the varying concrete compositions. Figure 4-6 displays diameter discrepancies between measured samples.

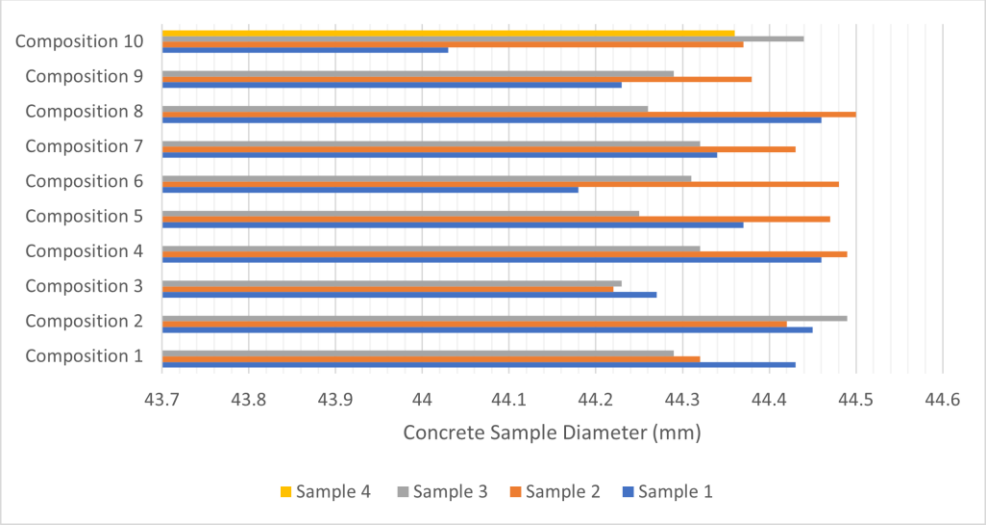

Figure 4-6: Concrete Sample Diameters

The second source of error caused by sample dimensions comes from the non-tested surface of the sample, the back of the sample. The backs of the samples were not flat surfaces resulting in there being an air cavity, or back cavity, located between the back of the sample and the rigid backed end of the impedance tube. This can cause potential error in the acoustic absorption measurements due to acoustic transmission through the sample into the air cavity. To test potential error caused by the airgaps, three different mounting techniques were tested on sample 1.1 and acoustic absorption measurements were compared. The three mounting orientations were as follows: orientation 1 - flat surface facing speaker (with back cavity), orientation 2 - non-flat surface facing the speaker (no back cavity), and orientation 3 – flat surface facing speaker with silicone vacuum grease filling the back cavity. While orientation 2 was supposed to mitigate the back cavity issue, it was found that the impedance tube design was not suitable for a non-symmetrically surfaced sample. The distance between M2 and the sample ($X2$) must meet the ASTM E1050-19 standard to insure mitigation of higher order modes which is dependent on the geometry of the surface being measured [16]. For non-symmetrical surfaces, $X2$ is required to be greater than twice the diameter of the impedance tube, a requirement that is not met by the M1-M2 setup [16]. While orientation 3 partially sealed the back cavity, likely bolstering accuracy, this technique was not utilized with all samples due to potential interference with measuring porosity post experimentation. The lubricant could have blocked surface pores, lowering water saturation and skewing porosity values. Further, the change in acoustic absorption measurements between orientations 1 and 3 was not deemed to be significant enough to justify this technique. The comparison of acoustic absorption measurements between orientations is shown in Figure 4-7. These samples were tested within the frequency range of 138 Hz to 4000 Hz.

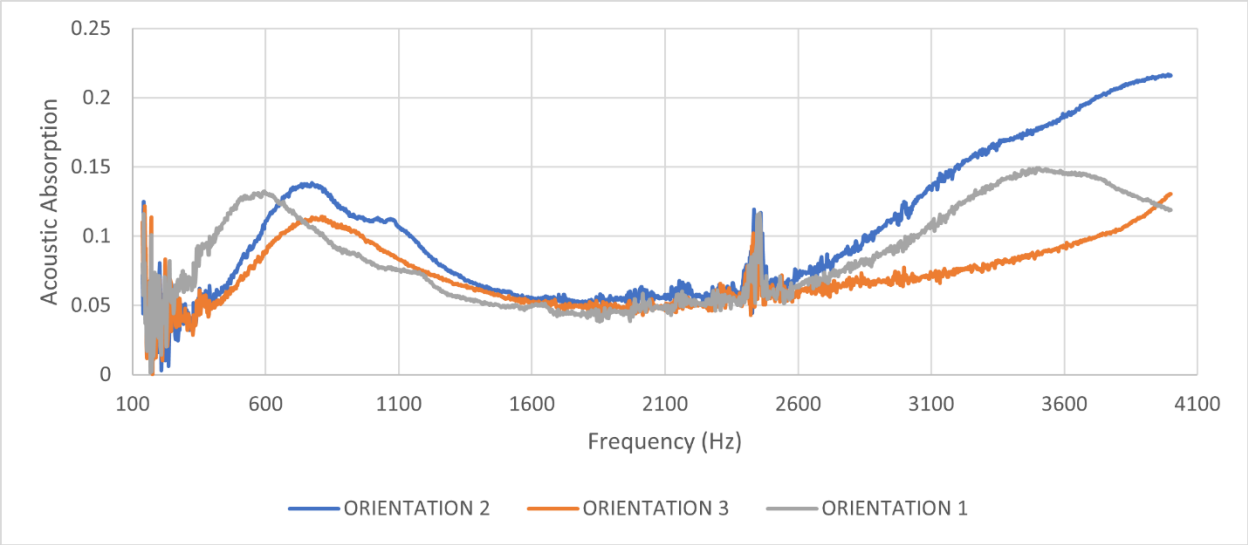

Figure 4-7: Sample Orientation Absorption Comparison

As seen in Figure 4-7, all orientations provided very similar results. However, orientation 2 was deemed invalid due to the nature of the impedance tube design, therefore, it was not considered further. This is because one of the stipulations for using the transfer function requires the surface of the material on which the emitted soundwave is reflected be flat and smooth [60]. Orientation 3 is seen to cause a decrease in the absorption measure at higher frequencies, while boasting higher absorption at lower frequencies, when compared to orientation 1. Across the frequency range, the data from all orientations was found to be most consistent across the range of approximately 1600 to 2600 Hz. This consistency in data at this frequency range is also seen in all measured samples shown in the following sections. This is significant, as it shows that while there are slight differences in values between the varying orientations, when examining the 1600 to 2600 Hz frequency range, orientation is not detrimental in observing the acoustic absorption of a sample. However, it is worth noting that at approximately 2500 Hz, there is a discrepancy where values differ by up to 0.607, which is significant. Absorption values spike drastically, and this was noticed across all samples measured. The exact cause of this discrepancy is not

known. Therefore, the significance in the difference in absorption values at this discrepancy are not believed to be largely representative of the results. While the accuracy of the impedance tube data was calculated to consist of the much larger frequency range of 57 Hz – 4400 Hz (see Table 4-2), data outside of the 1600 to 2600 Hz range is much more inconsistent between samples, as seen here between orientations as well. While potentially significant, all samples measured, even those of the same composition, had more erratic absorption measurements as frequencies increased beyond 3000 Hz further supporting that orientation has little impact on the nature of the measurements. In conclusion, while orientation 3 should provide the most accurate results in theory, absorption values were observed to be very consistent between all orientations in the mid frequency range of 1600 Hz to 2600 Hz, and consistently erratic outside of this range. Nonetheless, it is worth noting as a potential source of error.

Distortion in measurements generated by higher-order modes interfering with reflected plane waves during experiments are another source of potential error. This issue is briefly mentioned via the restrictions imposed on the impedance tube design regarding the distance between the sample and the nearest microphone to the sample ($X2$). Essentially, based on the stipulation that the material being tested, wood-infused concrete, is a flat surface

and symmetrical in shape, the ideal length for $X2$ is greater than half the diameter of the tube. These conditions are met. However, the material is not perfect. The nature of the pore and fiber distribution of the sample can, therefore, cause reflected waves to act in a non-ideal fashion, creating the potential for interference by higher-order modes [16].

Beyond the potential experimental errors related to sample mounting and calibration, no other significant sources of error were noticed. Furthermore, all measured values were within those values expected and showed consistency across varying trials.

Chapter 5

Results

Upon understanding how both impedance tube testing is performed and how the hybrid DBz-JCAL model estimates acoustic absorption, results can be obtained. In section 5.1, the impedance tube measurements will be examined and discussed using comparisons between absorption values of the varying compositions. In section 5.2, similar comparisons will be made using the estimated acoustic absorption values of the DBz-JCAL model. For the model, values of the estimated material properties will be provided for all samples. A discussion comparing the results of the impedance tube and model will be provided in Chapter 6. All 31 samples were examined in the model to allow for direct comparison of estimated acoustic absorption to measured acoustic absorption. To simplify charts, some comparisons will be done using the average absorption values of compositions.

5.1 Impedance Tube Results

The limitations on the acceptable frequency ranges for each microphone setup, M1-M2 and M1'-M2, were noted in Chapter 4. As such, two frequency ranges were examined when measuring acoustic absorption. A higher frequency range using M1-M2 at 138 Hz to 4466 Hz, and a lower frequency range using M1'-M2 at 58 Hz to 2572 Hz. While the lower frequency range is less than what was determined to be acceptable based on impedance tube dimensions, it was noted during the measurement of absorption in the M1-M2 setup

that a discrepancy of data occurred at approximately 2500 to 2600 Hz. These discrepancies were consistent across all samples and were likely due to resonant waves resulting from sample back cavities. However, this is not certain as not all samples had the same cavity space, and even when filled with vacuum seal, the abnormal values were still observed. Therefore, it was decided to limit the lower range to a peak value of 2572 Hz. Further, this discrepancy will not be considered when noting acoustic performance. Similarly, absorption values below 300 Hz and approaching 4466 Hz across all absorption measurements are erratic and do not accurately depict acoustic absorption. This behavior is likely due to being close to the respective limits of the frequency ranges examined.

Data will be examined first by comparing each composition without AE to its counterpart with AE. This will display the effects of AE on the acoustic performance. Following these comparisons, the fiber that has the greatest effect on acoustic absorption will be determined. Finally, each graph will include the acoustic data of the base concrete used, composition 1, to examine how each composition change bolstered or lowered the acoustic absorption.

5.1.1 Fiber-less Concrete

Compositions 1 and 2, those without fibers, acted as a baseline for deciding which of the other compositions bolstered acoustic absorption (Figure 5-1 and Figure 5-2). Composition 2, despite it containing AE, displayed an unexpected result across both high and low frequency ranges. The AE admixture, which is supposed to bolster porosity, is recorded to lower the average acoustic absorption below that of composition 1 without AE. Sample 2.3 is the only sample containing AE to boast greater acoustic absorption than composition 1, and only within the frequency range of 1284 Hz – 2800 Hz. This is interesting as the AE admixture, while lowering density in composition 2, did not increase absorption. While

surface porosity increased by 1-2%, the decrease in density indicates that the AE had a greater impact on the internal porosity than the surface porosity. Regarding specific values, the average absorption of composition 1 in the lower frequency range peaks at 0.142, while composition 2 peaks at 0.085. Values plateau to an average of 0.071 and 0.076 in composition 1 and 2, respectively, before reaching the end of the lower frequency range. Composition 2 obtained a higher average than 1 while plateauing due to the exceptionally high absorption of sample 2.3. Upon examining the higher frequency range, average absorption increased slightly from the plateau, with composition 1 being more absorptive than composition 2. Peak absorption in the higher frequency range for composition 1 is 0.131 and 0.094 for composition 2. Noticeably, absorption values of individual samples in both compositions begin to increase erratically or decrease when approaching the upper limit of the higher frequency range. These values are not considered when examining the absorption potential of the materials.

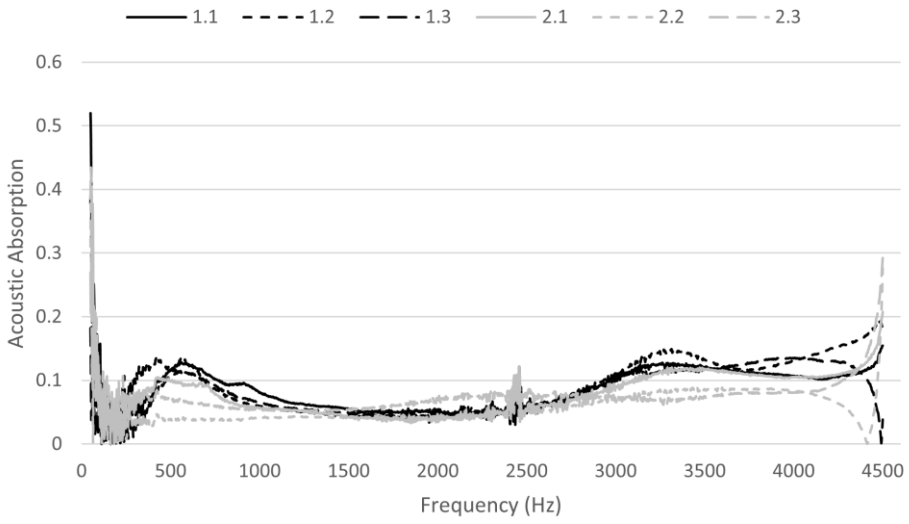

Figure 5-1: High Frequency Acoustic Absorption Measurements of Fiber-less Concretes

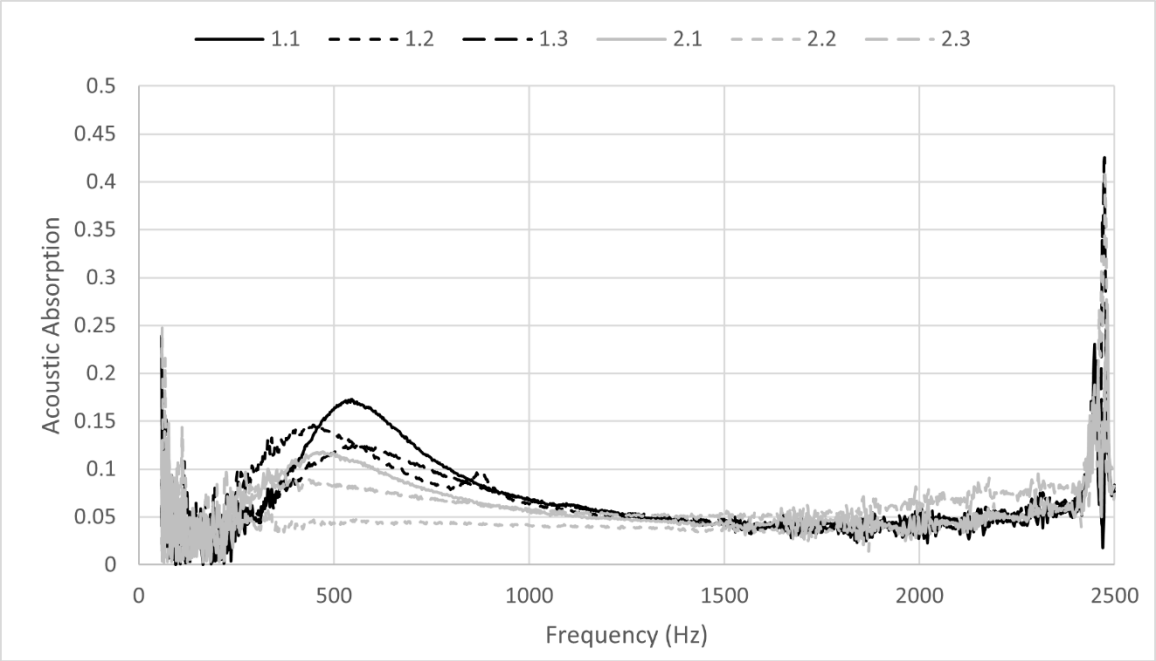

Figure 5-2: Low Frequency Acoustic Absorption Measurements of Fiber-less Concretes

5.1.2 FSD Concrete

Samples that contained FSD, the smallest of the aggregate forms, increased the acoustic absorption both with and without AE additives when compared to composition 1 (Figure 5-3 – Figure 5-5). Within the low frequency range, composition 3 and 10 both showed an increase in average acoustic absorption at all frequencies when compared to composition 1. An average low frequency peak absorption of 0.139 is noticed at 456 Hz and 0.232 at 546 Hz for composition 3 and 10, respectively. Of note, the lower frequency peaks were inconsistent between composition 3 samples. Sample 3.2 reached a peak 0.06, which was more absorptive than 3.1 and 3.3. Beyond the initial peaks, the same plateau trend is noticed as was seen in the fiber-less compositions. As values plateaued, composition 3 reached 0.108 and composition 10 reached 0.091 average absorption, while approaching 2500 Hz. However, sample 3.1 acted differently than other composition 3 samples, since absorption

increased until plateauing at 0.137 at 1700 Hz. In the higher frequency range, the net absorption increased across all samples compared to absorption at 2500 Hz. Average absorption of composition 3 increased as frequency increased, but was less absorptive than composition 1. Composition 10's average absorption began to increase in absorption as frequency increased, but not all samples acted in a similar way. Specifically, compositions 10.2 temporarily fell below composition 1, while 10.1 and 10.3 became more absorptive. Average high frequency peak absorption of 0.134 is noticed at 4446 Hz and 0.170 at 4280 Hz for composition 3 and 10, respectively. Interestingly, composition 10 containing AE is noted as having higher average acoustic absorption values than composition 3 without AE over a larger frequency range. This trend is opposite to what was noticed between composition 1 and 2, where compositions with AE were less absorptive. Comparatively, composition 10 appears to bolster higher and more consistent acoustic absorption properties than composition 3 in both the lower and higher frequency ranges.

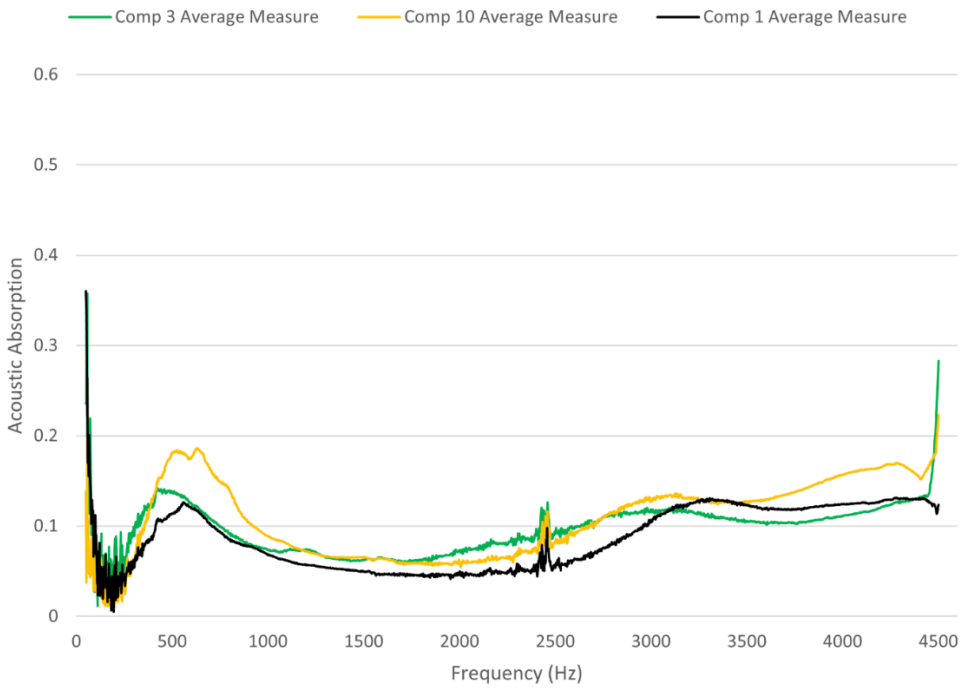

Figure 5-3: Average High Frequency Acoustic Absorption Measurement of FSD Concretes

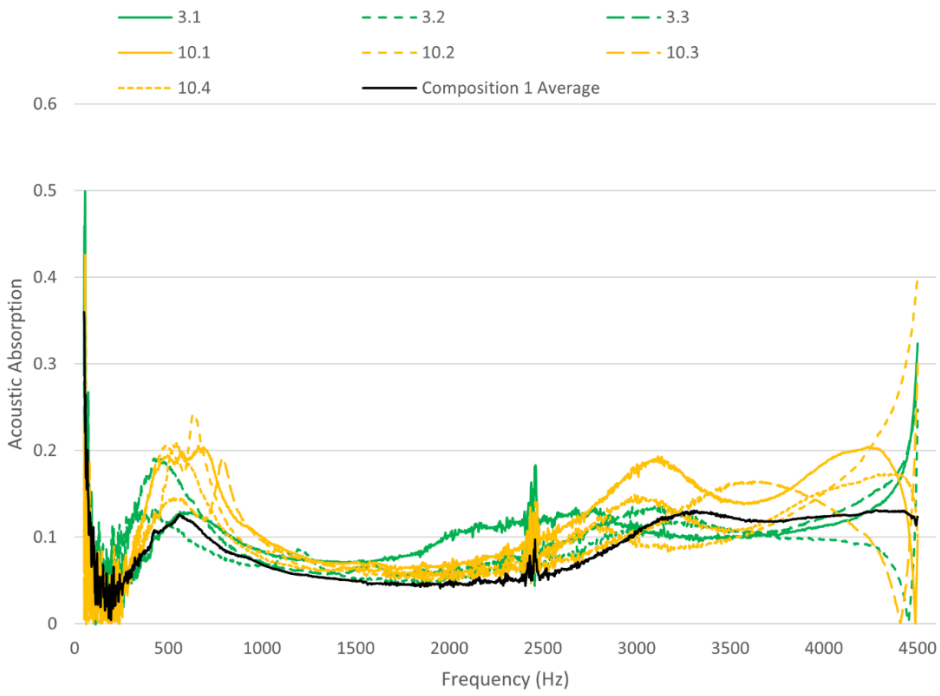

Figure 5-4: High Frequency Acoustic Absorption Measurements of FSD Concretes

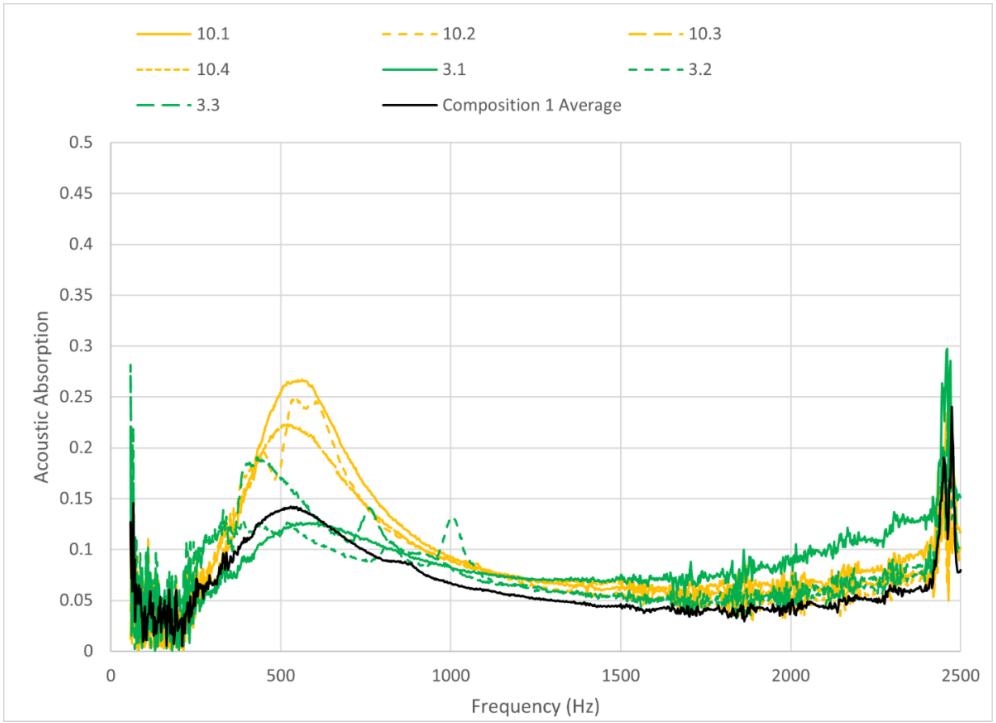

Figure 5-5: Low Frequency Acoustic Absorption Measurements of FSD Concretes

5.1.3 SD Concrete

Compositions 4 and 5 contain SD fibers (Figure 5-6 – Figure 5-8). Acoustic absorption values relative to composition 1 show consistent increase in absorption both with and without AE. As seen in all previous compositions, absorption values of all trials reached an initial peak in the lower frequency range before plateauing up to 2500 Hz. Specifically, average low frequency absorption peaked at 0.170 and 0.150 for compositions 4 and 5 respectively. Despite having a higher peak, the average composition 4 values fell below composition 5 at 1186 Hz. Of note, values did not plateau like in previous compositions. After the initial peak of the low frequency range, average absorption values of compositions 4 and 5 steadily increased into the high frequency range only plateauing at absorption values of 0.131 and 0.141 at 2808 Hz and 2818 Hz respectively. Average high frequency peak absorption is noticed beyond this plateau as frequency approached the upper limit. Peak high frequency averages were found to be 0.149 and 0.207 for compositions 4 and 5, respectively. Relative to the base concrete average, absorption increased by up to 0.178 for composition 4 and 0.121 for composition 5. Interestingly, while composition 4 boasted the highest individual acoustic absorption value, composition 5 containing AE was more absorptive over a greater frequency range. Unlike composition 4, composition 5 did not fall below the average absorption of composition 1. The addition of AE to composition 5 falls in line with the expectations of adding AE to the concrete composition (i.e. AE should both bolster porosity and increase acoustic absorption of the sample). Of note, composition 5 was on average denser than composition 4.

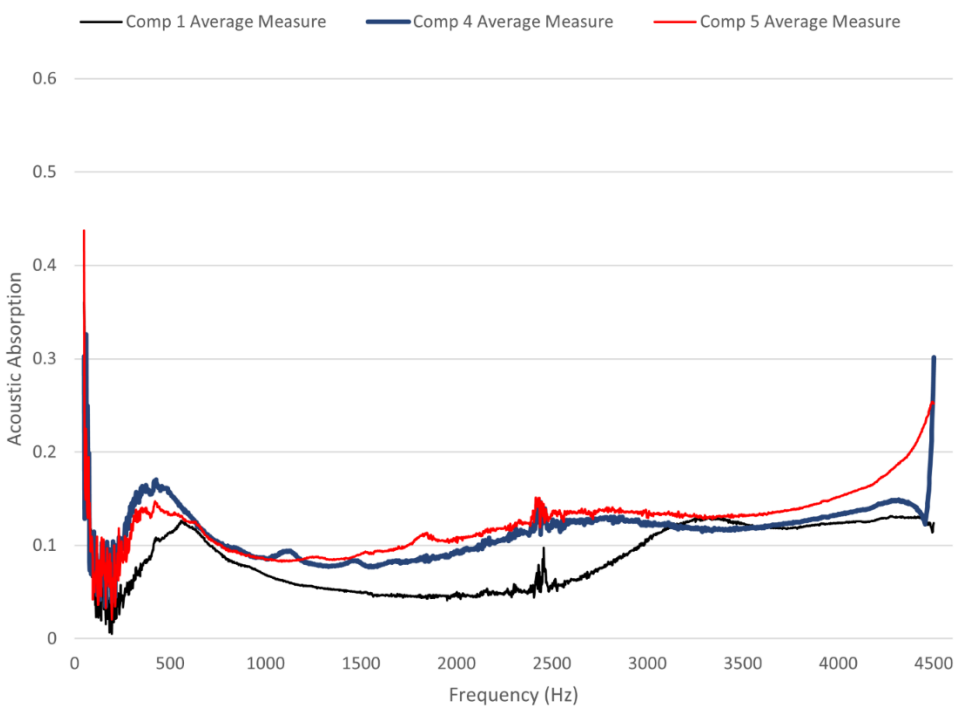

Figure 5-6: Average High Frequency Acoustic Absorption Measurement of SD Concretes

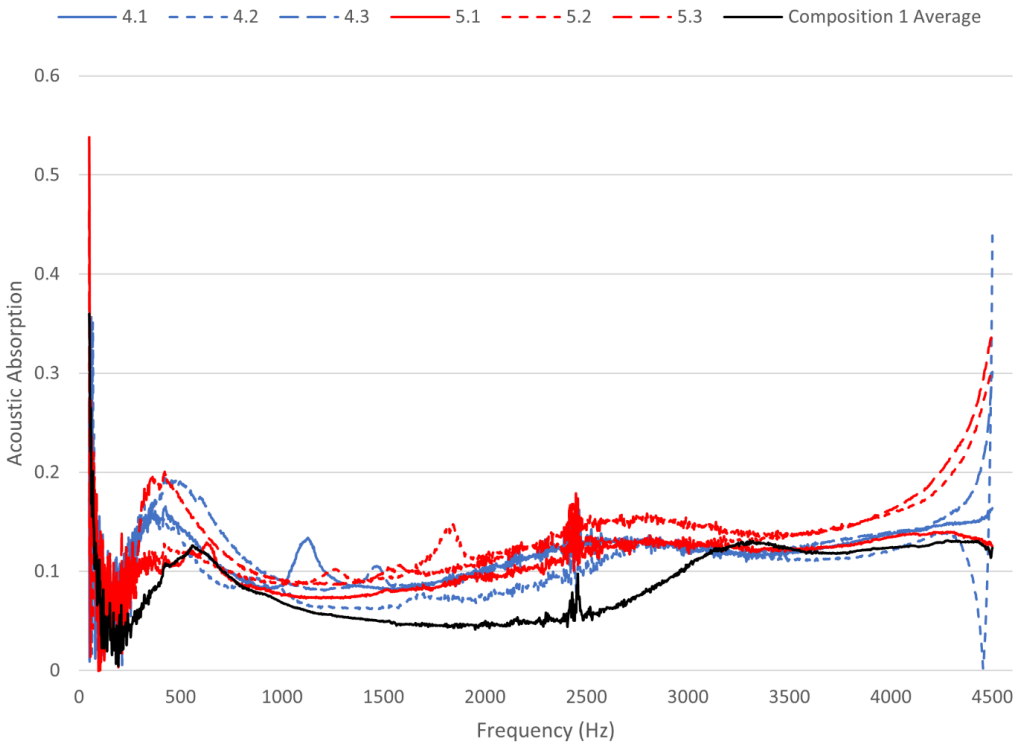

Figure 5-7: High Frequency Acoustic Absorption Measurements of SD Concretes

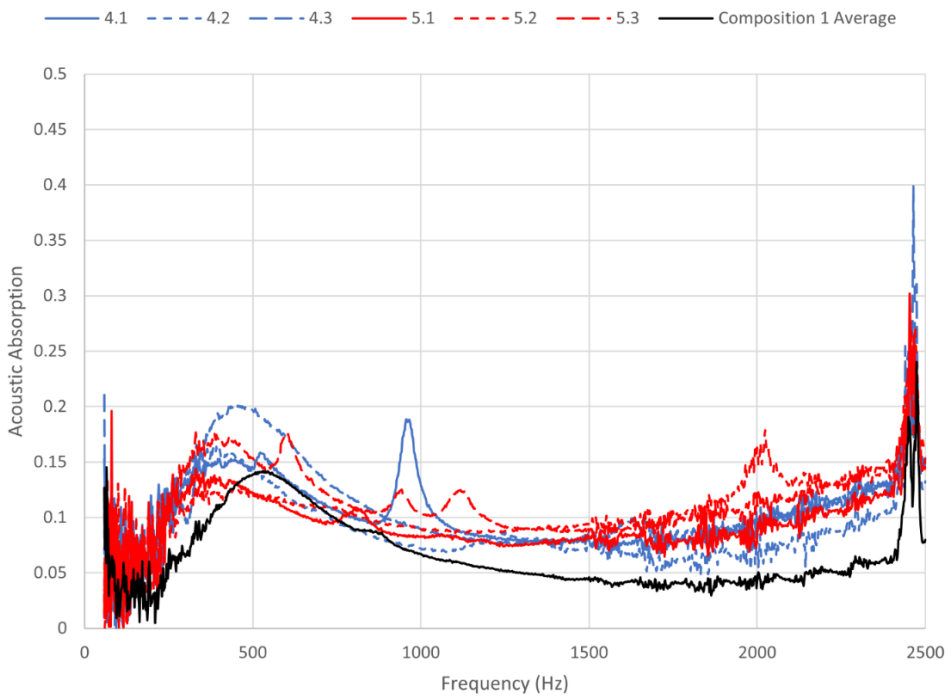

Figure 5-8*: Low Frequency Acoustic Absorption Measurements of SD Concretes*

5.1.4 2F Concrete

Compositions 6, 6.3, and 7 are interesting as they not only show how additives can alter absorption values, but also how the volumetric ratios of fibers, water, and concrete impact acoustic absorption (Figure 5-9 – Figure 5-11). Composition 6, referring to samples 6.1 and 6.2, utilized the same F/C ratios seen in the previously examined compositions. However, 6.3 and 7 had lower F/C and W/C ratios, and therefore, an increased concrete concentration. Composition 7 also contained AE. Considering the lower frequency range, composition 6 samples boasted significantly different initial low frequency peaks with 6.1 reaching 0.240 and 6.2 reaching 0.120. Despite the difference between peaks, both 6.1 and 6.2 realigned to similar values after plateauing as frequency approached 2500 Hz. Across all low frequencies, compositions 6.3 and 7 had worse absorption values than composition 6. Further, 6.3 and 7 performed poorly when compared to composition 1. At lower frequencies,

composition 6.3 performed slightly better than composition 7 reaching an average of 0.082 and 0.081, respectively, when approaching 2500 Hz. Within the higher frequency range, average composition 6 values remained consistently higher than composition 1, 6.3, and 7. Conversely, sample 6.1 drops to the same average absorption as composition 1 between 3800 and 4200 Hz. Average composition 7 values performed worse than composition 1, while 6.3 performed slightly better. The high frequency average peak absorption values are 0.246 at 4446 Hz, 0.145 at 3188 Hz, and 0.122 at 4442 Hz for compositions 6, 6.3, and 7, respectively. Examining composition 6, the use of 2F fibers proved to be quite effective at bolstering absorption across most frequencies with a near 0.1 increase in acoustic absorption when compared to 1.3 in the low frequency range. Compositions 6.3 and 7 perform as expected, whereby increasing the concrete concentration of the composition caused significant decrease in absorption. Nonetheless, 7.2 was an outlier, matching absorption values of 6.1 up to 2642 Hz. Interestingly, composition 7, containing AE, is both denser and less absorptive than 6.3 on average. The opposite would be expected given the use of AE. These results show the impact that F/C ratios have on acoustic performance, such that when the F/C ratio is increased by only 0.05 between 6.3 and 6, absorption values varied widely. Should the potential effect of F/C not be considered during acoustic design, acoustic performance could be impacted significantly.

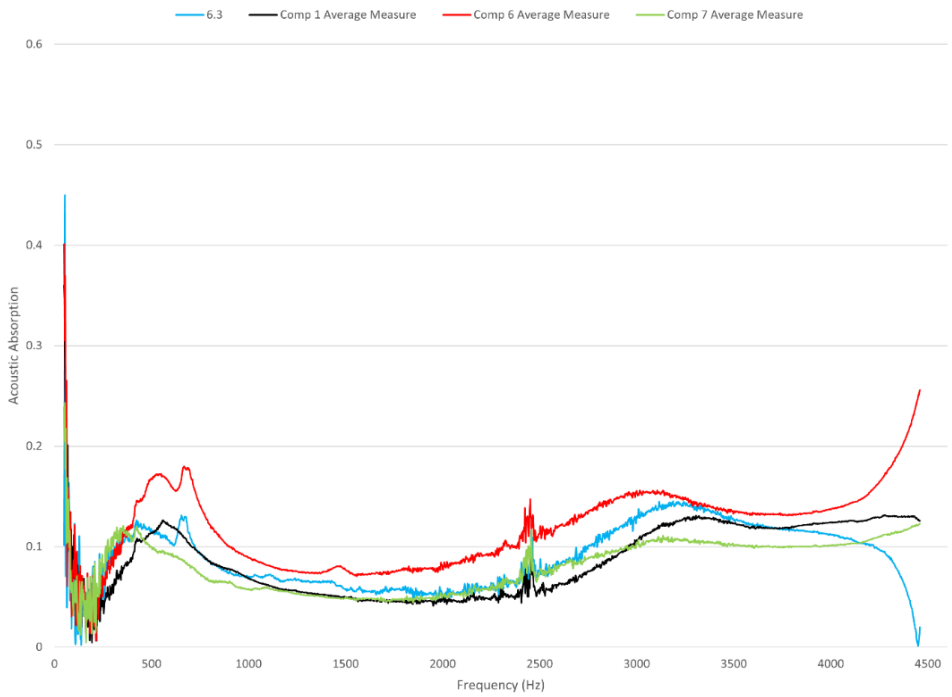

Figure 5-9: Average High Frequency Acoustic Absorption Measurement of 2F Concretes

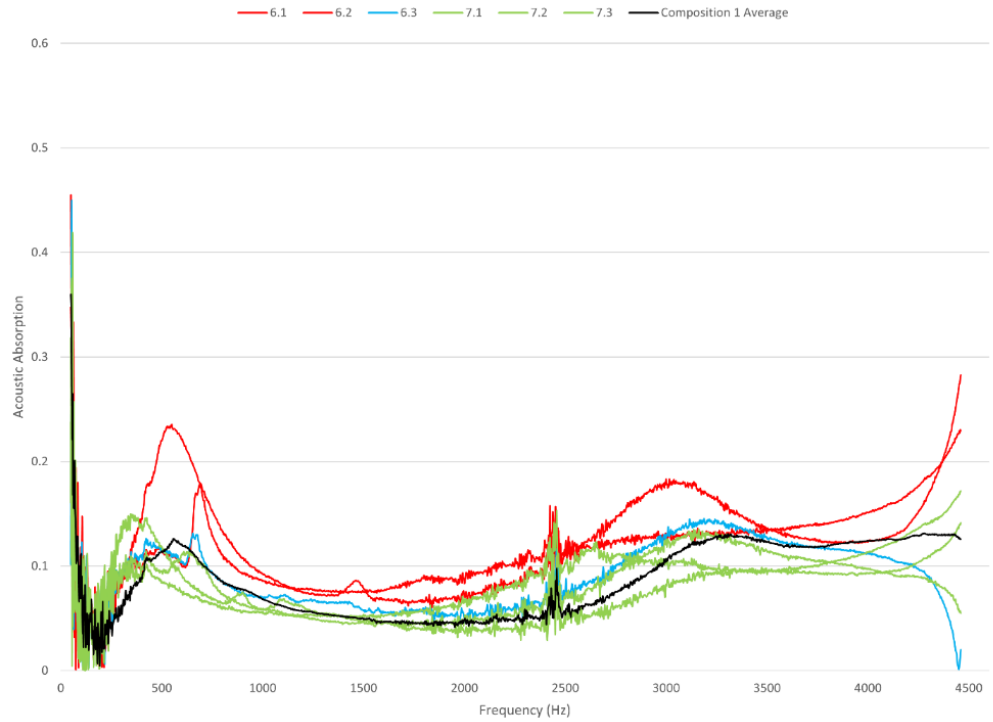

Figure 5-10: High Frequency Acoustic Absorption Measurements of 2F Concretes

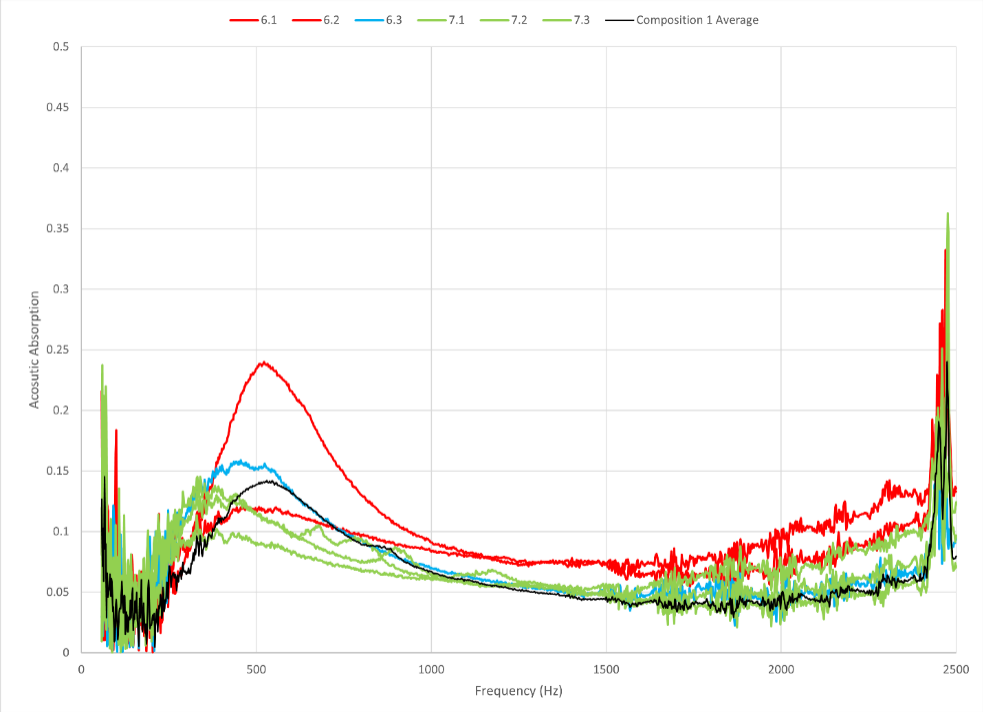

Figure 5-11: Low Frequency Acoustic Absorption Measurements of 2F Concretes

5.1.5 5F Concrete

The final two compositions, 8 and 9, are those containing 5F aggregates without and with AE, respectively (Figure 5-12 – Figure 5-14). Samples of composition 8 all performed worse than composition 1 across nearly all frequencies. The initial peak value of composition 8 reached an average maximum of 0.089 before plateauing to an average of 0.064 at 2500 Hz. Composition 9 performed better than 8 with an initial peak of 0.165. However, absorption dropped off steeply as values plateaued to an average 0.068 and fell below composition 1 at 1800 Hz. Within the higher frequency range, average absorption increased for both composition 8 and 9. However composition 8 remained below the average absorption of composition 1. An average high frequency peak absorption value of 0.102 is noticed at 3922 Hz and 0.278 at 4446 Hz for composition 8 and 9, respectively. Absorption for all samples of composition 9 exceed the average absorption of composition 1 above

3700 Hz by a significant amount. At their peaks, samples 9.1, 9.2, and 9.3 exceeded composition 1 by 0.088, 0.087, and 0.228 respectively. Compositions 8 and 9 reveal that once the fibers reach a size of 5F, fibers become detrimental to the absorption potential of the concrete across the mid-frequencies. This is important, as this reveals the limits of fiber potential in bolstering concrete absorption. Specifically, simply increasing fiber size does not guarantee an increase in acoustic absorption.

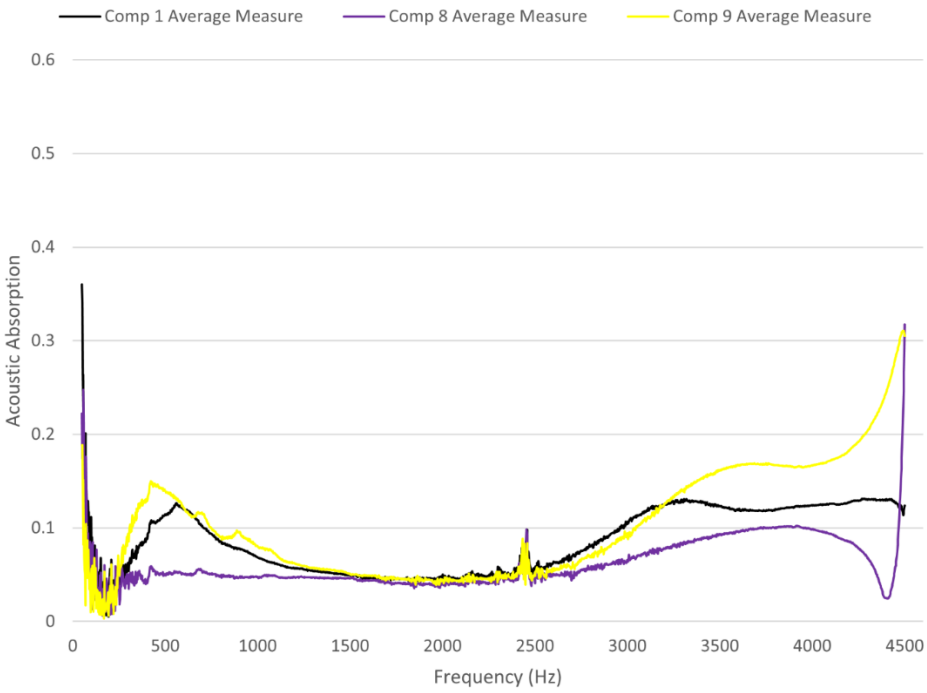

Figure 5-12: Average High Frequency Acoustic Absorption Measurement of 5F Concretes

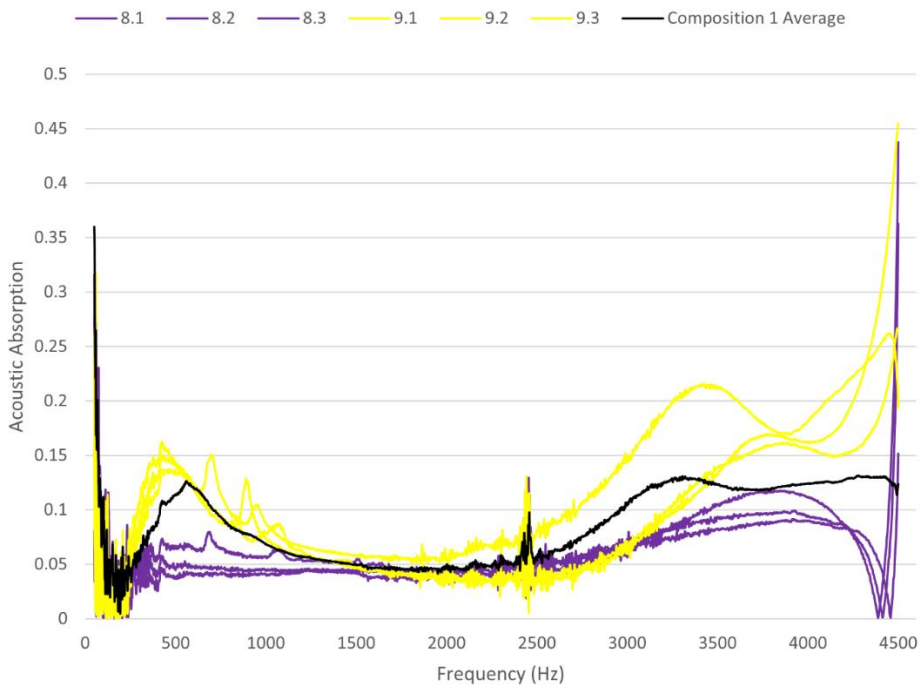

Figure 5-13: High Frequency Acoustic Absorption Measurements of 5F Concretes

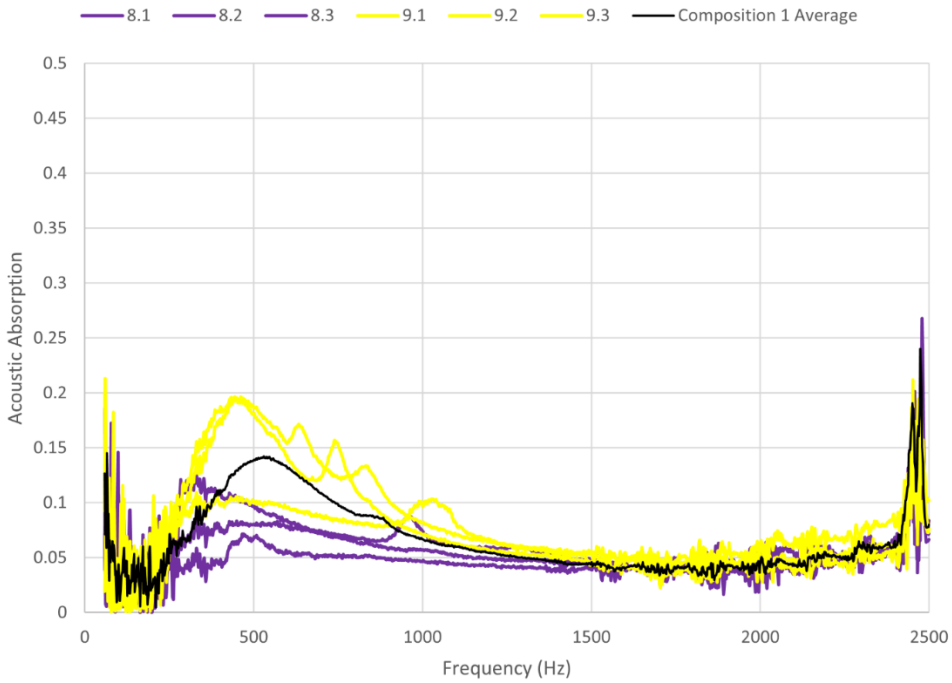

Figure 5-14: Low Frequency Acoustic Absorption Measurements of 5F Concretes

5.1.6 Impacts of AE Admixtures

By comparing each non-AE composition to its counterpart containing AE, the effects of AE on absorption can be examined. Inconsistency on how the AE affected final absorption results was noticed in compositions 2 and 7 where they performed worse than their non-AE counterparts. Further, while each comparison related absorption to composition 1 values, a more in-depth examination of fiber impact on absorption is required. This was done by comparing compositions without AE to one another showing how fiber form impacted absorption values. The same was done with compositions containing AE. These relationships are examined under both the small and large frequency ranges mentioned earlier.

Examining compositions without AE, acoustic performance are determined by comparing to composition 1 (Figure 5-15 and Figure 5-16). Only composition 8 containing 5F was found to have absorption values below those of composition 1 across all frequencies. Composition 6.3 was found to have absorption values equivalent to or only marginally better than composition 1 at lower frequencies. This similarity in absorption values between compositions 1 and 6.3 supports the conclusion that an increased concentration in concrete lowers absorption values, since very little improvement was observed in 6.3 even when using 2F fibers. Composition 3 was found to be only slightly more absorptive (0.042 greater) at lower frequencies when compared to composition 6.3. However, composition 3 had absorption values greater than those of 6.3 as frequencies increased into the higher frequency range, up to 2864 Hz. In fact, as the higher frequency limit was approached, composition 3 fell below the absorption values of base concrete, dropping to as low as 0.101. 6.3 also fell below the composition 1 threshold as the higher frequency limit was reached. Composition 4, containing SD, and 6, containing 2F, boasted the highest absorption values

of compositions without AE. At lower frequencies, composition 6 boasted higher absorption than 4 during initial peaks. Further, while both 4 and 6 plateaued, values were very similar. Composition 4's average peak was only 0.006 more absorptive than 6. Composition 6 reached the highest average absorption value of all compositions at 0.246 while approaching 4466 Hz. Of all the non-AE compositions, 2F and SD provided the best absorption values, with SD being better in the low frequency range and 2F in the higher frequency range. Therefore, compositions 4 and 6 best enhanced wood-aggregate concretes for acoustic absorption when considering constant F/C ratios.

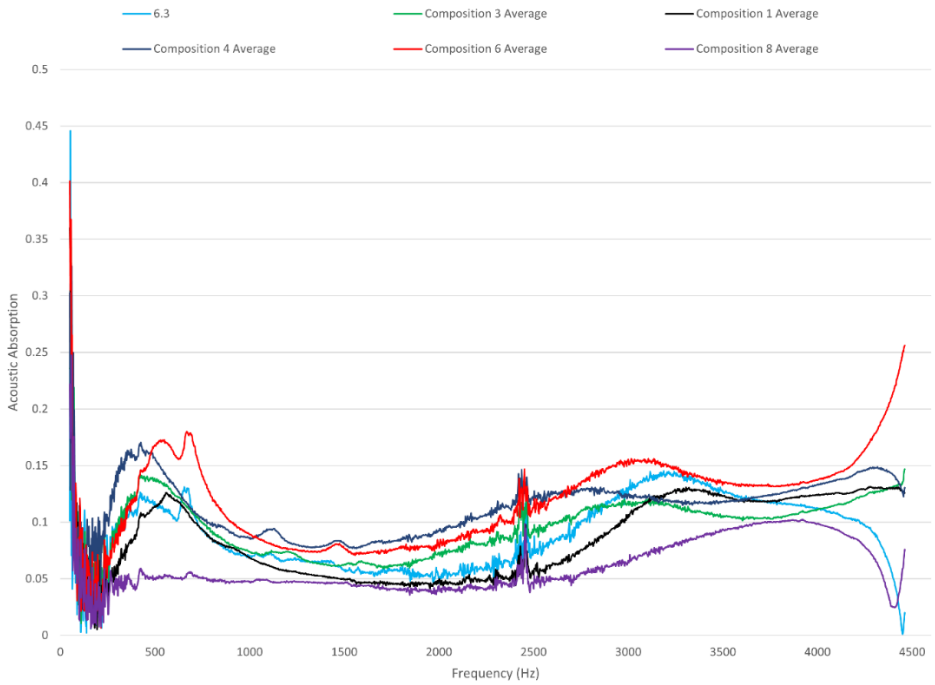

Figure 5-15: Average High Frequency Acoustic Absorption Measurements of Non-AE Concretes

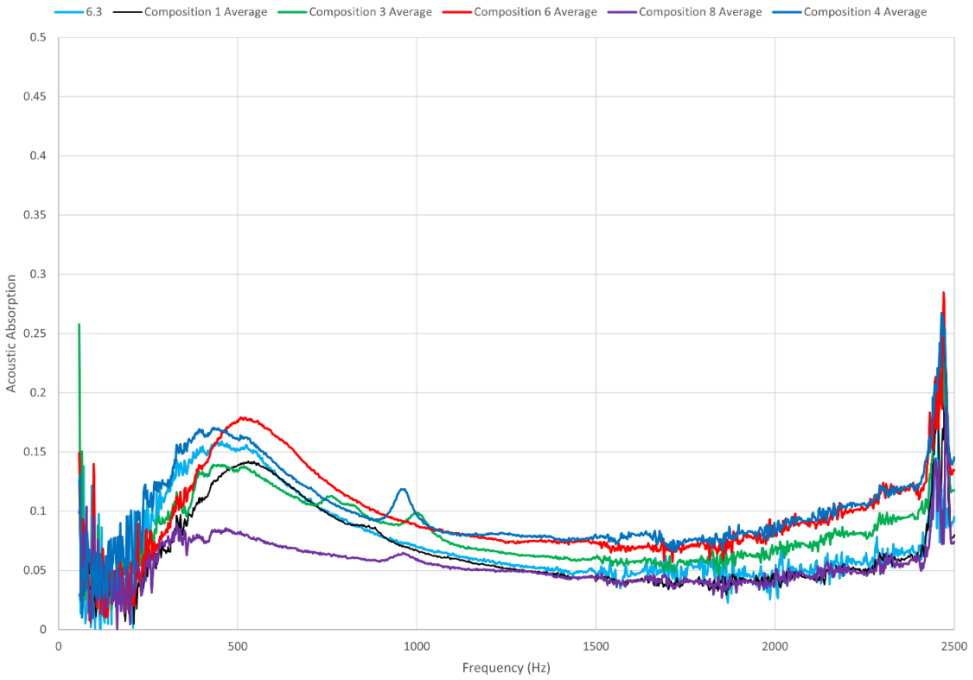

Figure 5-16: Average Low Frequency Acoustic Absorption Measurements of Non-AE Concretes

Examining AE compositions, similar results regarding optimum fibers are found (Figure 5-17 and Figure 5-18). Absorption performance of AE compositions were compared to the performance of composition 2. As noted earlier, composition 2 boasted lower absorption values than composition 1, its non-AE counterpart. At lower frequencies, all compositions boasted larger initial peak values than composition 2. Composition 10 reached the highest initial peak absorption value of 0.232. As frequency approached 2500 Hz and values plateaued, all compositions boasted higher absorption values than 2, other than composition 9. Compositions 10 and 7 peak absorption values exceeded composition 2, but only marginally. Composition 7 reached a peak plateau value of 0.081, while 10 reached 0.091, less than 0.02 greater than composition 2's plateau peak of 0.076. This is interesting given the impressive absorption values boasted by 10 at the initial peak. Compositions 7 and 9, containing 2F and 5F respectively, boasted the lowest absorption at low frequencies.

Composition 5 boasted significantly higher absorption values than all compositions as values plateaued. Specifically, as the frequency approached 2500 Hz, values consistently increased as frequency increased, and absorption reached 0.150. Entering the higher frequency range, composition 9 and 10 began to increase sharply. Composition 10 rose until matching the absorption values of composition 5, while composition 9 exceeded all other compositions as frequency increased. Compositions 5 and 10 reached a high frequency peak of 0.150 and 0.155, respectively, until the upper limit was reached. At this point, composition 5 increased sharpy to 0.207, while 10 only reached 0.170. Composition 7 increased slightly, but remained the least absorptive, only marginally exceeding composition 2. Composition 9 remained below composition 2 until steeply increasing at 2800 Hz, then peaking at 0.169 at 3762 Hz. Values then plateaued until the frequency range limit, where composition 9 boasted the highest absorption at 0.278. Based on these results, it is evident that composition 5, containing SD fibers, boasted the greatest absorption values over the largest frequency range. This matches the results found for samples without AE where composition 4 (also containing SD) boasted the highest absorption values. Of note, between 500 Hz and 1000 Hz, composition 10 also boasted good results with relatively high mid frequency values. Composition 7 further verified the effects of an increased concrete concentration on lowering absorption values, as displayed by the measured values. Had 2F fibers been examined under the same F/C ratios as composition 6, it would be expected that this composition would also boast high absorption values, as seen in composition 6. Interestingly, composition 9, while boasting the lowest absorption values, proved to be very effective at absorption in the higher and lower ends of the frequency range examined.

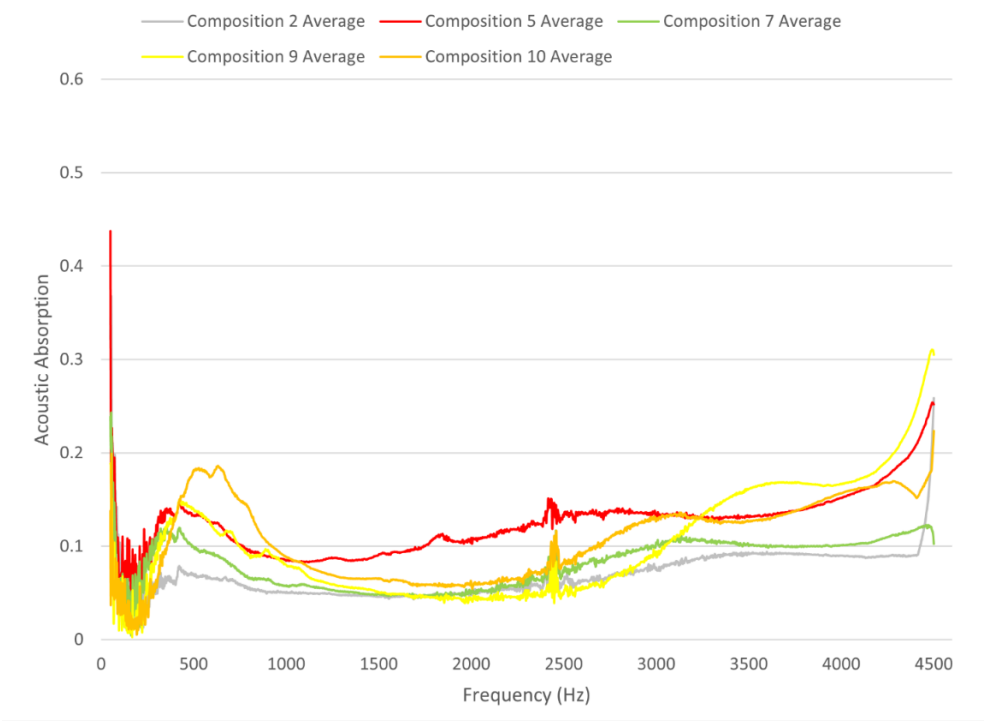

Figure 5-17: Average High Frequency Acoustic Absorption Measurements of AE Concretes

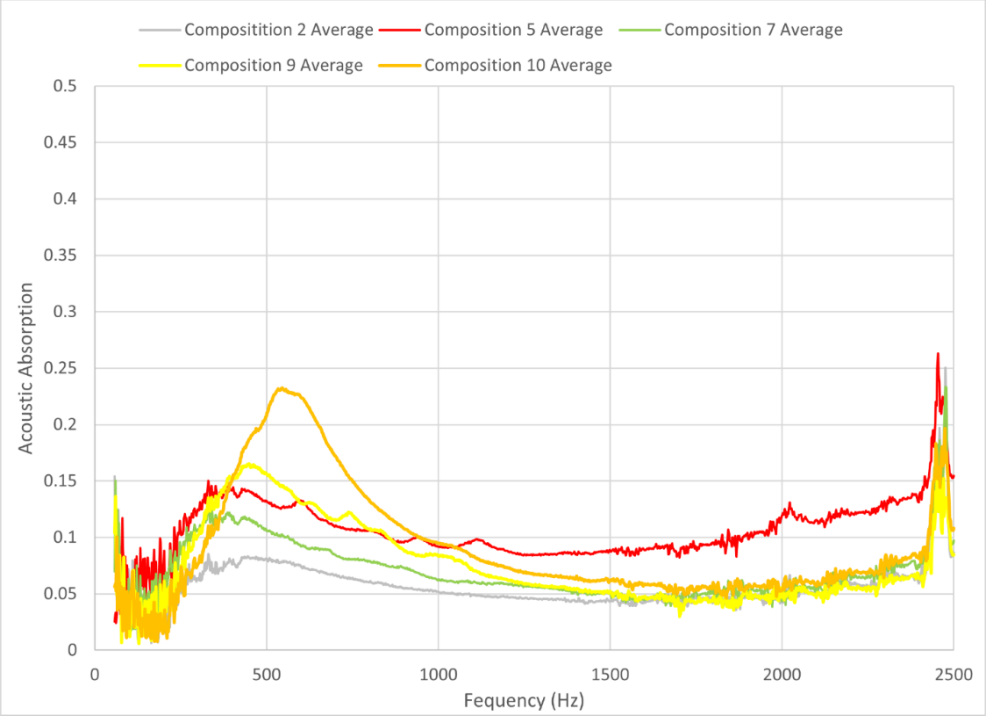

Figure 5-18: Average Low Frequency Acoustic Absorption Measurements of AE Concretes

Based on the results of impedance tube testing, composition 5, containing AE and SD, is the most absorptive concrete composition over the largest frequency range. Further, when compared to other fiber compositions, SD is the most absorptive in samples both with and without AE over the largest frequency range. A conclusion on the effect of using AE in the samples cannot be reached due to its inconsistent effect observed in the samples. Specifically, while AE was observed to increase absorption in compositions 5, 9, and 10 when compared to their non-AE counterpart compositions, compositions 2 and 7 saw a decrease in absorption relative to their non-AE counterpart compositions. While compositions 4 and 5 boast the highest absorption values across the largest frequency range, it is worth noting that some compositions boast higher absorption values at specific frequencies. For example, should a sample require better absorption above 3000 Hz, composition 6 would be a better composition. How the absorption of each composition relates to the material properties of each sample will be discussed in Chapter 6.

5.2 Model Results

Utilizing the hybrid DBz-JCAL model, acoustic absorption predictions for all samples containing wood fibers were calculated. Estimated acoustic absorption values were all found to follow a similar trend in which absorption values at lower frequencies (approaching zero) were found to be near zero. This, as mentioned in the limitations of the model, is to be expected since the DBz model is limited to a lower frequency of 171.8 Hz (see Table 3-2). Moreover, prediction of the dynamic properties at lower frequencies is not accurate in the JCAL model either [53], [54]. The upper frequency limit imposed on the estimations is 4600 Hz. This is to allow for simple comparison between the measured and estimated values, as the upper limit on the measured values was 4466 Hz. As frequencies increased, absorption increased over all frequencies. However, the rate of increase

decreased upon reaching 3000 Hz. It is worth noting that due to the method in which the airflow resistivity is estimated (by utilizing fiber radius and density), estimations of acoustic absorption for compositions 1 and 2, those without aggregate fibers, were not made. Results discussed in this section are for absorption only, a discussion related to the calculation of the complex variables and their potential impact on results will be examined in Chapter 6. Further, while impedance tube results will be mentioned in this section, comparison between the model and impedance tube results will also be discussed in Chapter 6.

5.2.1 FSD Concrete

Estimations of compositions 3 and 10, those containing FSD without and with AE, respectively, estimate absorption of composition 3 to be greater than 10 (Figure 5-19). Further, across all frequencies, absorption is found to only increase, although the rate of increase plateaus as the frequency exceeds 2000 Hz. Examining the average absorption estimations, composition 3 reaches a peak absorption of 0.22, while 10 reaches 0.19, a difference of 0.03. While averages provide an overall estimate on the compositions, the values are not always consistent making the averages less accurate in their representation of the material. The variation in absorption estimates stems from sample porosity across different samples. While each sample of a given composition is made of the same volumetric ratios of fibers, water, cement, and potentially AE, porosity values still vary due to the complex nature of the concrete curing process. Regarding composition 10, values vary widely relative to other compositions. Maximum absorption values peak between 0.168 and 0.215 across composition 10 samples due to the variance between porosity values, which ranged from 10.7% to 14.0%. In contrast, composition 3 sample porosities fell within 1% of

one another, as seen in Table 4-1. Interestingly, despite containing AE, composition 10 is estimated to be less absorptive and has a lower measured porosity.

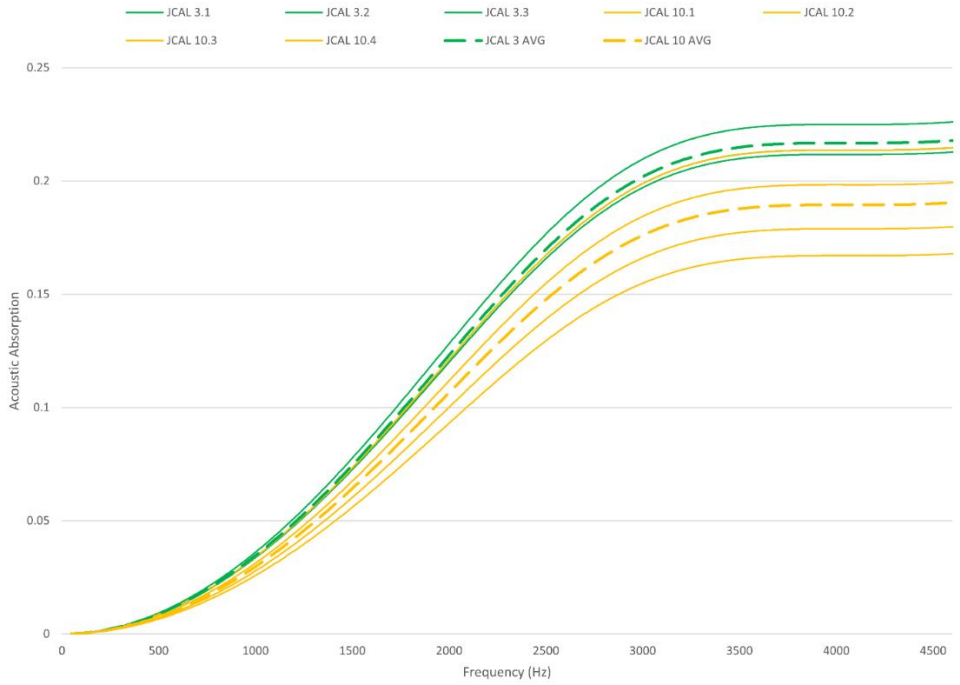

Figure 5-19: JCAL Acoustic Absorption Estimates of FSD Concretes

5.2.2 SD Concrete

Examining compositions 4 and 5 containing SD fibers, composition 5 is shown to have a lower acoustic absorption than composition 4 (Figure 5-20). Like compositions 3 and 10, the composition without AE is estimated to be more absorptive than that with AE. AE was accounted for through the input of porosity values of the samples into the model. While the AE additive should theoretically bolster the porosity of composition 5, the average measured porosity of composition 4 is found to be 3.75% higher than 5. Since the primary input used for estimating absorption is porosity, the samples with higher porosity are projected to be more absorptive. A change of only 1% in porosity can have a noticeable effect on the absorption estimation. Composition 4 reached an average peak of 0.250, while 5

reached an average peak of 0.199. The overall trend in the JCAL estimations for SD concretes is similar to that of FSD, whereby values continuously increased with frequency. However, the rate of increase decreases significantly as frequencies approach the higher frequency range. Naturally, as absorption values for SD are higher than those for FSD, the rate of increase is slightly higher for compositions 4 and 5.

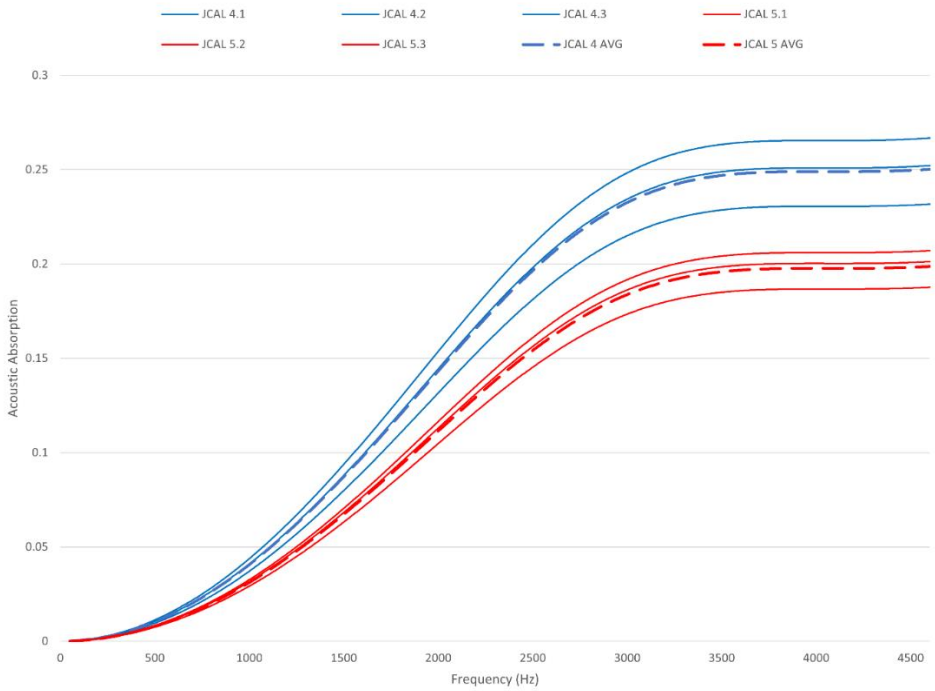

Figure 5-20: JCAL Acoustic Absorption Estimates of SD Concretes

5.2.3 2F Concrete

Figure 5-21 provides results for compositions 6 and 7. While all other sample compositions used the same F/C ratio, composition 6 is broken into two compositions based on concrete concentrations. 6.1 and 6.2 share the same F/C ratio as the other compositions, while 6.3 has decreased F/C and W/C ratios. Composition 7 has the same decreased F/C and W/C ratios, but with the inclusion of the AE additive. By increasing the amount of concrete in the sample, the porosity of the sample is decreased, which results in a lower estimate of

absorption. All samples followed the same trend of constant absorption increase across all frequencies. Composition 7 provides the lowest acoustic absorption that, based on the model's calculations, makes sense since it also has the lowest porosity. Reaching an average peak absorption of 0.115, composition 7 is 0.047 less than the average peak absorption of composition 6 at 0.162. Further, sample 6.3 at 0.158 has a lower absorption than 6 but is still quite absorptive relative to composition 7. While the calculated acoustic absorption values do not match those of the measured absorption values, the acoustic performance of the 2F compositions relative to one another mimics that of the 2F compositions' impedance tube data.

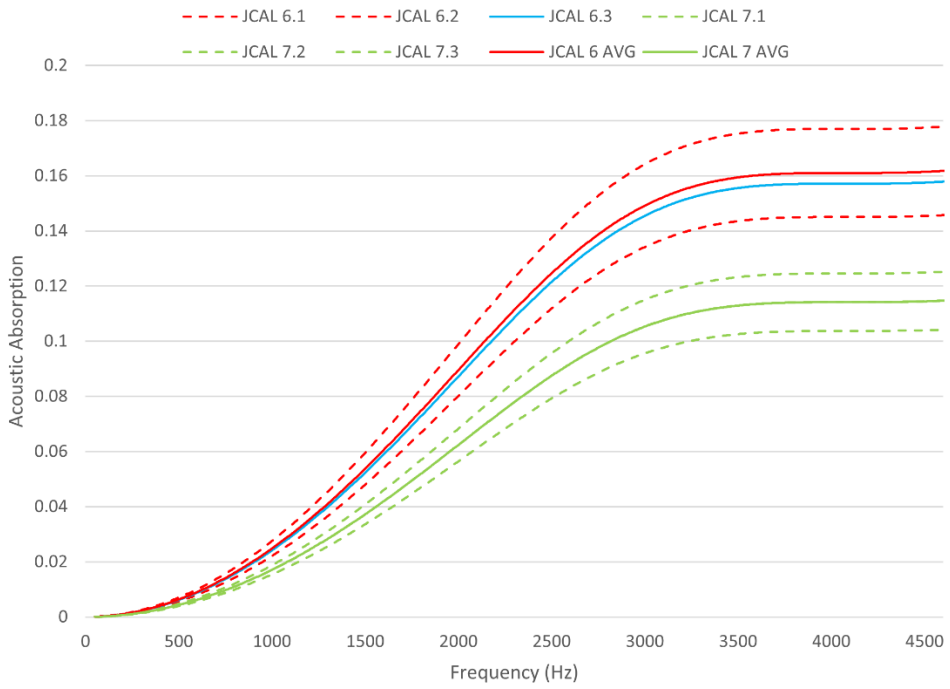

Figure 5-21: JCAL Acoustic Absorption Estimates of 2F Concretes

5.2.4 5F Concrete

Samples containing 5F had the least absorptive results (Figure 5-22). Estimations for both compositions 8 and 9 reached peak average absorptions of 0.104 and 0.095,

respectively. Absorption estimations of samples for both 8 and 9 remained within 0.01 of one another, except for 9.2, which had a porosity of 4.8%, nearly 2% less than the porosity values of the other samples of 8 and 9. Overall, composition 8 is found to be more absorptive than composition 9. Once again, this is not expected, since the inclusion of AE in composition 9 should bolster porosity, which in turn should bolster the absorption estimates, as per the model. Further, it is worth noting that the estimations for compositions 8 and 9 do not follow the trend of the measured results. In the impedance test, composition 8 is observed to be the least absorptive material of all compositions, whereas using the model it is estimated that 9 is marginally less absorptive than 8.

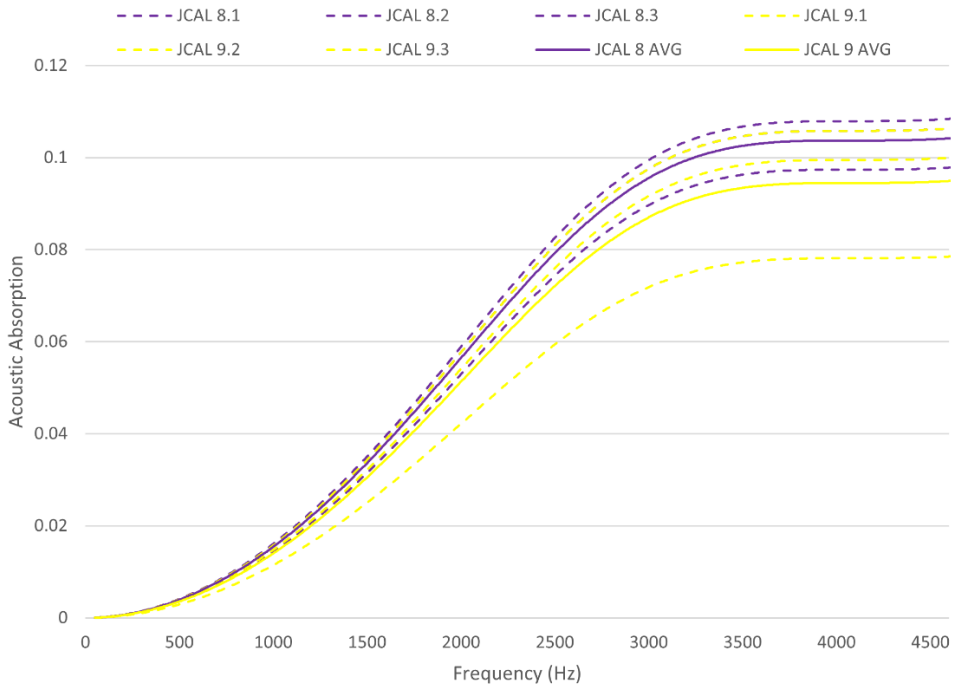

Figure 5-22: JCAL Acoustic Absorption Estimates of 5F Concretes

5.2.5 Impacts of AE Admixtures

When comparing the averages of all compositions, absorption is found to increase when the frequency increases, in general. As was done in the impedance measurement section,

composition averages will be compared to one another in two groups: without and with AE. Examining those without AE first, it is seen that composition 4, containing SD, was predicted to be the most absorptive of the compositions by a significant amount, reaching a peak absorption of 0.250 (Figure 5-23). Composition 3 was found to be the next most absorptive at 0.22, a difference of 0.03 absorption when compared to composition 4. Compositions 6 and 6.3, containing 2F, boast nearly identical absorption trends with the difference between peaks being less than 0.004. Average peak absorption values for 6 and 6.3 were estimated at 0.162 and 0.158, respectively. This is interesting given that 6.3 has a higher concrete concentration than 6. However, porosity values between the two are similar enough that the absorption estimates provided are nearly identical. By a large margin, composition 8 was estimated to be the least absorptive of the non-AE compositions, reaching a peak absorption of only 0.104.

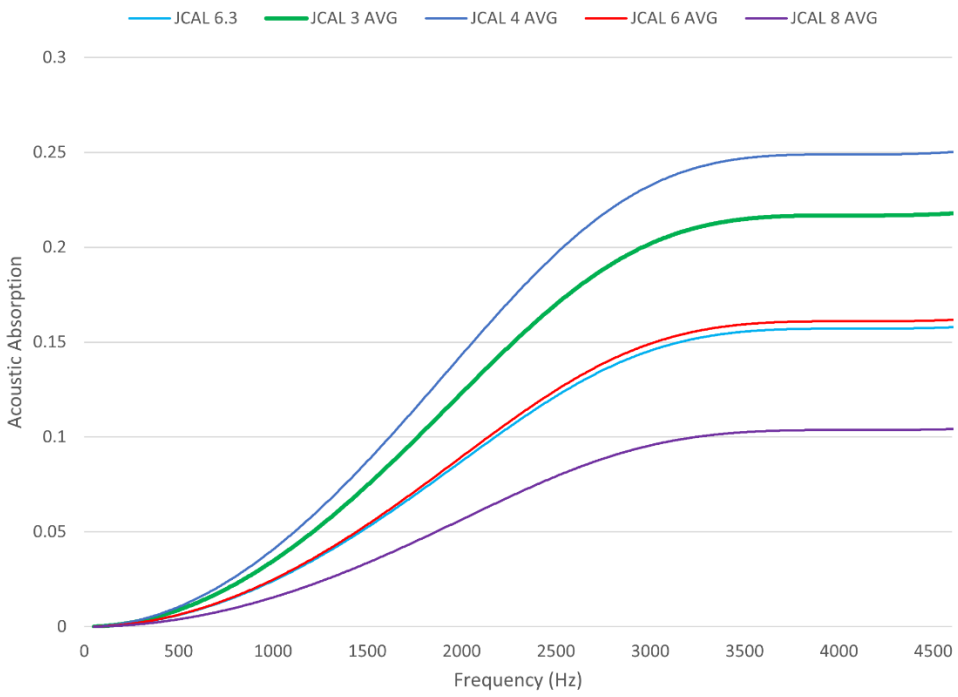

Figure 5-23: Average JCAL Acoustic Absorption Estimates of Non-AE Concretes

Finally, examining the estimations for those compositions containing AE, the following results were found (Figure 5-24). Compositions 5 and 10 boasted the highest estimations, with peak absorption values falling within less than 0.01 of each other. Composition 5, was found to be slightly more absorptive than 10, having a peak average absorption of 0.199, while 10 peaked at an average absorption of 0.19. Composition 7 was then found to boast the next lowest absorption values, reaching a peak average absorption of 0.115, significantly lower than composition 5. This large difference in acoustic performance was expected, as composition 7 had both a higher concrete concentration, as well as very low porosity values. Composition 9 was found to be the least absorptive, reaching a peak of 0.095, the lowest value of any composition, with or without AE.

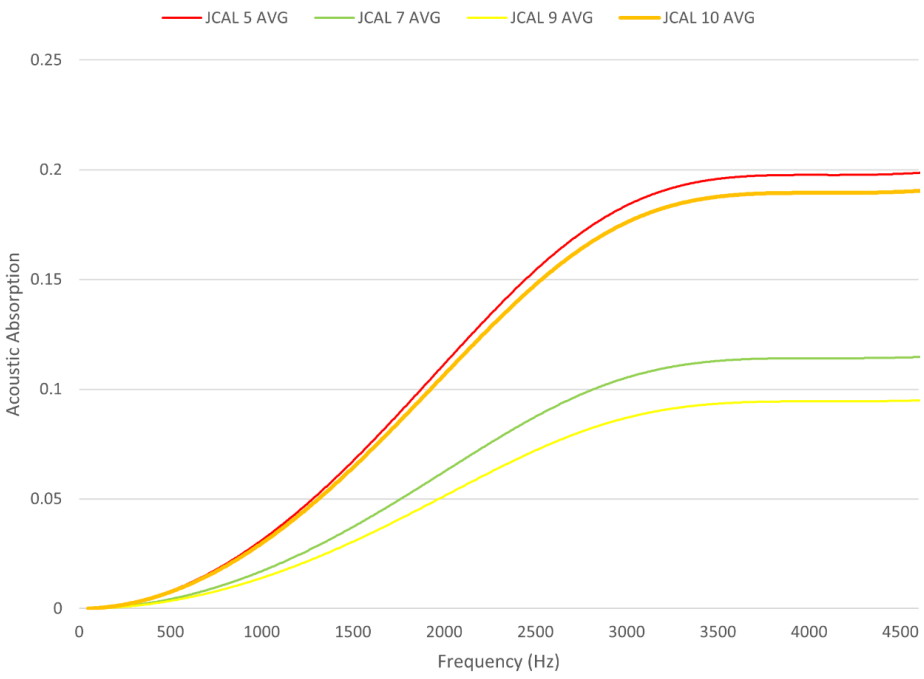

Figure 5-24: Average JCAL Acoustic Absorption Estimates of AE Concretes

Estimates made using the hybrid DBz-JCAL model, within the acceptable frequency range, are not particularly accurate over the entire range. However, there are similarities worth noting. The limits of both the model and the impedance tube data are noted in Table

3-2 and Table 4-2, respectively. Their shared acceptable range is between 1760 Hz and 4466 Hz. When comparing calculated estimations and experimental measurements, consistency between compositions varied widely across compositions, making conclusions about their relationships difficult (Figure 5-25 and Figure 5-26). However, within the acceptable data range, all absorption values obtained from both the model and impedance tube measurements remained below 0.3. This reveals that, while specific values at a given frequency are not particularly useful, the model does reflect, to some degree, the low absorptive properties of the concrete. This observation is substantial, as it reveals that there may be potential for improving the model to better represent wood-infused concretes. Furthermore, conclusions can be made based on specific trends and discrepancies between the measurements and estimations of individual compositions. This will be covered in Chapter 6.

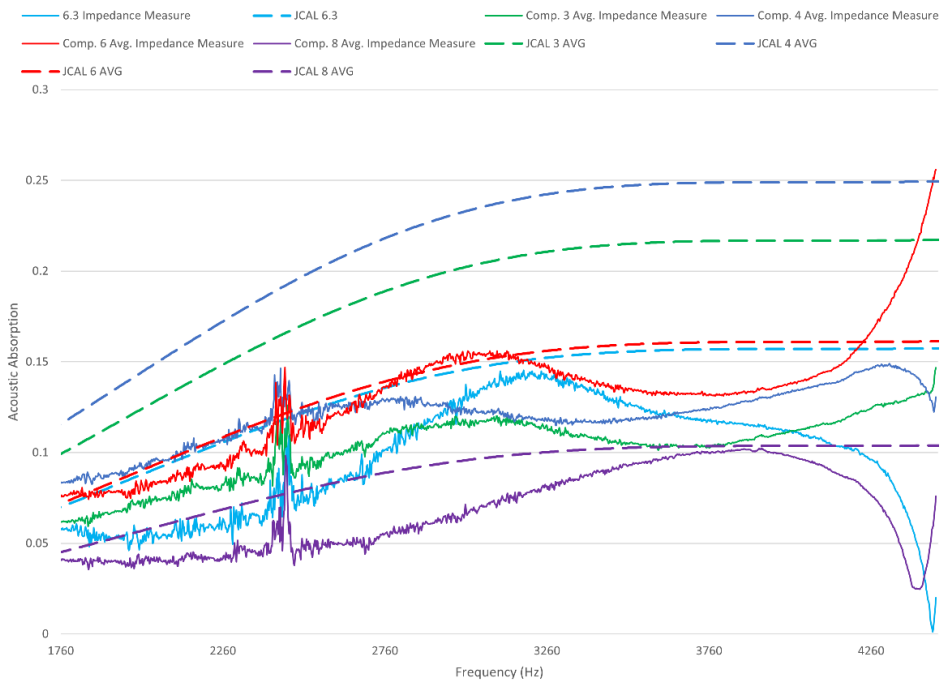

Figure 5-25: Comparison of Estimated and Measured Absorption of Non-AE Concretes

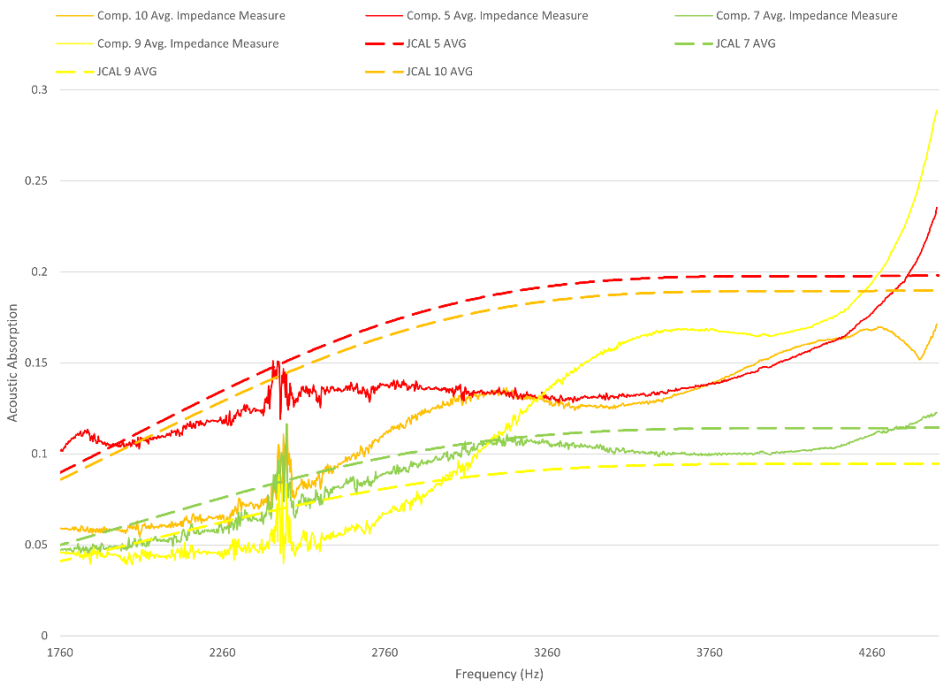

Figure 5-26: Comparison of Estimated and Measured Absorption of AE Concretes

Chapter 6

Discussion

While the DBz-JCAL model estimations and impedance tube measurements do not align exactly, they both provide interesting insight on the potential for making fibrous concrete absorption estimates. Within this section, the overall trends in the data, exact values, and effects of the varying material properties on absorption estimates and measurements will be examined. Given the imposed lower frequency limit of the DBz model and the higher frequency limit imposed by the impedance tube, comparisons will only be made in the frequency range of 1760 Hz and 4466 Hz.

Ability to predict real cement composition absorption values is, obviously, a significant factor in verifying the validity of the model. By comparing the average estimated and measured values between samples, the accuracy of the model will be discussed. When comparing, not all estimates were as accurate as others, and in most cases, the model estimated absorption values greater than those measured. First, considering compositions containing FSD (Figure 6-1), differences between estimated and measured absorption values for compositions 3 and 10 were found to be between 24.3% and 52.6%, and 9.7% and 54%, respectively. At its peak, the maximum difference between estimation and measurement for composition 3 is 0.11, a significant amount. Interestingly, given the resistivity value used was found using the radius of FSD, it was expected that these trials

would be the most accurate. Table 6-1 summarizes the differences between the estimates and measurements.

Table 6-1: Summary of Estimate and Measurement Results

Composition #	Peak Measured Absorption	Peak Absorption Difference	Model Maximum Error	Model Minimum Error
3	0.15	0.11	52.61	24.30
4	0.15	0.13	52.77	24.37
5	0.24	0.07	33.68	0.24
6	0.26	0.09	58.72	0.12
6.3	0.14	0.16	99.20	4.96
7	0.12	0.02	26.71	0.04
8	0.10	0.08	76.18	1.46
9	0.29	0.19	205.00	0.10
10	0.17	0.07	54.05	9.76

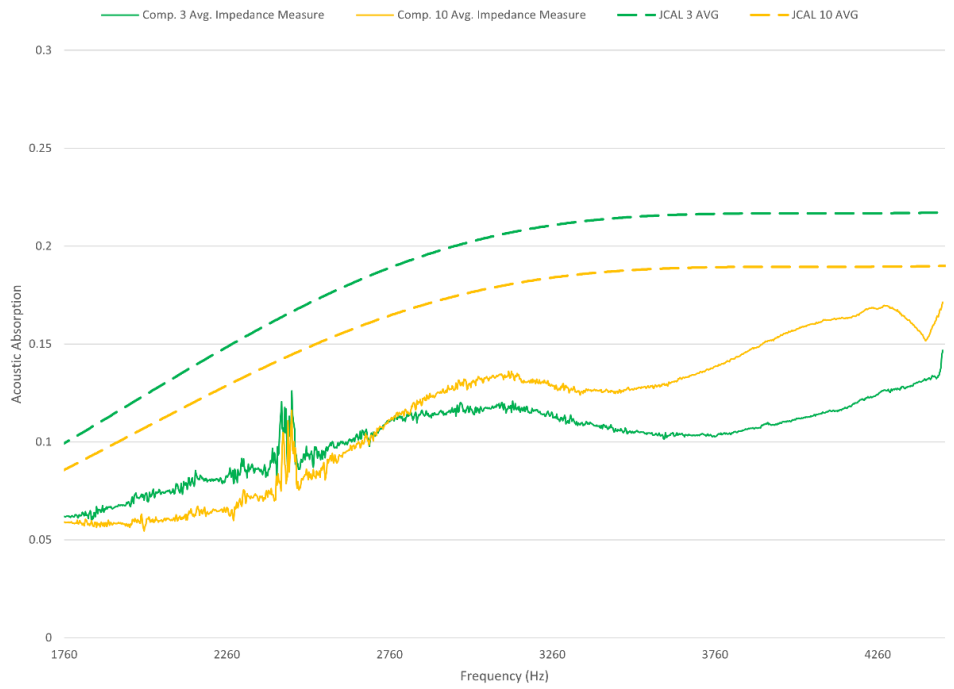

Figure 6-1: Comparison of Estimated and Measured Absorption of FSD Concretes

Compositions 4 and 5, containing SD, had similar discrepancies (Figure 6-2). While composition 5 estimates were more accurate than composition 4, estimates still overshot peak absorption by a significant amount. Perhaps most inaccurate, composition 4 boasted a

minimum and maximum difference of 24.4% and 52.8%, respectively. Composition 4 estimates were up to 0.130 greater than measured values. Composition 5 was slightly more accurate. However, as frequency increased, estimated accuracy decreased.

Figure 6-2: Comparison of Estimated and Measured Absorption of SD Concretes

Compositions 6, 6.3, and 7, those containing 2F, had varying levels of accuracy in their respective absorption estimates (Figure 6-3). While the estimations for 6.3 provided high values when compared to those measured, composition 6 and 7 were fairly accurate. In fact, composition 7's minimum and maximum difference values were 0.038% and 26.7%, significantly lower than the SD compositions. Further, composition 6 and 7 estimates did not overestimate values, as was seen in the FSD and SD composition estimates. Of note, while 6.3 estimations were higher than measured values, measured peak absorption estimates and measurements were equivalent.

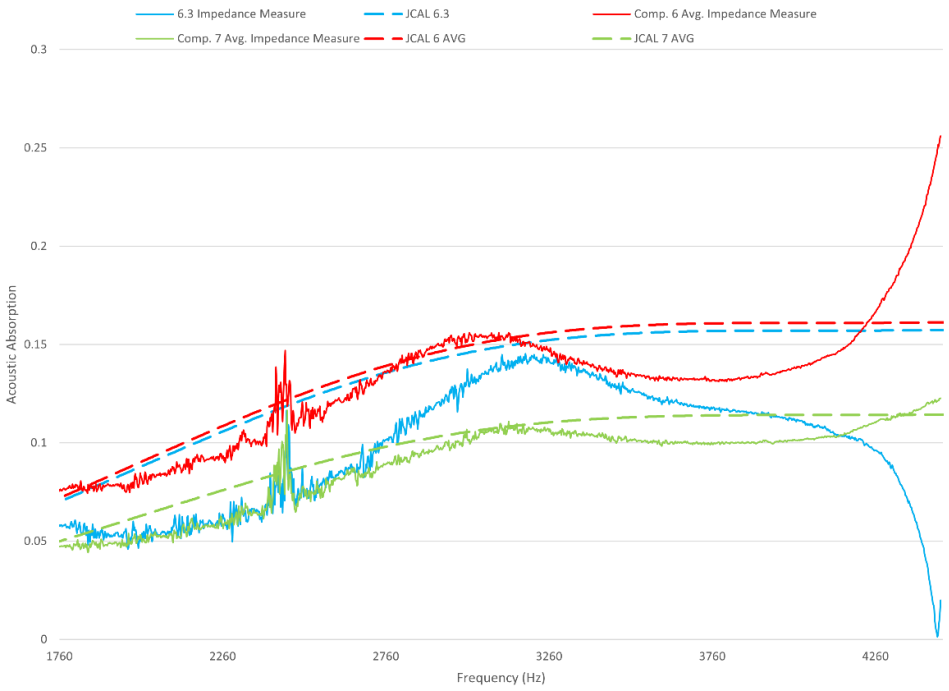

Figure 6-3: Comparison of Estimated and Measured Absorption of 2F Concretes

Looking at those compositions containing 5F (Figure 6-4), composition 8 estimates were found to overestimate absorption values until measurements reached peak absorption, at which point both estimations and measurements were equal. While composition 9 showed good initial estimates, measured values increased drastically at 2800 Hz, and thus, estimate differences increased as well. It is worth noting that sample 9.2 is the cause of this increase, as its values are higher relative to samples 9.1 and 9.3.

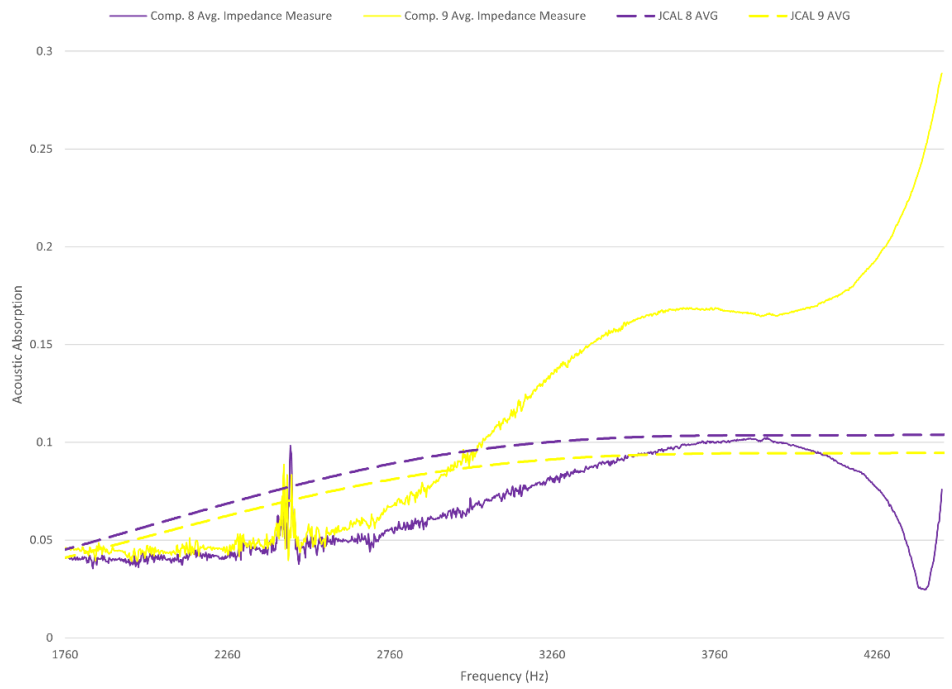

Figure 6-4: Comparison of Estimated and Measured Absorption of 5F Concretes

Three general trends were noticed in the data: good estimation, overestimation, overestimation until a high frequency peak. Unfortunately, due to variations in these trends, conclusions regarding the accuracy of the model's representation of the true acoustic absorption for each composition are not currently possible.

While exact values predicted by the model were not accurate, examining the overall trends in both estimated and measured values can provide insight on each process. In fact, while the model predicts a consistent mathematic relation, this consistency reduces accuracy due to the staggered nature of the absorption measurements. Potential sources for error in estimates can be noted throughout the calculations. First, while the estimated value for resistivity used is more reflective of concrete resistivity values than those found using other fiber radiuses, it is unlikely to be reflective of all composites [40], [57]. During model testing, it was found that by increasing resistivity values, lower absorption values were predicted. Therefore, for those compositions with excessively high absorption

estimates relative to measured values, 3, 4, 5, and 6.3, this could be a factor in their error. It was also noticed that as resistivity values decreased below a magnitude of 10^4 Ns/m^4, the overall trend in absorption values changed. This is important because concrete resistivity values fell within the range of 10^3 and 10^4 Ns/m^4. As resistivity values fell below 10^4 N/sm^4, a dip in absorption was noticed as values reached the higher frequency range before continuing to increase. Moreover, when comparing estimated higher limit tortuosity to the tortuosity values of hemp concrete projected by Glé et al., estimates were low [40]. In fact, tortuosity was estimated to be 1.0 for the wood-aggregate concretes, the same value found for many vegetable wools, implying pore geometry is like that of wools, which in reality it is not [40]. In fact, tortuosity values were projected to be 4.4 and 4.7 for the two hemp concretes used by Gle et al., suggesting that the estimates used in the DBz-JCAL model oversimplified the pore shape [40]. Like increasing the resistivity value, increasing the tortuosity value caused absorption values to decrease substantially. For example, increasing tortuosity values from only 1.0 to 2.0 caused absorption estimates to drop from a peak of 0.19 to 0.14. Proportionally decreased values were noticed across all other frequencies.

Although exact values of absorption were inaccurate, model data trends across all samples predicted correctly that net absorption increased as frequency increased. For the accepted frequency range shared between the model and the impedance tube, model estimations provided limited insight on general acoustic performance as frequency increased. Interestingly, while the shape of the estimated absorption trend line changed as resistivity values fell below the 10^4 Ns/m^4 threshold, net increase in absorption was still predicted. Beyond the accepted frequency range in which data was compared, the estimated trend and measured values varied significantly across compositions, as expected due to limitations.

While comparing the trends and exact absorption values between estimated and measured concrete compositions is important in determining the model's ability to predict the performance of individual samples, the ability to compare varying compositions to one another is also important. When considering the lower frequency range, the model accurately predicted which of the compositions were least absorptive, those being 8, 9, 6.3, and 7. However, the model predicted that 8 would be more absorptive than 9 when the opposite was found in the measured data. The remaining compositions, while both measured and estimated to be more absorptive, were not found to be well represented by the model. Examining the measured values at lower frequencies revealed that composition 5 was most absorptive, with 4, 6, 3, and 10 following suit in descending order. On the other hand, the model found 4 to be most absorptive with, 3, 5, 10, and 6 following suit in descending order. Therefore, at low frequencies, estimated absorption values did not accurately depict acoustic performance across all samples. However, when estimated absorption values were separated into compositions with and without AE, all but compositions 3 and 6 were found to be in the correct order of absorption at low frequencies. As such, the model was able to estimate correctly that utilization of SD fibers provided the most absorptive concrete composition in the low frequency range, that 5F was the least absorptive, and in AE samples, that FSD was more absorptive than 2F, especially in composition 7 of higher concrete concentration. While this is non-conclusive in verifying model accuracy, it is worth noting that the model was able to differentiate performance between samples, to a degree, at low frequencies. When examining the higher frequency range, due to the uniform trend of the estimated absorption, estimations were less accurate, as measured absorption values changed more drastically at higher frequencies. For example, while the measured order of most absorptive to least absorptive compositions are consistent across the low frequency range, as frequency increased beyond 2600 Hz, the

order changed drastically as compositions increased and decreased at varying rates. The estimated absorption values maintained the same order of most absorptive compositions across the entire frequency range examined due to the nature of the relations used.

Incorrect comparisons were likely a result of the model basing estimated absorption values primarily on porosity. While those samples of a higher porosity were measured to be comparatively more absorptive, generally, material density was noticed to impact absorption significantly in the measured values. For example, across all frequencies, composition 6 was measured to be more absorptive than composition 3 despite being 4% less porous. Of note, these two compositions are also the two non-AE compositions predicted incorrectly as to which was more absorptive, as seen in Figure 6-1 and Figure 6-3. Further, all compositions in the lower frequency range that boasted densities greater than 1400 kg/m^3 were found to be the least absorptive. It is worth noting that composition 10, despite having both high porosity and low density, was found to perform only marginally better than the denser compositions in the low frequency range. While the correlation between density and absorption was seen at lower frequencies, at higher frequencies a relation of density or porosity to measured absorption values became less apparent as absorption trends became less consistent. For example, composition 9, the least porous and second most dense composition boasted the highest absorption between 3300 Hz and 4466 Hz. As a basis for acoustic performance, the lower frequency range was deemed to be a more accurate representation due to more data being available from both M1-M2 and M1'-M2 microphone setups.

These results demonstrate that the model's current ability at predicting acoustic absorption is not great. However, the potential for improvement can be isolated to specific issues within the model. How these improvements could be developed and final conclusions are discussed in the following section.

Chapter 7

Conclusions and Future Work

7.1 Conclusions

While the methods used in the model are of empirical and semi-empirical sources, acoustic absorption estimations of the constructed concretes were not as accurate as expected. After performing experimental tests and examining the results, it was found that future work is required to improve the model.

Based on the results found when comparing model estimates to the measured values, the model does not provide an accurate estimation of acoustic absorption for fibrous concretes, nor does it consistently represent the complexities of the data trends in the measured absorption values. However, estimated absorption values were within the same general range as measured values. While the accuracy of the model was non-conclusive, the model showed potential in discerning acoustic performance relative to other compositions, as well as estimating general absorption trends. Interestingly, variations found between measurement and estimation across compositions did not appear to prioritize the same material properties. Specifically, estimations prioritized porosity as the limiting factor on acoustic performance, while impedance measurements showed that density of the material had a more impactful effect on absorption. Nonetheless, samples of a higher porosity boasted lower density, indicating a potential relationship between the two. While the two

variables may have a correlation when considering fibrous concretes, both the simplistic nature of the estimations made by the model and the lack of focus on density in calculations could be of detriment to the model and the accuracy of its estimations.

Beyond material density, other material properties that were found to be inaccurate, when compared to the literature, were airflow resistivity and tortuosity. Airflow resistivity values were initially predicted using the Tarnow method, which were found to hinder estimation accuracy [48]. The Tarnow method of estimating resistivity not only misrepresented the fiber arrangement and orientation, but also failed to meaningfully take into account that fibers were embedded in concrete [48]. This was found when inputting the varying values of fiber radius into the Tarnow model. Only the smallest fiber radius, FSD, returned values that were deemed realistic. The FSD resistivity values were, therefore, the only ones used in estimating the other resistivity values in Table 3-2, and misrepresented the properties of the concrete. These values also provided an impractical limitation on the DBz frequency limits, nullifying any potential practical acoustic property estimates. The tortuosity value estimations used in the model were also found to be inaccurate based on the literature, as they were lower than what was to be expected. This is important, as tortuosity defines the overall pore shape, or ease in which air flows through pores, and therefore, is significant in estimating the acoustic interactions of the material surface. Estimations were found to approach 1.00, a value more representative of traditional textiles and wools, while concrete values are estimated to be within the range of 4.0 to 5.0, and therefore, are less absorptive and have more complex pore shapes [40]. These low estimations were due to the JCAL model, which is generally used in predicting acoustic absorption of traditional textiles and wools.

Overall, while the use of the hybrid DBz-JCAL model was shown to provide reasonable estimates of the acoustic properties of fibrous materials in other studies, it failed to do so

with accuracy for fibrous concretes. Acoustic absorption values, based on the comparison of empirical data to model estimates, are generally overestimated at lower frequencies and do not accurately represent absorption values with any consistency at higher frequencies. Based on the data used in this study, there is potential in the model to provide relative comparisons on the acoustic performance of fibrous concretes across different compositions. However, further work would be required to quantify the comparisons. Further, the model's basis for estimating acoustic absorption is heavily weighted on the porosity of the fibrous concrete, while measurements of acoustic absorption show that density of the sample is likely more influential on acoustic performance. Unfortunately, density does not impact final estimates to a significant degree in the model's current state. The accuracy of the complex viscous and thermal property estimations is important as well, as they are the primary factors in estimating acoustic absorption, and in the model's current state, are not particularly representative of the concrete and have not been quantitatively verified in this study. Specifically, air flow resistivity estimation accuracy should utilize more information regarding the surface geometry of the concrete, as opposed to just the fibers. Higher limit tortuosity values also are lower than expected and provide a representation of the concrete pores that is oversimplified.

7.2 Future Work

Due to shortcomings in the model, improvements should be made to address them. Specifically, a greater representation of the concrete properties should be incorporated into the model. First, alterations to how the model handles material or acoustic properties should be examined in detail, and should be made to better represent density in the final absorption values. To improve model performance beyond density, further investigation into concrete airflow resistivity should be conducted. Specifically, an alternative to the way

the resistivity is found in the Tarnow model should be found or developed, since the current method for estimating resistivity provides values significantly lower than what is to be expected of concretes, based on a review of the literature [48]. A potential solution could be to use the Zwikker-Johnson-Kosten model, a hybrid model that, rather than treating the composition as fibrous, examines the composition as a granular material [40]. While the concrete contains fibers, the bulk of most concretes are composed of cement, a granular material, and therefore this, model may be able to provide more accurate estimates for both acoustic performance and material properties. This is only one alternative model, exploration into other models may provide better estimates of absorption by representing the concrete differently than the hybrid DBz-JCAL model presented in this thesis. Finally, the intention of the model is to allow for prediction of acoustic absorption with minimal inputs. However, having a large source of measured reference values for the development of the model would be beneficial in verifying estimations of all material properties, acoustic or otherwise. Specifically, values of viscous and thermal characteristic length and thermal permeability could only be compared to those of wools and textiles due to limited resources in the literature. Tortuosity and resistivity values of bio-fibrous concretes were also limited when verifying the model. Compiling vast amounts of empirical data regarding these material properties would be beneficial in the verification and improvement process of the model. Beyond material properties, limited information was found for predicting absorption values at frequencies above 5000 Hz. While not integral to improving the DBz-JCAL model examined in this paper, the measurement of higher frequency estimations of absorption would be beneficial to the model.

References

[1] S. Abbaszadeh, L. Zagreus, D. Lehrer, and C. Huizenga, "Occupant satisfaction with indoor environmental quality in green buildings," Jun. 2006, Accessed: Jan. 05, 2022. [Online]. Available: https://escholarship.org/uc/item/9rf7p4bs

[2] United States Geological Survey, "Cement in September 2021." Dec. 2021.

[3] H. K. Kim and H. K. Lee, "Influence of cement flow and aggregate type on the mechanical and acoustic characteristics of porous concrete," *Appl. Acoust.*, vol. 71, no. 7, pp. 607–615, Jul. 2010, doi: 10.1016/j.apacoust.2010.02.001.

[4] S. Amares, E. Sujatmika, T. W. Hong, R. Durairaj, and H. S. H. B. Hamid, "A Review: Characteristics of Noise Absorption Material," *J. Phys. Conf. Ser.*, vol. 908, p. 012005, Oct. 2017, doi: 10.1088/1742-6596/908/1/012005.

[5] H. Kuttruff, *Acoustics: An Introduction*. CRC Press, 2007.

[6] R. Fediuk, M. Amran, N. Vatin, Y. Vasilev, V. Lesovik, and T. Ozbakkaloglu, "Acoustic Properties of Innovative Concretes: A Review," *Materials*, vol. 14, no. 2, Art. no. 2, Jan. 2021, doi: 10.3390/ma14020398.

[7] Y. Chen, Q. L. Yu, and H. J. H. Brouwers, "Acoustic performance and microstructural analysis of bio-based lightweight concrete containing miscanthus," *Constr. Build. Mater.*, vol. 157, pp. 839–851, Dec. 2017, doi: 10.1016/j.conbuildmat.2017.09.161.

[8] Beijing University of Technology, Beijing, China, Y. Li, W. Dong, H. Li, and Z. Li, "Method of Vacuum Water Absorption to Determine the Porosity of Hardened Concrete," *Int. J. Struct. Civ. Eng. Res.*, 2015, doi: 10.18178/ijscer.4.3.282-286.

[9] E. Khankhaje *et al.*, "Properties of quiet pervious concrete containing oil palm kernel shell and cockleshell," *Appl. Acoust.*, vol. 122, pp. 113–120, Jul. 2017, doi: 10.1016/j.apacoust.2017.02.014.

[10] M. A. Kuczmarski and J. C. Johnston, "Acoustic Absorption in Porous Materials," Mar. 2011. Accessed: Jun. 29, 2022. [Online]. Available: https://ntrs.nasa.gov/citations/20110011143

[11] D. L. Johnson, J. Koplik, and R. Dashen, "Theory of dynamic permeability and tortuosity in fluid-saturated porous media," *J. Fluid Mech.*, vol. 176, no. 1, p. 379, Mar. 1987, doi: 10.1017/S0022112087000727.

[12] Y. Champoux and J. Allard, "Dynamic tortuosity and bulk modulus in air-saturated porous media," *J. Appl. Phys.*, vol. 70, no. 4, pp. 1975–1979, Aug. 1991, doi: 10.1063/1.349482.

[13] D. Lafarge, P. Lemarinier, J. F. Allard, and V. Tarnow, "Dynamic compressibility of air in porous structures at audible frequencies," *J. Acoust. Soc. Am.*, vol. 102, no. 4, pp. 1995–2006, Oct. 1997, doi: 10.1121/1.419690.

[14] J. Allard and Y. Champoux, "New empirical equations for sound propagation in rigid frame fibrous materials," *J. Acoust. Soc. Am.*, vol. 91, no. 6, pp. 3346–3353, Jun. 1992, doi: 10.1121/1.402824.

[15] M. E. Delany and E. N. Bazley, "Acoustical properties of fibrous absorbent materials," *Appl. Acoust.*, vol. 3, no. 2, pp. 105–116, Apr. 1970, doi: 10.1016/0003-682X(70)90031-9.

[16] "Standard Test Method for Impedance and Absorption of Acoustical Materials Using a Tube, Two Microphones and a Digital Frequency Analysis System." https://www.astm.org/e1050-19.html (accessed Aug. 10, 2022).

[17] A. Boubel, M. Garoum, S. Bousshine, and A. Bybi, “Investigation of loose wood chips and sawdust as alternative sustainable sound absorber materials,” *Appl. Acoust.*, vol. 172, p. 107639, Jan. 2021, doi: 10.1016/j.apacoust.2020.107639.
[18] A. Haapakangas, V. Hongisto, J. Varjo, and M. Lahtinen, “Benefits of quiet workspaces in open-plan offices – Evidence from two office relocations,” *J. Environ. Psychol.*, vol. 56, pp. 63–75, Apr. 2018, doi: 10.1016/j.jenvp.2018.03.003.
[19] S. Kang, D. Ou, and C. M. Mak, “The impact of indoor environmental quality on work productivity in university open-plan research offices,” *Build. Environ.*, vol. 124, pp. 78–89, Nov. 2017, doi: 10.1016/j.buildenv.2017.07.003.
[20] T. Chiu, “Noise Impact Study Update,” *LEA Consult. Ltd*, Accessed: Jan. 06, 2022. [Online]. Available: https://www.mississauga.ca/wp-content/uploads/2021/04/06150719/W5_6710_Noise_Impact_Study_Mar2021.pdf
[21] B. Peceño, C. Arenas, B. Alonso-Fariñas, and C. Leiva, “Substitution of Coarse Aggregates with Mollusk-Shell Waste in Acoustic-Absorbing Concrete,” *J. Mater. Civ. Eng.*, vol. 31, no. 6, p. 04019077, Jun. 2019, doi: 10.1061/(ASCE)MT.1943-5533.0002719.
[22] M. Antoun, C. A. Issa, G. Aouad, and N. Gerges, “Sustainable masonry blocks: Olive wood waste as substitute for fine aggregates,” *Case Stud. Constr. Mater.*, vol. 15, p. e00590, Dec. 2021, doi: 10.1016/j.cscm.2021.e00590.
[23] E. V. Aghimien, O. H. Akinkuoroye, and O. T. Adams, “Assessment of wood waste generated in selected sawmills in Kajola local government area of Oyo state,” *J. Res. For. Wildl. Environ.*, vol. 12, no. 2, Art. no. 2, Aug. 2020, Accessed: Dec. 19, 2021. [Online]. Available: https://www.ajol.info/index.php/jrfwe/article/view/198390
[24] University of BC Okanagan, “Pulp Mill Waste Hits the Road Instead of the Landfill,” *GSTDTAP*, Apr. 2021, Accessed: Dec. 19, 2021. [Online]. Available: http://119.78.100.173/C666//handle/2XK7JSWQ/321609
[25] Y.-Y. Kim, K.-M. Lee, J.-W. Bang, and S.-J. Kwon, “Effect of W/C Ratio on Durability and Porosity in Cement Mortar with Constant Cement Amount,” *Adv. Mater. Sci. Eng.*, vol. 2014, p. e273460, Apr. 2014, doi: 10.1155/2014/273460.
[26] M. Li, M. Khelifa, and M. El Ganaoui, “Mechanical characterization of concrete containing wood shavings as aggregates,” *Int. J. Sustain. Built Environ.*, vol. 6, no. 2, pp. 587–596, Dec. 2017, doi: 10.1016/j.ijsbe.2017.12.005.
[27] F. C. Jorge, C. Pereira, and J. M. F. Ferreira, “Wood-cement composites: a review,” *Holz Als Roh- Werkst.*, vol. 62, no. 5, pp. 370–377, Oct. 2004, doi: 10.1007/s00107-004-0501-2.
[28] T. S. Tie, K. H. Mo, A. Putra, S. C. Loo, U. J. Alengaram, and T.-C. Ling, “Sound absorption performance of modified concrete: A review,” *J. Build. Eng.*, vol. 30, p. 101219, Jul. 2020, doi: 10.1016/j.jobe.2020.101219.
[29] P. He, M. U. Hossain, C.-S. Poon, and D. C. W. Tsang, “Mechanical, durability and environmental aspects of magnesium oxychloride cement boards incorporating waste wood,” *J. Clean. Prod.*, doi: 10.1016/j.jclepro.2018.10.015.
[30] A. S. Banawair, G. M. Qaid, Z. Adil, and N. Mohd Nasir, “The strength of lightweight aggregate in concrete – A Review,” *IOP Conf. Ser. Earth Environ. Sci.*, vol. 357, p. 012017, Nov. 2019, doi: 10.1088/1755-1315/357/1/012017.
[31] The Engineering Toolbox, “Concrete Properties,” 2008. https://www.engineeringtoolbox.com/concrete-properties-d_1223.html (accessed Jan. 07, 2022).
[32] Portland Cement Association, “Aggregates.” https://www.cement.org/cement-concrete/concrete-materials/aggregates (accessed Jan. 06, 2022).

[33] E. Tudor *et al.*, "Acoustic Properties of Larch Bark Panels," *Forests*, vol. 12, p. 887, Jul. 2021, doi: 10.3390/f12070887.
[34] E. M. Tudor, A. Dettendorfer, G. Kain, M. C. Barbu, R. Réh, and Ľ. Krišťák, "Sound-Absorption Coefficient of Bark-Based Insulation Panels," *Polymers*, vol. 12, no. 5, Art. no. 5, May 2020, doi: 10.3390/polym12051012.
[35] A. C. C. Warnock, "Factors affecting sound transmission loss," *Can. Build. Dig.*, p. 7 p., Jul. 1985, doi: 10.4224/20328703.
[36] M. Pereira, J. Carbajo, L. Godinho, P. Amado-Mendes, D. Mateus, and J. Ramis, "Acoustic behavior of porous concrete. Characterization by experimental and inversion methods," *Mater. Constr.*, vol. 69, no. 336, Art. no. 336, Dec. 2019, doi: 10.3989/mc.2019.03619.
[37] W. G. A. Hussein, A. A. Al-Sultan, and F. H. Al-Ani, "Acoustic and thermal insulation properties of recycled aggregate mortar," *IOP Conf. Ser. Mater. Sci. Eng.*, vol. 1067, no. 1, p. 012022, Feb. 2021, doi: 10.1088/1757-899X/1067/1/012022.
[38] P. Glé, T. Blinet, and C. Guigou-Carter, *Acoustic performance prediction for building elements including biobased fibrous materials*. 2018.
[39] C. Zwikker and C. W. Kosten, *Sound absorbing materials*. New York: Elsevier Pub. Co., 1949. Accessed: Jan. 07, 2022. [Online]. Available: https://catalog.hathitrust.org/Record/001479870
[40] P. Glé, "Acoustic performance prediction for building elements including biobased fibrous materials," *Conf. Proc.*, p. 8, 2018.
[41] F. G. Praticò, R. Fedele, and P. G. Briante, "On the Dependence of Acoustic Pore Shape Factors on Porous Asphalt Volumetrics," *Sustainability*, vol. 13, no. 20, Art. no. 20, Jan. 2021, doi: 10.3390/su132011541.
[42] G. Taraldsen, "The Delany-Bazley Impedance Model and Darcy's Law," *Acta Acust. United Acust.*, vol. 91, pp. 41–50, Jan. 2005.
[43] R. Sreeja, "Sound Propagation Analysis in Porous Fibrous Acoustic Absorbers Using Johnson-Champoux-Allard Lafarge (JCAL) Model & Delaney Bazley Model," *Int. J. Appl. Eng. Res.*, vol. 16, 2021, Accessed: Jan. 14, 2022. [Online]. Available: https://www.ripublication.com/ijaer21/ijaerv16n5_11.pdf
[44] S. Chakraborty, S. K. Saha, J. C. Pandey, and S. Das, "Experimental characterization of concentration of nanofluid by ultrasonic technique," *Powder Technol.*, vol. 210, no. 3, pp. 304–307, Jul. 2011, doi: 10.1016/j.powtec.2011.03.035.
[45] *CRC HANDBOOK of THERMOPHYSICAL and THERMOCHEMICAL DATA*. CRC Press, 2020. doi: 10.1201/9781003067719.
[46] Y. S. Touloukian and T. Makita, "Thermophysical Properties of Matter - The TPRC Data Series. Volume 6. Specific Heat - Nonmetallic Liquids and Gases," THERMOPHYSICAL AND ELECTRONIC PROPERTIES INFORMATION ANALYSIS CENTER LAFAYETTE IN, Jan. 1970. Accessed: Jun. 29, 2022. [Online]. Available: https://apps.dtic.mil/sti/citations/ADA951940
[47] A. D. Pierce, *Acoustics: An Introduction to Its Physical Principles and Applications*. Springer, 2019.
[48] V. Tarnow, "Airflow resistivity of models of fibrous acoustic materials," *J. Acoust. Soc. Am.*, vol. 100, no. 6, pp. 3706–3713, Dec. 1996, doi: 10.1121/1.417233.
[49] J. Liu, F. Ren, and H. Quan, "Prediction Model for Compressive Strength of Porous Concrete with Low-Grade Recycled Aggregate," *Materials*, vol. 14, no. 14, Art. no. 14, Jan. 2021, doi: 10.3390/ma14143871.

[50] "Standard Test Method for Density, Absorption, and Voids in Hardened Concrete." https://www.astm.org/c0642-21.html (accessed Aug. 15, 2022).
[51] Md. Safiuddin and N. Hearn, "Comparison of ASTM saturation techniques for measuring the permeable porosity of concrete," *Cem. Concr. Res.*, vol. 35, no. 5, pp. 1008–1013, May 2005, doi: 10.1016/j.cemconres.2004.09.017.
[52] O. Doutres, Y. Salissou, N. Atalla, and R. Panneton, "Evaluation of the acoustic and non-acoustic properties of sound absorbing materials using a three-microphone impedance tube," *Appl. Acoust.*, vol. 71, no. 6, pp. 506–509, Jun. 2010, doi: 10.1016/j.apacoust.2010.01.007.
[53] R. Panneton and X. Olny, "Acoustical determination of the parameters governing viscous dissipation in porous media," *J. Acoust. Soc. Am.*, vol. 119, no. 4, pp. 2027–2040, Apr. 2006, doi: 10.1121/1.2169923.
[54] X. Olny and R. Panneton, "Acoustical determination of the parameters governing thermal dissipation in porous media," *J. Acoust. Soc. Am.*, vol. 123, no. 2, pp. 814–824, Feb. 2008, doi: 10.1121/1.2828066.
[55] G. Benoit, C. Heinkélé, and E. Gourdon, "Characterizing a porous road pavement using surface impedance measurement: A guided numerical inversion procedure," *J. Acoust. Soc. Am.*, vol. 134, no. 6, pp. 4782–4791, Dec. 2013, doi: 10.1121/1.4824971.
[56] M. Mastali, P. Kinnunen, H. Isomoisio, M. Karhu, and M. Illikainen, "Mechanical and acoustic properties of fiber-reinforced alkali-activated slag foam concretes containing lightweight structural aggregates," *Constr. Build. Mater.*, vol. 187, pp. 371–381, Oct. 2018, doi: 10.1016/j.conbuildmat.2018.07.228.
[57] M. Degrave-Lemeurs, P. Glé, and A. Hellouin de Menibus, "Acoustical properties of hemp concretes for buildings thermal insulation: Application to clay and lime binders," *Constr. Build. Mater.*, vol. 160, doi: 10.1016/j.conbuildmat.2017.11.064.
[58] R. Iştoan, D. Manea, L. Plesa, R. Iernuţan, and M. Dumitran, "Acoustic and thermal properties of hemp-cement building materials," *Procedia Manuf.*, vol. 32, pp. 208–215, Jan. 2019, doi: 10.1016/j.promfg.2019.02.204.
[59] Y. Champoux and M. R. Stinson, "Measurement of the characteristic impedance and propagation constant of materials having high flow resistivity," *J. Acoust. Soc. Am.*, vol. 90, no. 4, pp. 2182–2191, Oct. 1991, doi: 10.1121/1.401645.
[60] "Standard Test Method for Impedance and Absorption of Acoustical Materials Using A Tube, Two Microphones and A Digital Frequency Analysis System." https://www.astm.org/e1050-08.html (accessed Aug. 11, 2022).
[61] R. Ďuriš and E. Labašová, "The design of an impedance tube and testing of sound absorption coefficient of selected materials," *IOP Conf. Ser. Mater. Sci. Eng.*, vol. 1050, no. 1, p. 012003, Jan. 2021, doi: 10.1088/1757-899X/1050/1/012003.
[62] International Organization for Standardization, "ISO 10534-2:1998 Acoustics — Determination of sound absorption coefficient and impedance in impedance tubes — Part 2: Transfer-function method," *ISO*. https://www.iso.org/cms/render/live/en/sites/isoorg/contents/data/standard/02/28/22851.html (accessed Aug. 11, 2022).

Appendix A

MATLab Code

A.1 Sample MATLab Model Output

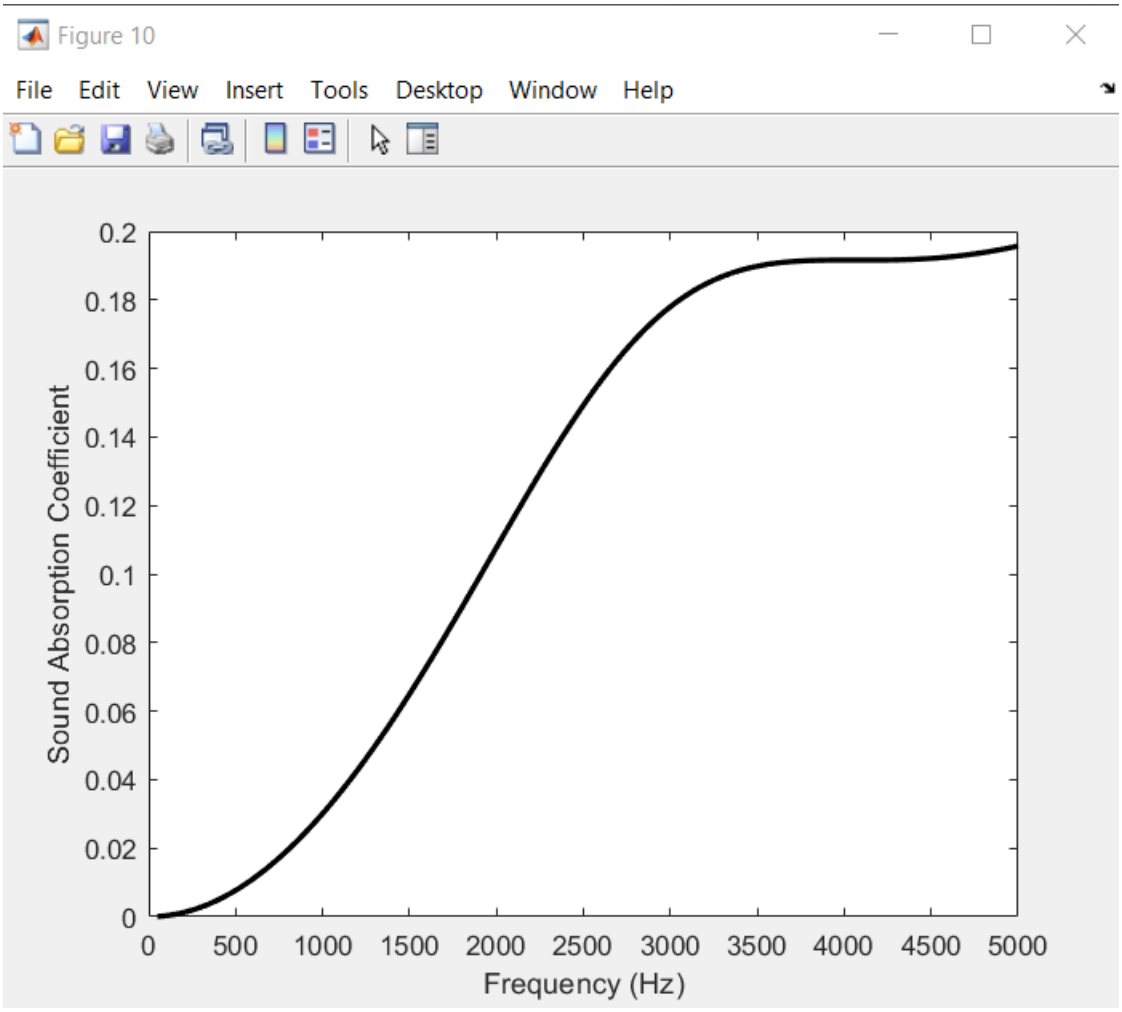

Figure A-7-1: Model Output of Estimated Acoustic Absorption for Sample 10.4

A.2 MATLab Model Code

```
%% Hybrid Johnson-Champoux-Allard-Lafarge and Delany-Bazley Acoustic Absorption Model Integration
% 10/28/2022 - By Matthew Lorimer

% Code based on JCAL method code by Luc Jaouen & Dominic Pilon, further
% reference and information at apmr.matelys.com
clear all
close all
%% First must define constants required for environment and materials

T0 = 22.8; % initial air temperature [C]
T = T0 + 273.16; % temperature in Kelvin [K]
R = 287.031; %universal gas constant [J/kg*K]
P0 = 101650; %air pressure (accepted pressure) [Pa]
rho0 = P0/(R*T); %density of air [kg/m3]
c0 = 20.047*sqrt(T); % speed of sound in air [m/s]
ka = (c0^2)*(rho0); % isentropic bulk modulus of air [Pa]

h = 0.047; % [m] thickness of final barrier

% Due to nature of the JCAL viscous and thermal properties at higher frequencies,
% need a higher frequency range for values - appoach infinity
```

```
syms freq %allows for calculations as frequency approaches infinity
% syms angular frequency that approaches infinity
omegaFreq = 2*pi.*freq; %[Hz]

%Frequency Range 1, used in plotting [Hz]
xx1 = 50; % [Hz] lower limit
%freq increment
yy1 = 5; % [Hz]
%max freq limit
zz1 = 20000; % [Hz] upper limit - threshold of human hearing

% Frequency Range 2, used in Excel to compare to experimental data
% as max frequency of impedance data is aprox. 4700 Hz
%Frequency Range 2 [Hz]
xx2 = 50; %[Hz] lower limit
%freq increment
yy2 = 5; % [Hz]
% max freq limit
zz2 = 5000; % [Hz] upper limit - threshold of human hearing

f = xx1:yy1:zz1;   % [Hz] frequency range in plot
omega = 2*pi.*f;   % [Hz] angular frequency of f

f2 = xx2:yy2:zz2;  % [Hz] frequency range in plot in excel
```

```
omega2 = 2*pi.*f2; % [Hz] angular frequency of f2

%% Reference air qualities based on temperature - taken from MATELYS JCAL code
% Dynamic viscosity of air for 100 K < T < 600 K
visc0=7.72488e-8*T-5.95238e-11*T^2+2.71368e-14*T^3;   % [Ns/m²]

% Specific heat at constant pressure (J.kg-1.K-1; 260 K < T < 600 K)
Cp    = 4168.8*(0.249679-7.55179e-5*T+1.69194e-7*T^2-6.46128e-11*T^3);

% Thermal conductivity of air
thermCond = 2.624e-02 * ( (T/300)^(3/2) * (300+245.4*exp(-27.6/300))/(T+245.4*exp(-
27.6/T)) );


%Final properties of air found using these values
Cv = Cp-R; %specific heat at constant volume [J/K*kg]
gamma = Cp/Cv; %ratio of specific heats [-]

% Prandtl number ratio of momentum diffusivity to thermal diffusivity
Pr = visc0*Cp/thermCond; % [-] Prandtl Number - established formula

%% Material / fibre properties that are known / assumed / or to be goal in calculating
Air Resistivity
%porosity found through water saturation of pores of concrete
porous = 0.1242; % composition porosity (example used sample 10.4)
```

```
%For this calculation, utilize the Tarnow method for airflow resistivity
r = 7.5*10^-5; %FSD, fiber radius [m]

rhoFIB = 155.7; %density of fibres [kg/m3]
rhoMAT = 1242.16; %density of concrete  sample[kg/m3]
d = rhoMAT/rhoFIB; %density ratio

% b is square root of area per fibre, [m]
b2 = (r*sqrt(pi*rhoFIB/rhoMAT))^2; % [m2]

coefFirst = 4*visc0*pi/(b2);
sigma = coefFirst*(1/(0.64*log(1/d) - 0.737 + d)); % [Ns/m4], airflow resistivity

%% Can not substitute known values into the dynamic bulk modulus and density equations
% Characteristic Impedance using DBz model
Zc = rho0*c0*(1 + 0.0571.*(rho0.*f./sigma).^-0.754 - 1j*0.087.*(rho0.*f./sigma).^-0.732);
% 0.01 < f/sigma < 1.00 as per DBz model

%Characteristic wave number using DBz model
kc = (omega./c0).*(1 + 0.0978.*(rho0.*f./sigma).^-0.7 - 1j*0.189.*(rho0.*f./sigma).^-0.595);
```

```
% then using the characteristic impedance and wave number, the dynamic
% density and bulk modulus can be found
K_Dyn = omega.*Zc./kc; %Dynamic Bulk Modulus
rho_Dyn = Zc.*kc./omega; %Dynamic Density

%Require values to approach infinity for the calculation of toruosity,
%therefore need to define the dynamic bulk modulus and density using syms
%frequency
%Impedance
ZcFreq = rho0*c0*(1 + 0.0571.*(rho0.*freq./sigma).^-0.754 -
1j*0.087.*(rho0.*freq./sigma).^-0.732);
%wave number
kcFreq = (omegaFreq./c0).*(1 + 0.0978.*(rho0.*freq./sigma).^-0.7 -
1j*0.189.*(rho0.*freq./sigma).^-0.595);
%dyanmic bulk modulus
K_DynFreq = omegaFreq.*ZcFreq./kcFreq;
%dynamic density
rho_DynFreq = ZcFreq.*kcFreq./omegaFreq;

%% Now must find the missing JCAL parameters needed
% higher freq limit of tortuosity, thermal permeability, and both
% thermal and viscous characteristic lengths

% Can then find upper limit on tortuosity and charactersitic length with the
```

```
% syms variable as frequency approaches infinity

% higher frequency limit of tortuosity [-]
upperTortLim = limit((1/rho0).*(real(rho_DynFreq) - sqrt((imag(rho_DynFreq).^2) -
(sigma*porous./omegaFreq).^2)), freq, inf);

% converting syms variable to number useable in calculations and plotting
upperTort = double(upperTortLim)

upperTortVAL = upperTort; % useable variable saved here [-]

% With the known values of tortuosity and porosity, can find the viscous char lengh of
% using JCAL model formulae for viscous effects

%viscous characteristic length as frequency approaches infinity [m]
viscLength = upperTort.*sqrt((2*visc0*rho0)./(omega.*imag(rho_Dyn).*(rho0*upperTort
- real(rho_Dyn))));

figure(1) % plotting the viscous characteristic length over frequency
set(gca,'fontsize',12)
plot(f,real(viscLength),'k-','LineWidth',2)
hold on
%plot(meas(:,1),meas(:,9),'r-','LineWidth',2)
plot(f,imag(viscLength),'b-','LineWidth',2)
hold on
```

```
plot(f,abs(viscLength),'r-','LineWidth',2)
%plot(meas(:,1),meas(:,10),'r-','LineWidth',2)
xlabel('Frequency (Hz)')
ylabel('Real (B) and Imag. (U) Parts of Viscous Char Length (m)')
set(gca,'Ylim')

%saving parts of viscous length separately and as total value
viscLengthVALimg = imag(viscLength(1,3991)); % imaginary part of viscous characteristic length
viscLengthVALreal = real(viscLength(1,3991)); % real part of viscous characteristic length
viscLengthVAL = viscLengthVALreal + viscLengthVALimg; % viscous characteristic length [m]

%% Using viscous properties, can find thermal characteristic length
% calculation placeholder
placeHold = sqrt(2*visc0./(rho0.*omega.*Pr));

%ratio of dynamic bulk modulus to bulk modulus of air
ratioK = K_Dyn./ka;
% relation to specific heat
gammaRatio = gamma.*ratioK;

% calculation placeholders
numTherm = porous - ratioK;
```

```
denTherm = porous - (gamma.*ratioK);
imVal = (numTherm./denTherm).^2;
imVal2 = -1.*imag(imVal);

%Thermal characteristic length (m)
thermLength = placeHold.*(sqrt(2)).*(imVal2.^-0.5);

figure(2) % plotting the thermal characteristic length in relation to frequency
set(gca,'fontsize',12)
plot(f,real(thermLength),'k-','LineWidth',2)
hold on
%plot(meas(:,1),meas(:,9),'r-','LineWidth',2)
plot(f,imag(thermLength),'b-','LineWidth',2)
hold on
plot(f,abs(thermLength),'r-','LineWidth',2)
%plot(meas(:,1),meas(:,10),'r-','LineWidth',2)
xlabel('frequency (Hz)')
ylabel('Real (B) and imag. (U) parts of visc therm length (m)')
set(gca,'Ylim')

% thermal characteristic length saved in imaginary and real parts
thermLengthVALimg = imag(thermLength(1,3991)); % imaginary part of thermal characteristic length
thermLengthVALreal = real(thermLength(1,3991)); % real part of thermal characteristic length
```

```
thermLengthVAL = thermLengthVALreal + thermLengthVALimg; % thermal characteristic length (m)

%% Can find the thermal permeability through the use of similar relation
% calculation placeholders
placeHold2 = placeHold.^2;

% bulk modulus in relation to porosity of material
Keq = K_Dyn./porous;
% ratio of porous bulk modulus to bulk modulus of air
ratioKeq = Keq./ka;
% relation of bulk modulus to specific heats
ratioGammaKeq = gamma.*ratioKeq;

% calculation placeholders
numPerm = 1 - ratioKeq;
denPerm = 1 - ratioGammaKeq;
reValEq = (numPerm./denPerm).^2;
reValEq2 = -1.*real(reValEq);

% calculation of thermal permeability [m2]
thermPerm = (porous.*placeHold2./2).*(reValEq2.^-0.5);

% plotting thermal permeability in relation to frequency
figure(3)
```

```
set(gca,'fontsize',12)
plot(f,real(thermPerm),'k-','LineWidth',2)
hold on
%plot(meas(:,1),meas(:,9),'r-','LineWidth',2)
plot(f,imag(thermPerm),'b-','LineWidth',2)
hold on
plot(f,abs(thermPerm),'r-','LineWidth',2)
%plot(meas(:,1),meas(:,10),'r-','LineWidth',2)
xlabel('Frequency (Hz)')
ylabel('Real (B) and Imag. (U) parts of Thermal Termeability (m2)')
set(gca,'Ylim')

% thermal permeability saved as imaginary and real parts
thermPermVALimg = imag(thermPerm(1,3991)); % imaginary part of thermal permeability
thermPermVALreal = real(thermPerm(1,3991)); % real part of thermal permeability
thermPermVAL = thermPermVALreal + thermPermVALimg; % thermal permeability

%% All properties for JCAL calculations of KDyn and rhoDyn are accounted for
% Plug all properties into final JCAL formulae to solve for acoustic absorption

% calculation placeholders
aCoef = gamma*P0/porous;
bCoef = gamma - (gamma-1);
```

```
oneCoef = upperTortVAL*rho0/porous;
twoCoef = sigma*porous./(1j.*omega2.*rho0.*upperTortVAL);
threeCoef =
(1j*4.*(upperTortVAL.^2).*visc0*rho0.*omega2)/((sigma^2).*(viscLengthVAL.^2).*(porous^
2));

% dynamic density recalculated through JCAL model [kg/m3]
rhoDyn_JCAL = oneCoef.*(1 + twoCoef.*sqrt(1 + threeCoef));

% graph of dynamic density from JCAL method in relation to frequency
figure(5)
set(gca, 'fontsize',12)
plot(f2,real(rhoDyn_JCAL),'k-','LineWidth',2)
hold on
%plot(meas(:,1),meas(:,9),'r-','LineWidth',2)
plot(f2,imag(rhoDyn_JCAL),'b-','LineWidth',2)
hold on
plot(f2,abs(rhoDyn_JCAL),'r-','LineWidth',2)
%plot(meas(:,1),meas(:,10),'r-','LineWidth',2)
xlabel('Frequency (Hz)')
ylabel('Real (B) and Imag. (U) Parts of Dynamic Density (kg/m3)')
set(gca,'Ylim')

% calculation placeholders for dynamic bulk modulus
cCoef = porous*thermCond*1j./(thermPermVAL.*Cp*rho0.*omega2);
```

```
dCoef =
1j*4*Cp*rho0.*omega2.*(thermPermVAL.^2)./(thermCond.*(porous^2).*(thermLengthVAL.
^2));

Kden1 = sqrt(1 + dCoef);
Kden2 = bCoef.*((1 - cCoef.*Kden1).^-1);

% dynamic bulk modulus over frequency [Pa]
KDyn_JCAL = aCoef./Kden2;

% output graph of dynamic bulk modulus from JCAL method in relation to frequency
figure(6)
set(gca, 'fontsize',12)
plot(f2,real(KDyn_JCAL),'k-','LineWidth',2)
hold on
%plot(meas(:,1),meas(:,9),'r-','LineWidth',2)
plot(f2,imag(KDyn_JCAL),'b-','LineWidth',2)
hold on
plot(f2,abs(KDyn_JCAL),'r-','LineWidth',2)
%plot(meas(:,1),meas(:,10),'r-','LineWidth',2)
xlabel('Frequency (Hz)')
ylabel('Real (B) and Imag. (U) Parts of Dynamic Bulk Modulus (Pa)')
set(gca,'Ylim')

%% Finally, relating to the original Zc and kc formulae, absorption can be calculated
```

```
% Using the Dynamic Bulk Modulus and the Dynamic density, solve for the
% characteristic impedance and wave number from the JCAL solved K and rho

% characteristic impedance calculation [Pas/m]
impChar = sqrt(rhoDyn_JCAL.*KDyn_JCAL);
% wave number calculation [m-1]
waveNum = omega2.*sqrt(rhoDyn_JCAL./KDyn_JCAL);

% output graph of characteristic impedance in relation to frequency
figure(7)
set(gca, 'fontsize',12)
plot(f2,real(impChar),'k-','LineWidth',2)
hold on
%plot(meas(:,1),meas(:,9),'r-','LineWidth',2)
plot(f2,imag(impChar),'b-','LineWidth',2)
hold on
plot(f2,abs(impChar),'r-','LineWidth',2)
%plot(meas(:,1),meas(:,10),'r-','LineWidth',2)
xlabel('Frequency (Hz)')
ylabel('Real (B) and Imag. (U) Parts of Characteristic Impedance (Pas/m)')
set(gca,'Ylim')

% output graph of wave number in relation to frequency
figure(8)
set(gca, 'fontsize',12)
```

```
plot(f2,real(waveNum),'k-','LineWidth',2)
hold on
%plot(meas(:,1),meas(:,9),'r-','LineWidth',2)
plot(f2,imag(waveNum),'b-','LineWidth',2)
hold on
plot(f2,abs(waveNum),'r-','LineWidth',2)
%plot(meas(:,1),meas(:,10),'r-','LineWidth',2)
xlabel('Frequency (Hz)')
ylabel('Real (B) and Imag. (U) Parts of Wave Number (m-1)')
set(gca,'Ylim')

% Can then use the relations in the Delany Bazley models acoustic
% absorption application to find the acoustic absorption
% This model of impedance (impOnWall) is under the assumption that the
% surface being examined is rigidly backed, therefore it can apply here as
% a concrete absorber on a wall.

% calculating impedance on surface of sample
impOnWall = -1j .* impChar./tan(waveNum.*h); %[kg/m2s]

% calculating acoustic absorption
alpha = 1 - ( abs( (impOnWall-rho0*c0)./(impOnWall+rho0*c0) ) ).^2; %[-] unitless

% Output graph of surface impedace on the sample surface in relation to frequency
figure(9)
```

```
set(gca, 'fontsize',12)
plot(f2,real(impOnWall),'k-','LineWidth',2)
hold on
%plot(meas(:,1),meas(:,9),'r-','LineWidth',2)
plot(f2,imag(impOnWall),'b-','LineWidth',2)
hold on
plot(f2,abs(impOnWall),'r-','LineWidth',2)
%plot(meas(:,1),meas(:,10),'r-','LineWidth',2)
xlabel('Frequency (Hz)')
ylabel('Real (B) and Imag. (U) Parts of Impedance on Wall (kg/m2s)')
set(gca,'Ylim')

 % output graph of acoustic absorption coefficient in relation to frequency
figure(10)
set(gca, 'fontsize',12)
plot(f2,alpha,'k-','LineWidth',2)
xlabel('Frequency (Hz)')
ylabel('Sound Absorption Coefficient')
set(gca,'Ylim')

%% Output Data to Excel for Comparison to Impedance Tube Measurements
filename = 'alphaDataHolding.xlsx';
writematrix(alpha, filename, 'Sheet', 1, 'Range', 'A1')
```